GEOCHEMISTRY AND MINERALOGY OF TONGUE RIVER MEMBER COAL FROM THREE MONTANA COAL MINES

by

Caroline McColl Gottschalk

A thesis submitted in partial fulfillment
of the requirements for the degree

of

Master of Science

in

Earth Science

MONTANA STATE UNIVERSITY
Bozeman, Montana

May 2010

©COPYRIGHT

by

Caroline McColl Gottschalk

2010

All Rights Reserved

APPROVAL

of a thesis submitted by

Caroline McColl Gottschalk

This thesis has been read by each member of the thesis committee and has been found to be satisfactory regarding content, English usage, format, citation, bibliographic style, and consistency and is ready for submission to the Division of Graduate Education.

Dr. David Mogk

Approved for the Department of Earth Science

Dr. Stephan G. Custer

Approved for the Division of Graduate Education

Dr. Carl A. Fox

STATEMENT OF PERMISSION TO USE

In presenting this thesis in partial fulfillment of the requirements for a master's degree at Montana State University, I agree that the Library shall make it available to borrowers under rules of the Library.

If I have indicated my intention to copyright this thesis by including a copyright notice page, copying is allowable only for scholarly purposes, consistent with "fair use" as prescribed in the U.S. Copyright Law. Requests for permission for extended quotation from or reproduction of this thesis in whole or in parts may be granted only by the copyright holder.

Caroline McColl Gottschalk

May 2010

ACKNOWLEDGEMENTS

I would like to thank Dr. David W. Mogk, advisor, for help with development and refinement of my project, and for intensive editing. Many thanks to the ICAL staff for training on, support with, and the use of instruments. Thank you to Nelson Eby, University of Massachusetts-Lowell, for providing instrumental neutron activation analysis data. Many thanks to Mr. Kent Salitros from Rosebud Coal Mine, Mr. Daryl Myran from Absaloka Coal Mine, and Mr. Bill Pruitt from Decker Coal Mine for the generosity of allowing me to analyze coal from their mines. My special thanks to Eugene Morigeau for sticking with me and giving me the emotional support I needed. Without it, I would not have completed this thesis.

TABLE OF CONTENTS

1. INTRODUCTION 1

Geologic Setting 1
Goals 7
Objectives 8
Rational 9
General Coal Information 9
Composition of Coal 12

2. ANALYSIS AND RESULTS 16

3. INSTRUMENTAL NEUTRON ACTIVATION ANALYSIS (INAA) 17

4. X-RAY POWDER DIFFRACTION (XRD) 27

Instrumentation 27
Sample Preparation 27
Experimental Conditions 28
Analytical Results 28
Discussion 31

5. SCANNING ELECTRON MICROSCOPY (SEM) 32

Instrumentation 32
Sample Preparation 32
Experimental Procedures 33
Analytical Results 34
Discussion 37

6. X-RAY PHOTOELECTRON SPECTROSCOPY (XPS) 41

Instrumentation 41
Sample Preparation for Bulk Coal Surveys 42
Experimental Procedures for Bulk Coal Surveys 43
Analysis Procedures for Bulk Coal Surveys 44
Analytical Results 44
Additional Surveys Beyond the Bulk Coal 48
Multiplex Analysis of XPS Spectra 49
Results from Multiplex Analysis of XPS Spectra 50
Discussion of Multiplex Analysis of XPS Spectra 54

TABLE OF CONTENTS - CONTINUED

7. TIME-OF-FLIGHT SECONDARY ION MASS SPECTROMETRY (ToF-SIMS) 57

Instrumentation 57
Sample Preparation 58
Experimental Procedures for Positive Spectrum 58
ToF-SIMS- Analysis of Positive ToF-SIMS Spectra with 4 Minutes Sputtering 59
ToF-SIMS- Data for Positive ToF-SIMS Spectra with 4 Minutes Sputtering 60
Analysis of ToF-SIMS Images 62
Additional Search for Trace Elements Using ToF-SIMS 63
Analysis of Negative ToF-SIMS Spectra with 4 Minutes Sputtering 66

8. DISCUSSION 68

Composition 69
Mineralogy 70
Focus on Nitrogen and Sodium 72
Hazards Potential 74
Human Health Implications for Trace Elements in Coal 75
Suggestions for Future Work 78

REFERENCES CITED 79

APPENDICES 87

APPENDIX A: Note from Nelson Eby 88
APPENDIX B: Specific JCPDF Card File Numbers 90
APPENDIX C: Sampling Of SEM Images 92
APPENDIX D: Sampling of EDS Spectra 98
APPENDIX E: Sampling Of XPS Surveys 101
APPENDIX G: Elements in U.S. Coals by Rank, and U.S. and Worldwide Averages, Compiled by the National Research Council (1980) 109

LIST OF TABLES

Table Page

1. Samples Names and Abbreviations. 2

2. INAA Dataset..... 18

3. Relative Amounts of Potentially Hazardous Elements. 26

4. Summary of Minerals Identified in Three Montana Coal Mines (Ab, D, Rb) Using XRD. 31

5. Minerals in each Sample Based on SEM Imaging and EDS Elemental Analysis. 34

6. Minerals in each Component Based on SEM/EDS Interpretations. 36

7. Classification of Pyrite in this Study According to Alonso-Azcárate et al. (2001) and Murowick and Barnes (1987). 40

8. Complete Argonne Coals List with Locations and Ranks. 46

9. XPS Peak Positions from the Literature Exhibiting the Chemical Shifts Associated with Various Ionic States. 50

10. Relative Concentrations of Various N, S, and O Components Determined by XPS Curve Fittings. 51

11. Components Listed by Decreasing Abundance Based on Positive ToF-SIMS after Four Minutes Sputtering..... 61

12. Maximum Peak Counts for Select Elements Based on Positive ToF-SIMS after Four Minutes Sputtering..... 64

13. Top Ten Components, Found by Negative ToF-SIMS after 4 Minutes Sputtering, Listed in Order of Decreasing Abundance. 67

14. Na atomic concentration as determined by XPS in various coal mines..... 75

15. Elements in U.S. Coals by Rank, and U.S. and Worldwide Averages. 110

LIST OF FIGURES

Figure Page

1. Map of Colstrip coalfield and surrounding area. (Figure from Roberts et al., 1999b). 3

2. Map of Decker Coalfield and surrounding area. (Figure from Roberts et al., 1999a). 3

3. Map of the PRB and surrounding area. (Figure from Flores and Bader, 1999). 5

4. Partial stratigraphic column of the Powder River basin, including the Fort Union Formation. Modified from Flores (2004). 6

5. Representation of nitrogen functionalities (Fletcher et al., 2008). 13

6. Periodic table showing hazardous air pollutants found in coal denoted by circles and elements routinely found in coal in general by rectangles. 15

7. LILE and LREE concentrations as determined by INAA. 20

8. HFSE and middle to heavy REE concentrations as determined by INAA. 21

9. Transition metals, chalcophile elements, and a platinum group element (Ir) as determined by INAA. 22

10. Degree of LREE enrichment shown by the ratio of La_n to Yb_n as determined by INAA. 24

11. Chondrite-normalized REE diagram for samples from Absaloka mine as determined by INAA. 24

12. Chondrite-normalized REE diagram for samples from Decker mine as determined by INAA. 25

13. Chondrite-normalized REE diagram for samples from Rosebud mine as determined by INAA. 25

14. Absaloka coal XRD results. 29

15. Decker coal XRD results. 30

LIST OF FIGURES - CONTINUED

Figure Page

16. Rosebud coal XRD results. 30

17. SEM image of kaolinite in an ash rich part of a sample from D low 1% Na. 37

18. SEM images of cubo-pyritohedra pyrite from a sulfide rich piece from Ab 1 (top) and dendritic pyrite from a sulfide rich piece from Ab 2 (bottom).. 40

19. Pie charts illustrating atomic concentrations based on XPS in coal samples from three coal mines. 45

20. Relative atomic concentration according to XPS, excluding carbon and oxygen, for Absaloka, Decker, Rosebud, and each of the APCSP coals (Weitzsacker and Gardella, 1992). 47

21. Absolute at.% of Na and N in various Montana coals determined by XPS. 48

22. A representative N 1s XPS profile and the XPS curve fits for a Decker coal sample. Deconvoluted peaks correspond to 1) pyrrolic nitrogen, 2) pyridinic nitrogen, and 3) quaternary nitrogen. 52

23. A representative S 2p XPS profile and the XPS curve fit for an Absaloka coal sample. Sulfur here is recognized only as thiophenes. 52

24. A representative N 1s XPS profile and the XPS curve fits for a Decker coal sample. Deconvoluted peaks correspond to 1) pyrrolic nitrogen, 2) pyridinic nitrogen, and 3) quaternary nitrogen. 53

25. A representative S 2p XPS profile and the XPS curve fits for a Decker coal sample. Deconvoluted peaks correspond to 1) thiophenes and 2) pyrite. 53

26. representative N 1s XPS profile and the XPS curve fits for a Rosebud coal sample. Deconvoluted peaks correspond to 1) pyrrolic nitrogen, 2) pyridinic nitrogen, and 3) quaternary nitrogen. 54

LIST OF FIGURES - CONTINUED

Figure Page

27. Proportion of nitrogen in quaternary form versus carbon content based on high resolution XPS surveys from the Absaloka, Decker and Rosebud coal mines. 55

28. ToF-SIMS elemental maps for D low Na 8% of aluminum (left) and silicon (right). Scale bars are 100 micron each. Intensity scale, far right, shows the number of ions coming into the detector per a given unit of time with lighter colors indicating more ions. 63

29. ToF-SIMS total ion image from RB Upper. Scale bar is 100 micron. Intensity scale, far right, shows the number of ions coming into the detector per a given unit of time with darker colors indicating more ions. This scale also applies to the next three images..... 65

30. ToF-SIMS Cr+ ion image from RB Upper. Scale bar is 100 micron. 65

31. ToF-SIMS Mn+ ion image from RB Upper. Scale bar equals 100 micron. 66

32. ToF-SIMS Zn+ ion image from RB Upper. Scale bar equals 100 micron. 66

33. Na in ppm as determined by INAA in various coal mines. 73

34. Na atomic concentration as determined by XPS in various coal mines. 74

35. Comparison of uranium levels in coal in comparison to other natural sources (from USGS, 1997). 78

36. D low 1% Na ash rich. Kaolinite with platy habit. 93

37. D low 8% Ash rich. Dominantly kaolinite, pyrite is also detected in low abundance throughout. 94

38. RB Upper Powder. Kaolinite and dolomite are the dominant minerals in this powder made in absence of visible ash and sulfide heterogeneities. 95

39. RB CLEP Powder. Pyrite is the dominant mineral in this powder made in absence of visible ash and sulfide heterogeneities..... 96

LIST OF FIGURES - CONTINUED

Figure Page

40. Ab 1 Sulfide rich. Cubo-pyritohedra pyrite dominants this sulfide component. 97

41. Ab 2 Sulfide rich. Dendritic pyrite dominants this sulfide component. 97

42. EDS spectra of pyrite in a powder from RB CLEP; note pyrite is pure. 99

43. EDS spectra of kaolinite in a powder from Ab 4. 99

44. EDS spectra of mostly quartz and some pyrite in a sulfide rich piece from RB 1. 100

45. Spectra of XPS peaks. Auger peaks are also present; these are commonly wider such as displayed by the labeled O KLL peaks. 104

46. ToFSIMs spectra gathered in positive mode after four minutes sputtering of Ab 2. 106

47. ToFSIMs spectra gathered in positive mode after four minutes sputtering of D low Na 8%. 107

48. ToFSIMs spectra gathered in positive mode after four minutes sputtering of RB Upper. 108

ABSTRACT

The geochemistry and mineralogy of coal from the Absaloka, Rosebud, and Decker mines located in the Powder River Basin in Montana have been characterized to determine the bulk composition of inorganic constituents in the coal; mineralogy of the coal, including the identity, morphology, composition and distribution of minerals present; occurrence and distribution of potentially hazardous trace elements; and chemical state of selected elements (N, O, S). These data were acquired using instrumental neutron activation analysis (INAA), X-ray powder diffraction (XRD), scanning electron microscopy (SEM) and energy dispersive spectroscopy (EDS), X-ray photoelectron spectroscopy (XPS), and time of flight mass spectrometry (ToF-SIMS). In aggregate, these analytical techniques provide complementary information and also allow for cross-technique comparison of results.

Overall the Montana coals contain mineral assemblages that are typical of coals described from across the United States and the world. Comparing Montana Powder River basin coal versus the rest of the United States coals, Montana Power River has, overall, a remarkably lower abundance of potentially hazardous elements. XRD analysis revealed kaolinite in all samples, variably present are quartz, illite, calcite, dolomite, gypsum, and pyrite. SEM/EDS imaging and analysis confirmed the occurrence of these mineral phases and the dominance of kaolinite in ash layers. Pyrite is the primary sulfide mineral that occurs in a variety of crystal forms that could affect its solubility, and therefore, potential for acid release. Pyrite occurs as a pure compound with no As nor other potentially hazardous element as part of a solid solution. However XPS analysis of sulfide rich areas reveal a concentration of Se and Co suggesting these elements are sorbed onto the pyrite surfaces.

This study provided a reconnaissance overview of the geochemistry and mineralogy of these Montana coal mines. Future work could include a more detailed chemical stratigraphy of the coal-producing layers to better characterize the distribution of minerals and elemental components in the coal, and to determine the processes responsible for their occurrence and distribution. The results of this study are applicable to the future development of clean coal technologies and to address the potential environmental and health impacts of coal combustion.

CHAPTER 1

INTRODUCTION

Coal is the most abundant energy source, and dependency on it is predicted to increase as oil and gas reserves run out (Nabeel et al., 2000) and industrializing countries such as India and China demand ever-increasing abundances of coal-generated energy. Additionally, there is a growing concern over environmental and health impacts of coal combustion products and products formed from them; potentially hazardous compounds and elements include SO_x (Thomas, 2002), NO_x (Smith, 2005), As, Be, Cd, Hg, Mn, Ni, Pb, Sb, Se, (Finkelman, 1994), and Th (Kizilshtein and Kholodkov, 1999). To mitigate numerous potential environmental hazards of coal combustion, it is important to understand the mode and distribution of these potentially hazardous or toxic elements. This will provide information for the minimization of hazardous gaseous and solid (fly ash) waste products, and is an important step towards development of clean coal technology (Kolker and Finkelman, 1998).

Geologic Setting

Three Montana coal mines from the Powder River Basin (PRB), Absaloka, Decker, and Rosebud, were selected for detailed geochemical and mineralogical studies to characterize the occurrence and distribution of inorganic components of coal at these locations. Within each mine representative samples were collected from known production units. Table 1 lists the samples according to coal mine; names provided by companies are followed in parentheses by abbreviations used throughout this study.

Table 1. Samples Names and Abbreviations.

Absaloka	Decker	Rosebud
Absaloka 1 (Ab 1)	Dietz 1 low[1] 1% Na D7 (D low Na 1%)	Rosebud 1 high Na (RB 1)
Absaloka 2 (Ab 2)	Dietz 1 low 8% Na (D lower Na 8%)	Rosebud 2 low Na (RB 2)
Absaloka 3a (Ab 3a)		Rosebud high sulfur Upper zone top 6 inch (RB Upper)
Absaloka 3b (Ab 3b)		Rosebud CELP high sulfur (RB CELP)
Absaloka 4 (Ab 4)		

[1]The 'low' in the Decker sample names is an indication of physical placement, it does not correspond to amount of Na

The Absaloka Mine (Figure 1) is a 15,000-acre single pit surface mine complex located near Hardin Montana, operated by Westmoreland resources (Westmoreland.com-resources, 2009). It produces 7 – 7.5 million tons of coal annually from a coal bed formed by the coalescing of the Rosebud and the Robinson bed and the Rosebud-McKay coal bed (Ellis et al., 1999). It was developed to supply coal to Midwestern utilities, as it continues to do today (Westmoreland.com-resources, 2009).

The Rosebud Mine (Figure 1) is a 25,000 acre surface mine complex located in the northern PRB near Colstrip, Montana, operated by Western Energy Company (Westmoreland.com-rosebud, 2009) (Richards, 2008). It produces coal from the Rosebud coal bed (Roberts et al., 1999b). The most productive coal mine in Montana (Richards, 2008), it produces 10 to 13 million tons of coal annually, most of which goes to the Colstrip Power Station (Westmoreland Rosebud website, 2009).

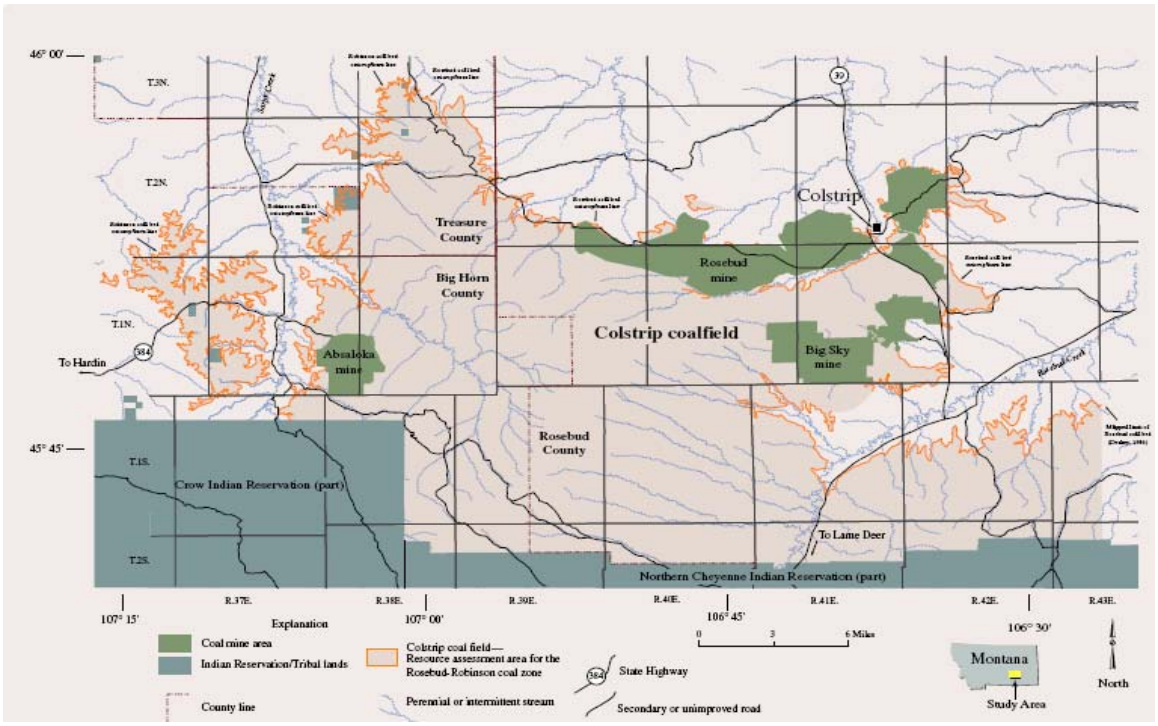


Figure 1. Map of Colstrip coalfield and surrounding area.
(Figure from Roberts et al., 1999b).

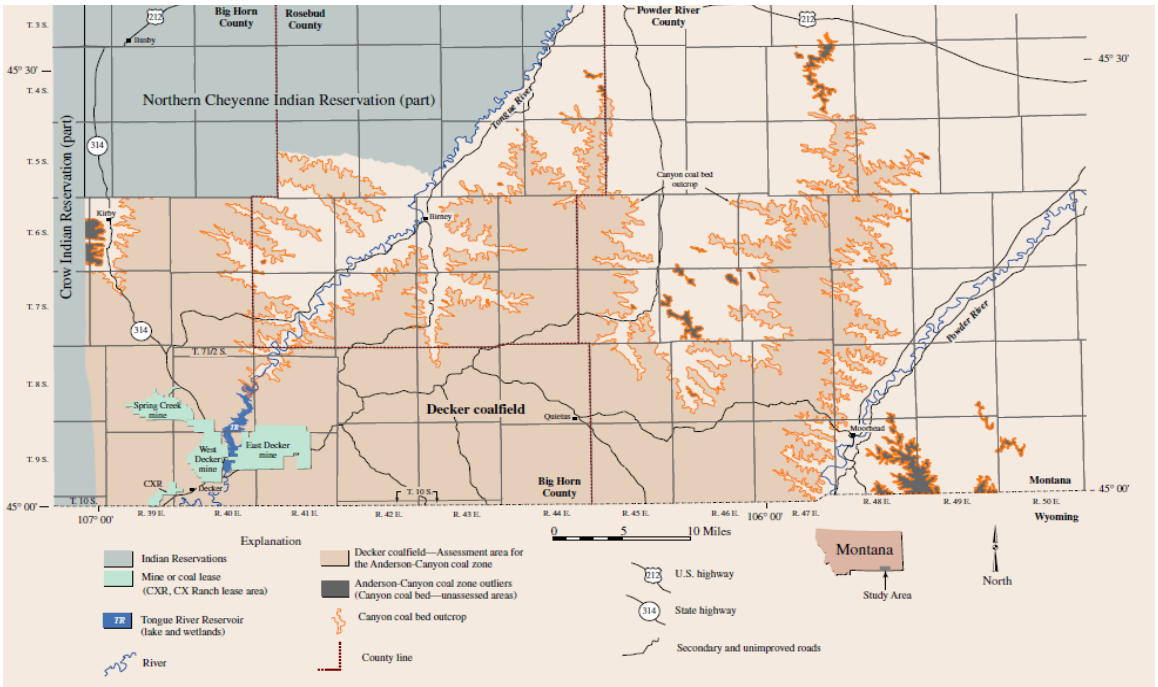


Figure 2. Map of Decker Coalfield and surrounding area.
(Figure from Roberts et al., 1999a).

Decker Coal Company operates in the northwest section of the PRB southeast of Big Horn County, Montana (Kennecott Website, 2009), producing a maximum of 12 million tons of coal per year. The coal is mostly marketed to Midwestern utilities (Kennecott Website, 2009). Decker Coalfield (Figure 2) includes the Spring Creek, East Decker, and West Decker surface mines (Roberts et al., 1999a).

The Absaloka, Rosebud (Roberts et al., 1999b) and Decker (Roberts et al., 1999a) Mines all primarily derive their coal resources from the Tongue River Member of the Palaeocene Fort Union Formation. The Fort Union Formation is the dominant coal bearing Formation of the Decker coalfield, although also present is up to 120 m of the Wasatch Formation, a coal bearing unit of similar lithology (Roberts et al., 1999a) that overlies the Fort Union Formation (Kong et al., 1993). The coal of the Colstrip coalfield, including the Absaloka and Rosebud Mines, is mainly found in the Tongue River Member of the Fort Union Formation, with some additional coal present in the Tullock and Lebo Members (Ellis et al., 1999). Only the Tongue River Member crops out in the Decker Coal field (Roberts et al., 1999a). The coal deposits in the Tongue River Member are flat-lying and near the surface (many at a depth of less than 45 m), making them economically advantageous to mine (Struck, 1975).

The Powder River Basin (PRB) (Figure 3), a 12,000 plus square mile asymmetrical structural basin, is one of many coal-bearing basins in the Northern Rocky Mountains and Great Plains region (Ellis et al., 1999). The stratigraphy of the coal beds is quite variable in both horizontal and vertical dimensions, and occur in a complex geometry wherein coal beds typically merge, split, or are otherwise discontinuous in the subsurface (Ellis et al., 1999).

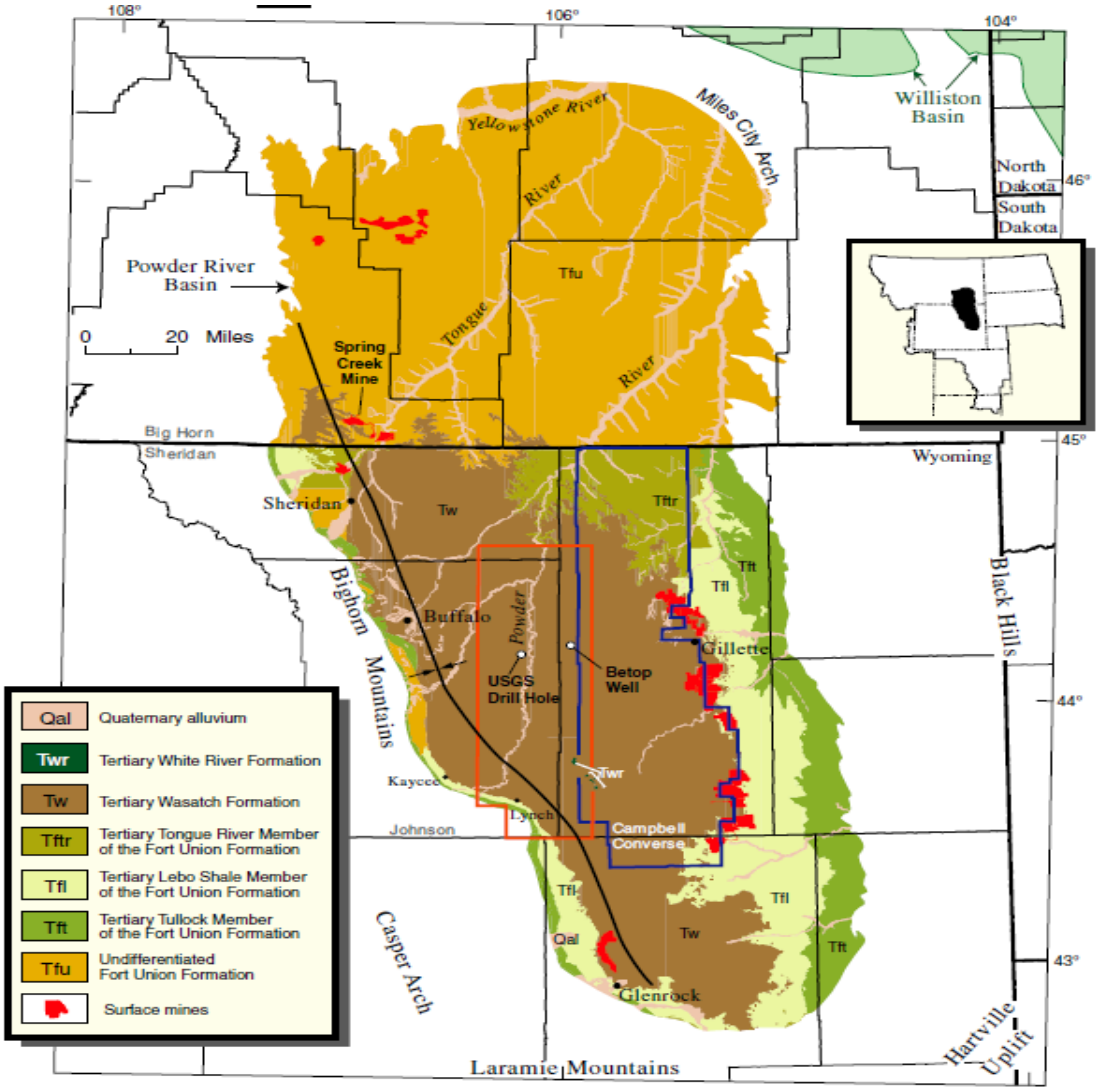


Figure 3. Map of the PRB and surrounding area.
(Figure from Flores and Bader, 1999).

The Fort Union Formation is stratigraphically situated between the overlying Wasatch Formation and the underlying Lance Formation (Flores and Bader, 1999) as displayed in Figure 4. The Fort Union Formation is often assigned a Paleocene age and the Wasatch Formation an Eocene age, but the exact position of this age boundary is debated (Flores and Bader, 1999). The Fort Union Formation was deposited in a fluvial environment undergoing processes of avulsion (Flores and Bader, 1999). This caused a

high degree of vertical variability of the coal beds and abundant splits and merges (Flores and Bader, 1999).

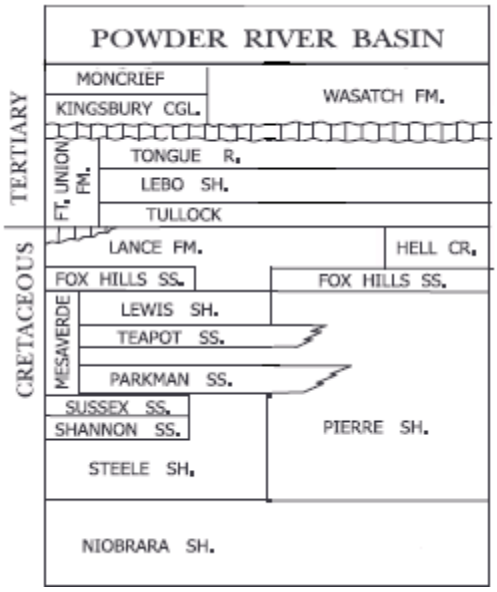


Figure 4. Partial stratigraphic column of the Powder River basin, including the Fort Union Formation. Modified from Flores (2004).

The Fort Union Formation is comprised of the Tullock Member overlain by the Lebo overlain by the Tongue River Member (Roberts et al., 1999a). The Tullock Member contains weathered sandstone beds with some coal beds of varying thickness (Flores and Bader, 1999). The Lebo Member contains abundant mudstone and weathered sandstone but little coal (Flores and Bader, 1999). The Tongue River Member contains mudstone (Flores and Bader, 1999) and hosts the most and thickest coal beds of the Formation (Flores et al., 1999).

Coal of the Tongue River Member is mostly low ash, low sulfur, and of subbituminous rank (Hildebrand, 1986). Typical coal beds of the Tongue River Formation are 6 – 9 m thick, with thicker beds towards the top of the member (Flores et al., 1999). The upper part of the Tongue River Member is the Anderson-Canyon coal

zone, which includes the Anderson, Dietz 2, Dietz 3, Kirby, Cox and Canyon coal beds (Roberts et al., 1999a). The lower part of the Tongue River Member is the Rosebud-Robinson coal zone, which contains the Robinson coal bed, overlain by the McKay coal bed which is, in turn overlain by the Rosebud coal bed (Ellis et al., 1999). The Rosebud-Robinson coal zone is estimated to reach 110 m thick within the Colstrip Coalfield (Ellis et al., 1999).

More detailed geochemical and mineralogical data on these localities is lacking. The next sections outline what additional information is sought, methods used, and significance of the information.

Goals

The goal of this study is to characterize the geochemistry and mineralogy of naturally occurring coal found in the PRB of Montana. Specific questions that are addressed in this study include:

1.) What elements are present? A primary outcome of this study is an inventory of major and trace elements that are present in coal from the PRB in Montana.

2.) What is the distribution of these elements in PRB coal; do these elements occur as a dispersed component of the coal, or are they preferentially accumulated either in or on minerals present in the coal?

3.) What is the mineralogy of these coal deposits, and what is the role of mineral phases in controlling elemental distribution? What is the variation of composition of mineral phases in PRB coals?

4.) What functional forms of nitrogen and sulfur are present, and how much occurs of each type?

5.) How do the geochemistry and mineralogy of these coals compare in different sites within a mine, and at different mines? How does the geochemistry and mineralogy of these coals compare with other coal deposits?

Objectives

Numerous independent analytical techniques have been used in this study to characterize the geochemistry and mineralogy of Montana coal. These techniques have been used for phase identification, geochemical analysis of major and trace elements, and determination of the occurrence and distribution of these elements in coal. The methods used in this study are bulk analysis of major and trace elements using instrumental neutron activation analysis (INAA); mineral phase identification using X-ray powder diffraction (XRD); characterization of size, morphology, and texture of coal samples using scanning electron microscopy (SEM); phase discrimination using backscattered electron imaging (BSE); elemental analysis of mineral phases using energy dispersive spectrometry (EDS); elemental surveys and characterization of molecular ions and chemical state using X-ray photoelectron spectroscopy (XPS), and time of flight secondary ion mass spectroscopy (ToF-SIMS). These complementary methods provide a comprehensive geochemical and mineralogical characterization of these coal samples.

Rational

This work characterizes coal samples from the Absaloka, Rosebud, and Decker mines. It is important to characterize concentrations, distribution and forms of elements and overall coal structure (Kizilshtein and Kholodkov, 1999; Nabeel, 2000). This work needs to be done on a small scale (Kizilshtein and Kholodkov) as is done here. In particular focus is paid to nitrogen, sulfur and potentially toxic metals described in later sections.

This study characterizes coal of Absaloka, Decker, and Rosebud Mines, and the results may be utilized in forming mine operation decisions. Additionally it allows for more formal comparison between Montana coals with coal globally. Before developing the narrative of geochemistry and mineralogy of Montana coal mines it is important to step back and review coal.

General Coal Information

Coal is a fossil fuel, meaning it is a nonrenewable energy source formed by decomposition of organic matter to hydrocarbons (Kotz et al., 2006). The energy output depends on the carbon to hydrogen ratio; lower ratios result in greater energy output (Kotz et al., 2006). The energy output from coal is heat, and coals are classified according to heat potential (Kotz et al., 2006). Heat content of anthracite coal also known as hard coal is 36 to 37 kJ/g, for bituminous coal also known as soft coal heat content is 29 to 37 kJ/g, and for lignite also known as brown coal it is 28 to 30 kJ/g (Kotz et al., 2006). Therefore, in going from lignite to anthracite the productivity of burning increases, however, anthracite coal is uncommon so bituminous coal is commonly used

(Kotz et al., 2006). An additional advantage of bituminous coal is that its softness makes for easier pulverization, as required for modern commercial boilers (Thomas, 2002).

Processes of coal combustion cause concentrations of different element species in the various products (Gong et al., 1999). Pyrolysis is the first stage of coal combustion (Stanczyk, 2004), whereby heat induces breakdown of internal organic structure (Williams et al., 2000). Pyrolysis causes devolatilization (Williams et al., 2000), which is the removal of vaporizable material (Speight, 2005). Char, gaseous tars, and combustible gases form and sequentially burn (Williams et al., 2000). Char burns slow leaving behind ash (Williams et al., 2000), the noncombustible remnants of complete coal combustion (Speight, 2005).

Coal is a very heterogeneous substance (Fyfe et al., 1982), made up of organic and inorganic compounds (Thomas, 2002). The organic portion consists of compounds known as macerals (Weitzsacker and Gardella, 1992). Vitrinite, liptinite, and inertinite are the three types of macerals, though further subdivisions are also recognized (Weitzsacker and Gardella, 1992). The inorganic portion, also referred to as mineral matter, includes ash content as well as water and oxides eliminated during combustion (Thomas, 2002). Degree of association with organics, and thereby ease of separation, is the basis for classification of mineral matter (Speight, 2005). Inherent mineral matter is closely associated with organics, whereas adventitious mineral matter is more easily removed (Speight, 2005). The term impure describes coals with a high mineral content (Thomas, 2002). These minerals may reside in distinct bands or be dispersed throughout the coal (Thomas, 2002). Fractures, known as cleats, commonly provide accommodation

space for mineral precipitates including carbonates and sulphides (Thomas, 2002). Mineral accumulations also may occur as veins within the coal (Thomas, 2002).

On average, clay minerals constitute 60 - 80 % of the mineral content of coal (Thomas, 2002). Different clay mineral compositions are typical of different depositional environments (Thomas, 2002). Illite and kaolinite tend to dominant marine and non-marine influenced coals, respectively (Thomas, 2002). The clay mineral assemblage also correlates with coal rank (Ward and Christie, 1994). Increased pressure and temperature can cause alteration to secondary clay minerals such as chlorite (Thomas, 2002). With the introduction of water, clay minerals swell which can weaken surrounding rock (Thomas, 2002). Therefore, structural danger associated with coal mines in high clay areas is recognized (Thomas, 2002). Additionally, since clays hold onto water, they can interfere with both draining and dewatering of coal mines (Thomas, 2002).

The variations in coal composition reflect variations in precursor peat. Peat, plant matter that has undergone some carbonization (Speight, 2005), may reveal information on the character and distribution of coal beds (Cameron et al., 1989). However, this depends on the major simplifying assumption that early stages present today are similar to previous states of late stages present today (Cameron et al., 1989). Still, specifics of coal forming peat beds in general correlate with differently characterized coal deposits (Thomas, 2002). The overall ecosystem, vegetation characteristics, humidity and sediment input of a peat bed determines coal bed dimensions and maceral content (Thomas, 2002). With respect to transport and sequestration of elements transported in ground water,

Composition of Coal

Coal has been studied using a variety of techniques including bulk (atomic absorption spectroscopy, AAS) and surface (XPS) techniques as part of the Argonne Premium Coal Sample Program (APCSP). Elements universally present as determined by XPS for a variety of coals done for the APCSP are carbon, oxygen, nitrogen, aluminum and silicon (Weitzsacker and Gardella, 1992). Sulfur, though commonly detected, is usually present at levels right around the detection limit for XPS (Weitzsacker and Gardella, 1992). Calcium and sodium were sometimes detected (Weitzsacker and Gardella, 1992). Whole rock analysis of coal using AAS on a variety of coals revealed the presence of Al, Ca, Fe, K, Na, Ti, Ba, Be, Cd, Co, Cr, Cu, Li, Mn, Ni, Pb, Sr, V, Y, and Zn (Weitzsacker and Gardella, 1992).

One major element of concern in coal is nitrogen. Coal combustion releases NO_x (Franco and Diaz, 2009) which contributes to human health complications, acid rain, smog, global warming, (Smith, 2005) and depletion of stratospheric ozone (Beer, 2000). Although a vague correlation exists between total nitrogen concentration and NO_x emissions, a good prediction of NOx emissions requires information of modes of occurrence (Kambara et al., 1995). Kambara et al. (1995) propose NOx emissions can be predicted; NOx index = ([QN] + [PdN] + [PrN]/[C]) x [QWPW + PWCI) with [QN], [PdN], [PrN] and [C] standing for quaternary-N, pyridinic-N, and pyrrolic-N. In order of decreasing abundance, organic nitrogen in raw coal is made of pyrrolic, pyridinic, quaternary and amino forms (Kelemen et al., 1998) (Figure 5).

> "In the pyrrolic structure N-5, the sp3- hybridized N atom is connected to one H atom and two C sp2 atoms. In the pyridinic structure N-6, the N atom is connected to two sp2- hybridized C atoms. In quaternary structure

> N-Q, the N atom is situated in a graphen layer and connected to three sp2-hybridized C atoms" (Stanczyk, 2004, p. 405- 406).

Both pyrrolic and pyridinic structures are ring structures, and they have very similar stabilities, though pyridinic structures are slightly more stable (Stanczyk, 2004). Review of the literature does not reveal significance of pyrrolic versus pyridinic structure; however, determination of the different nitrogen functionalities is a well established procedure and future work may reveal significance of different proportions of the forms.

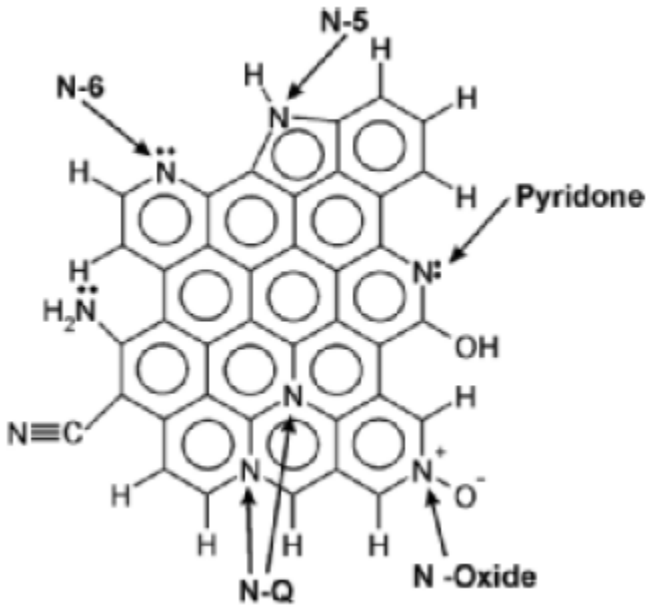


Figure 5. Representation of nitrogen functionalities (Fletcher et al., 2008).

Another element of concern is sulfur. Overall, PRB coal is low in sulfur, a main reason it is of high demand (Considine, 2009). Sulfur in coal occurs in many states including organic sulfur, pyritic sulfur, and sulphate minerals (Thomas, 2002). Sulfur is undesirable because of pollution and corrosion issues (Thomas, 2002). Sixty percent of SO_2 emission in the United States is attributable to burning coal (Kotz et al., 2006). A study of coal ashes from subbituminous and bituminous coal from Canadian power plants

reveals feed coals with higher sulfur concentrations tend to produce fly ashes with greater levels of chalcophile elements such as As, Cd, Hg, Mo, Ni, and Pb (Goodarzi, 2006). Additionally, the fly ashes of higher sulfur coals tend to have higher concentrations of iron-bearing minerals (Goodarzi, 2006), and for coal of the Krepoljin Brown Coal basin (East Serbia), a positive correlation is noted between availability of sulphates and pyritization of Fe (Devic and Pfendt, 2007).

A third undesirable element in coal is sodium. Sodium leaves behind an undesirable residue in boilers after coal combustion (Chadwick and Domazetis, 1995). Unfortunately, high sodium levels are an issue with Montana coal (Kunce et al., 2004). Sodium levels for coal in the northwestern PRB are typically greater than 0.2 weight percent; variations directly correlate with local ground water chemistry (Hildebrand, 1986).

Additionally, coal concentrates many trace elements that are potentially hazardous (Figure 6). As, Be, Cd, Hg, Mn, Ni, Pb, Sb, Se, and U are all elements found in coal which are recognized as hazardous air pollutants under the 1990 Clean Air Act (Finkelman, 1994). Additionally Th, not noted on the table, deserves attention since it is a natural radionuclide (Kizilshtein and Kholodkov, 1999). While it is fundamental that hazardous elements mobilized during coal combustion are problematic, the specifics including maximum acceptable levels are not clear (NRC, 1980).

A study based on ten coal samples from the United States found B, S, Ni, Zn, Ga, Ge, Sr, Y, Mo, Sn, Sb, I, Ba, Pr, Nd, Sm, Eu, Ho, Pt, Hf, Pt, Hg, Pb, Tl, Bi, and U in greater concentrations than for the earth's crust overall (Kronberg et al., 1981). Ba and Sr are particularly abundant in these coals, with concentrations existing sometimes in excess

of one tenth of a weight percent (Kronberg et al., 1981). Meanwhile Cl, V, Cr, Br, and Rb were found in greater concentrations in the crust overall than in these coals (Kronberg et al., 1981). Elements such as Cu, Ni, Cd, Hg, and Ag, are coal waste products either beneficial if recycled or detrimental if dispersed into the environment (Finkelman, 1997).

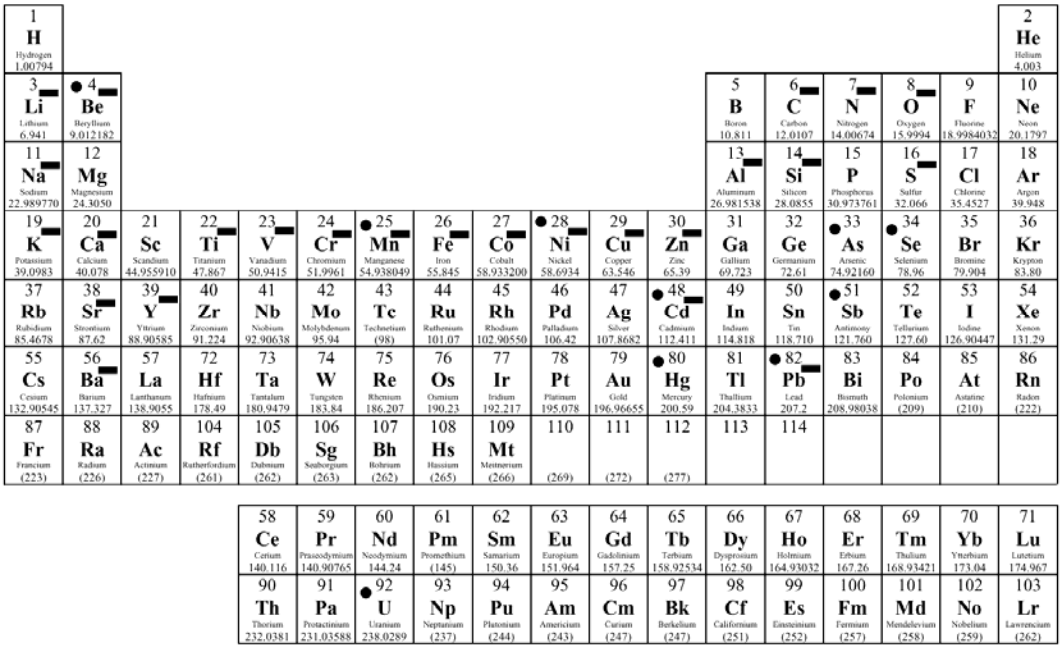


Figure 6. Periodic table showing hazardous air pollutants found in coal denoted by circles and elements routinely found in coal in general by rectangles.

Although remarkable similarity persists between trace elements concentrations of coals of different regions (Kronberg et al., 1981), trace element concentration also varies considerably between coal fields (Kizilshtein and Kholodkov, 1999). Similarly, variation exists for trace element distribution between organic and inorganic phases, which determines the final form of release of the element (Kizilshtein and Kholodkov, 1999).

CHAPTER 2

ANALYSIS AND RESULTS

The bulk composition of these coals was measured, particularly for trace elements, using INAA. The mineral content of these coals for bulk samples was determined by XRD, and the more detailed morphology, size and distribution of minerals was determined using SEM and BSE imaging, and composition of the minerals was determined using EDS. The final two techniques, XPS followed by ToF-SIMS, are surface analysis techniques, with angstrom scale depths of analysis. Whereas SEM work mostly focuses on elements located in mineral phases, XPS analysis is mostly focused on surface elements located throughout the carbon matrix. XPS results include surveys of elements distributed in the coal and additional information on the bond state of polyvalent elements (e.g. N, S). ToF-SIMS also generates surveys of elements and molecular compounds, and also produces micro-scale imaging of the distribution of elements on the surface of the coal.

CHAPTER 3

INSTRUMENTAL NEUTRON ACTIVATION ANALYSIS (INAA)

Instrumental neutron activation analysis, INAA, determines elemental concentrations in bulk samples (Eby, 2007). It works by subjecting the sample to a neutron flux, causing many elements to produce radioactive nuclides (Eby, 2007). When the radioactive nuclides decay, gamma rays are emitted (Eby, 2007). The energies of the gamma rays are characteristic of the elements, and by comparing to standards the amounts of different elements present are quantified (Eby, 2007). The elements determinable by INAA are limited based on how different elements react to neutron fluxes (Eby, 2007).

INAA was done to determine the concentration of the following elements in each of the eleven samples: Fe, Na, K, Sc, Cr, Co, Ni, Zn, Rb, Cs, Sr, Ba, La, Ce, Nd, Sm, Eu, Gd, Tb, Ho, Tm, Yb, Lu, Zr, Hf, Ta, Th, U, As, Sb, W, Ag, Ir, and Se. Representative samples were selected for analysis from 11 samples of PRB coals. These samples avoided coal that included visible ash layers or sulfide concentrations. The coals samples were ground to a fine powder with a mortar and pestle. Analysis was performed by Nelson Eby from University of Massachetts Lowell and details on the analytical methods are provided in Appendix A. The full INAA dataset is presented in Table 2.

Table 2. INAA Dataset.

	RB1	RB1	RB2	RBU	RB CELP	D low Na 1%	D low Na 8%	Ab1	Ab2	Ab2	Ab3a	Ab3b	Ab4
Fe	291[2]	337	445	1133	4179	1172	1448	2464	3221	3260	2150	148780	781
Na	1	1	349	75	90	553	3195	916	843	860	911	187	558
K	nd[3]	nd	140	169	414	195	nd	nd	nd	7	nd	nd	nd
Sc	0.68	0.69	0.85	2.36	7.16	0.61	0.55	0.81	1.04	1.04	0.88	3.23	1.29
Cr	1.13	1.18	2.36	7.20	13.13	0.92	0.54	2.93	3.72	3.67	3.61	14.43	3.92
Co	0.56	0.56	0.42	0.34	0.69	0.55	0.45	0.97	0.87	0.88	1.04	0.55	1.02
Ni	1.5	1.4	nd	nd	8.0	nd	nd	2.5	4.2	3.8	4.0	nd	3.4
Zn	1.4	1.5	1.5	2.1	11.6	0.9	0.9	2.0	1.8	2.0	2.1	2.3	1.9
Rb	nd	0.1	0.2	nd	0.6	nd	nd	nd	nd	0.2	nd	7.5	0.6
Cs	nd	0.01	0.01	nd	nd	0.03	0.04	nd	nd	0.01	nd	nd	0.12
Sr	137	136	228	172	69	171	164	456	498	499	498	128	389
Ba	14.5	14.4	46.0	70.1	114.7	227.9	57.8	74.8	106.4	105.6	100.1	133.9	43.6
La	0.40	0.41	6.07	7.79	9.25	1.39	0.05	4.53	6.53	6.63	7.17	9.20	7.30
Ce	6.11	6.13	6.56	15.40	18.36	2.19	0.12	7.80	9.81	10.08	11.32	16.86	12.69
Nd	2.22	2.15	1.91	6.66	8.72	0.98	0.10	2.84	2.90	2.90	3.66	7.02	4.48
Sm	0.08	0.08	0.33	1.60	2.00	0.12	0.13	0.49	0.55	0.54	0.64	1.60	0.84
Eu	0.096	0.098	0.072	0.406	0.571	0.036	0.038	0.108	0.123	0.125	0.134	0.462	0.174
Gd	0.43	0.45	0.31	1.62	2.66	0.15	0.20	0.53	0.62	0.55	0.66	2.81	0.90
Tb	0.071	0.070	0.052	0.368	0.555	0.022	0.028	0.071	0.085	0.088	0.087	0.418	0.120
Ho	0.09	0.09	0.07	0.39	0.64	0.03	0.03	0.09	0.09	0.10	0.09	0.51	0.12
Tm	0.027	0.026	0.022	0.156	0.276	0.010	0.011	0.030	0.035	0.037	0.034	0.218	0.047
Yb	0.137	0.139	0.141	1.189	2.179	0.066	0.076	0.187	0.252	0.260	0.221	1.954	0.334
Lu	0.016	0.017	0.022	0.185	0.354	0.011	0.011	0.030	0.035	0.038	0.032	0.330	0.050
Zr	26	26	26	84	234	10	7	14	33	26	23	224	33
Hf	0.41	0.42	0.45	2.01	4.49	0.21	0.07	0.41	0.53	0.54	0.40	5.71	0.82
Ta	0.049	0.050	0.088	0.280	0.569	0.030	0.010	0.047	0.075	0.075	0.054	0.835	0.107
Th	0.89	0.89	0.84	3.98	6.99	0.25	0.10	0.78	1.15	1.14	0.91	4.85	2.28
U	0.316	0.321	0.883	1.496	5.357	0.147	0.103	0.478	0.662	0.641	0.639	2.464	0.847
As	0.02	0.02	0.54	3.28	4.98	0.10	0.08	0.80	0.98	0.98	0.91	5.81	0.90
Sb	0.52	0.54	0.36	0.72	1.76	0.06	0.03	0.23	0.31	0.31	0.22	4.84	0.25
W	0.02	0.02	0.98	0.38	1.14	0.05	0.11	0.45	0.25	0.22	0.34	2.49	0.28
Ag	nd	nd	nd	nd	nd	nd	nd	nd	0.07	0.08	nd	0.14	nd
Ir	nd	nd	587	1076	1994	nd	nd	nd	nd	300	407	945	nd
Se	0.45	0.47	0.24	1.15	1.73	0.11	0.19	0.58	0.63	0.63	0.51	2.88	0.39

[1]Data from Nelson Eby
[2]All in ppm, except it is ppb for Ir
[3]nd = not determined

Large ion lithophile (LILE) and light rare earth elements (LREE) in PBR coal as measured by INAA (Figure 7) display no consistent pattern of enrichment; though a subset of the group, La and Ce, do display a similar pattern of enrichment. High field strength elements (HFSE) and middle to heavy REE PBR coal as measured by INAA

(Figure 8) are enriched in Ab 3b, RB Upper and RB CLEP. These elements are typically immobile in ground water (except for U and Th) and therefore more likely reflect detrital concentration than secondary concentration processes. These elements mostly occur in trace minerals (e.g. zircon and titanite). Transition metals, chalcophile elements, and platinum group element, Ir, in PBR coal as measured by INAA (Figure 9) show a weak pattern of enrichment at either Ab 3b or RB CLEP; their enrichment pattern may be seen as an intermediate between the LILE and LREE (no enrichment pattern) and the HFSE and middle to heavy REE (enriched at Ab 3b, RB Upper, and RB CLEP). The most similar enrichment patterns are seen for the pairing of Sc and Ir and for the grouping of Sb, As, and Se.

These patterns are presented below in bar graphs. The column labeled average refers to the average of samples of this study. The column labeled SRM 1635 is an INAA analysis of a reference sample subbituminous coal prepared by the National Institute of Standards and Technology, USA (Suzuki and Hirai, 1992). To differentiate between elements present in very low amounts and elements for which no data is recorded, reference must be made to the INAA dataset above for this study or to “Multielement Analysis of Environmental Reference Materials by Instrumental Neutron Activation” (Suzuki and Hirai, 1992) for SRM 1635.

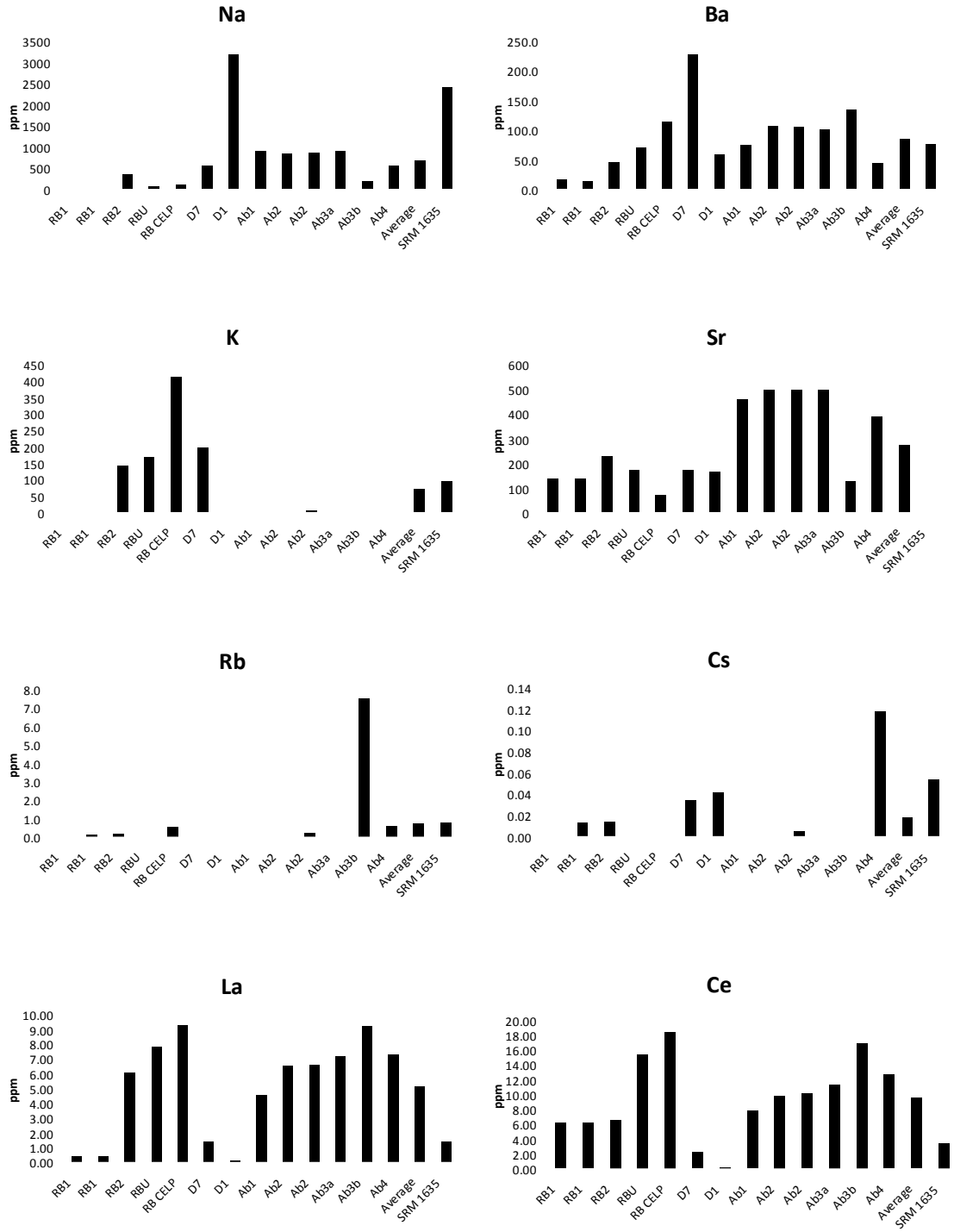


Figure 7. LILE and LREE concentrations as determined by INAA.

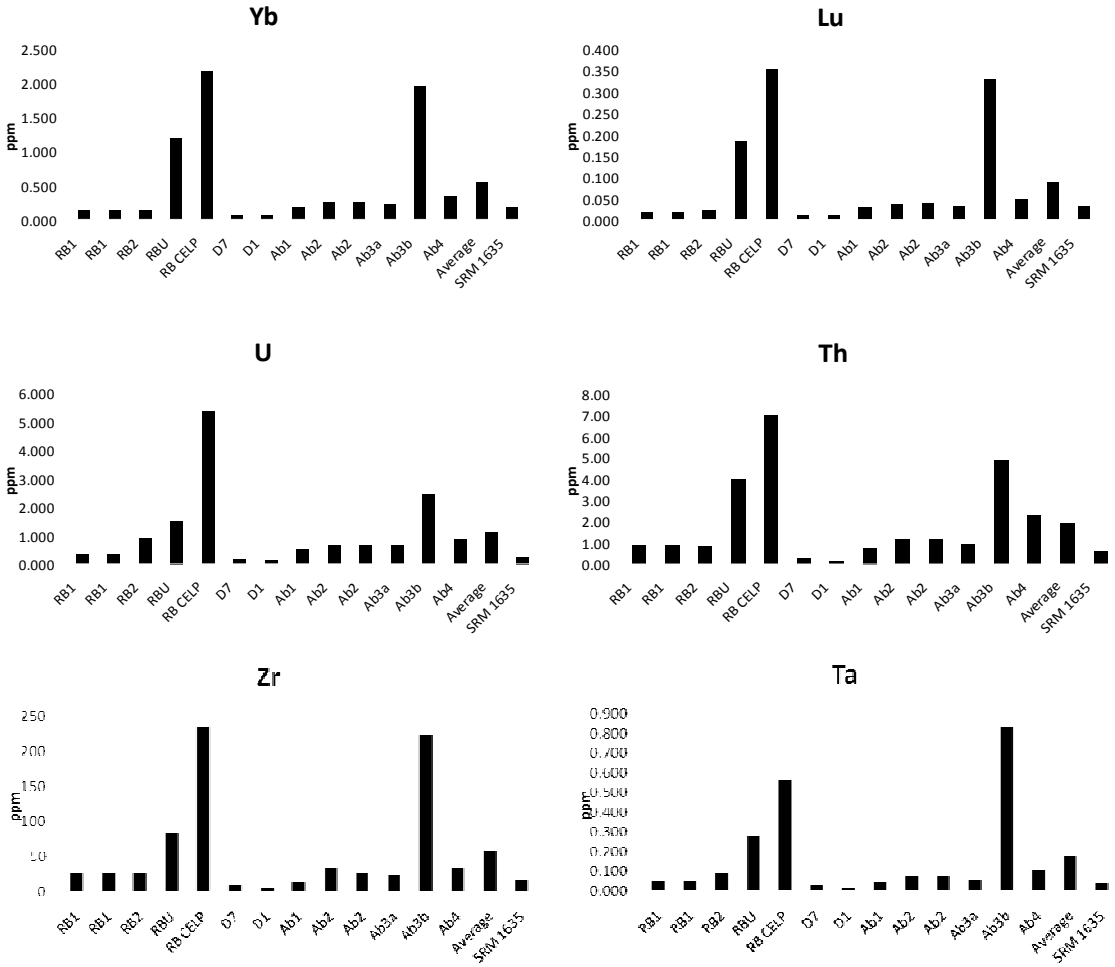


Figure 8. HFSE and middle to heavy REE concentrations as determined by INAA.

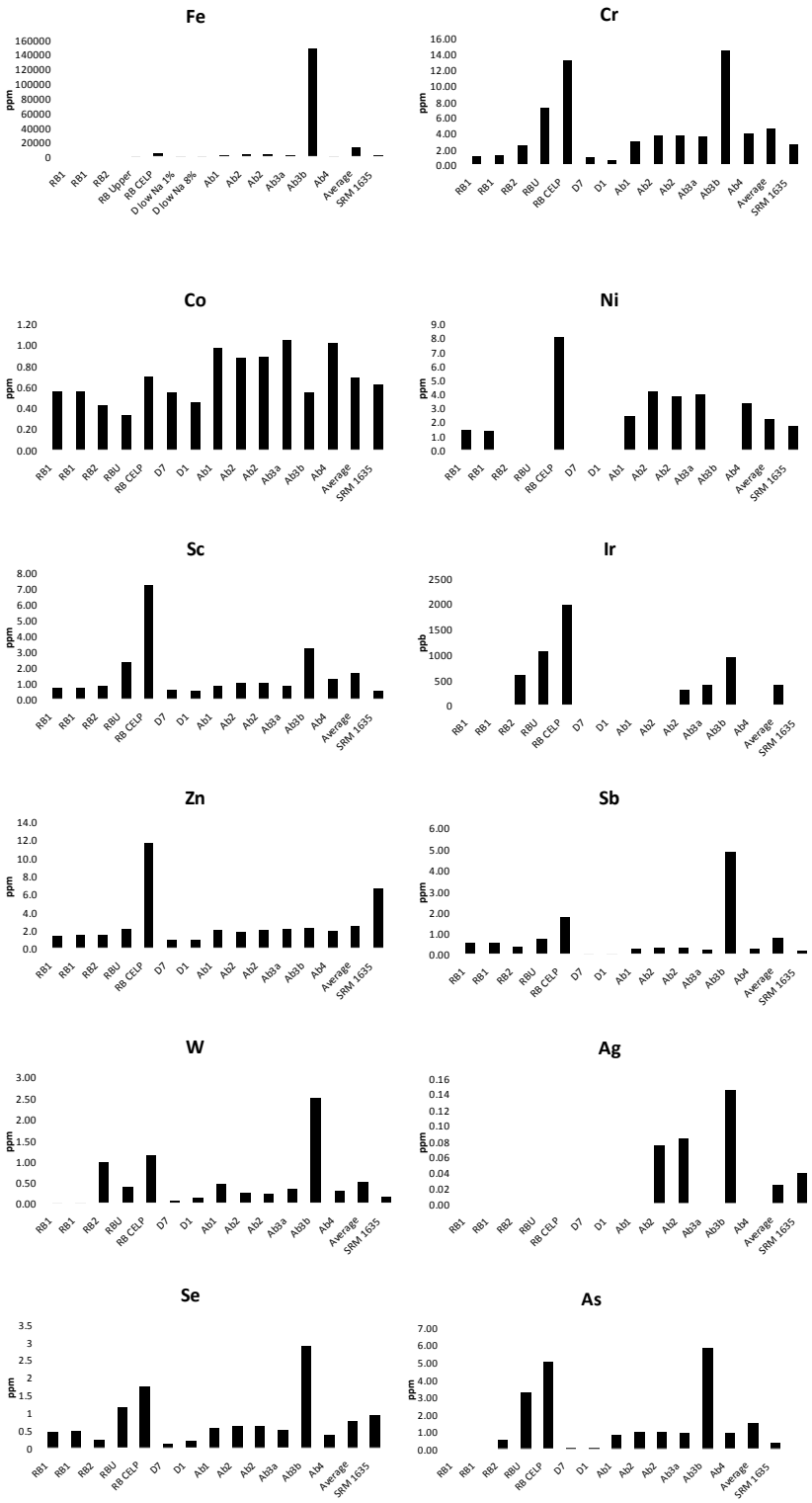


Figure 9. Transition metals, chalcophile elements, and a platinum group element (Ir) as determined by INAA.

Chondrite-normalized rare earth element diagrams are plotted in Figures 11-13 using the normalization values of Nakamura (1974). Overall, the samples are LREE enriched (ranging from 0.15 to 28.04 La_n) and have negative europium anomalies. The degree of LREE enrichment is illustrated in Figure 10 which shows the La_n/Yb_n ratio for all samples. These REE patterns are characteristic of a granitic source area. However, total REE abundances are lower than expected for granitic rocks (Cullers and Graf, 1984) and samples with $La_n/Yb_n < 10$ may indicate mixing with another source material, possibly a more mafic crustal component. Unusual depletion of LREEs is evident at the Decker Mine (La, Ce, Nd), and at the Rosebud Mine (La, Sm).

At Absaloka, all samples except Ab 3b plot nearly identically and are LREE enriched, have a negative europium anomaly and slight HREE depletion. Ab 3b, has less LREE enrichment and slight HREE enrichment. The two Decker sites plot similarly from Sm through Lu; in this range, both display a slight negative europium anomaly, slight LREE enrichment, and insignificant effects with respect to the HREE. However, D low Na 1% displays enrichment in the LREE, whereas, D low Na 8% displays depletion in the LREE; these variations (enrichment and depletion) are more extreme than variations present at other sites in this study. At Rosebud, Rb2, RB Upper, and RB CLEP all display negative europium anomalies and LREE enrichment. However LREE enrichment is distinctly highest for RB 2, and RB 1 is distinctly depleted of La and Sm

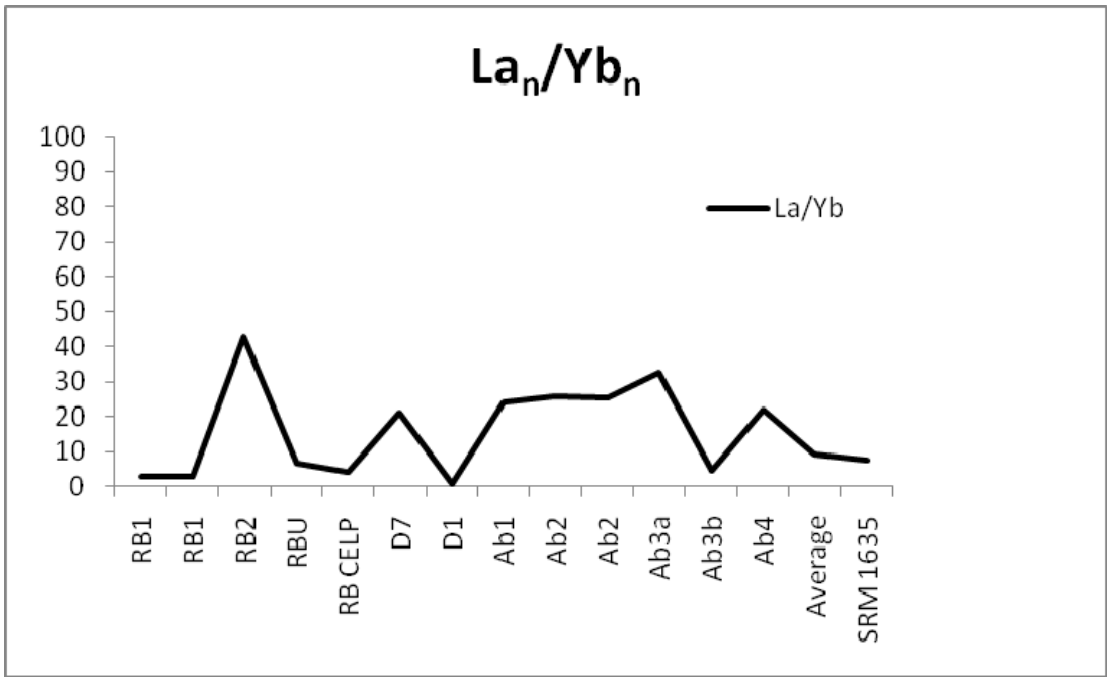


Figure 10. Degree of LREE enrichment shown by the ratio of La_n to Yb_n as determined by INAA.

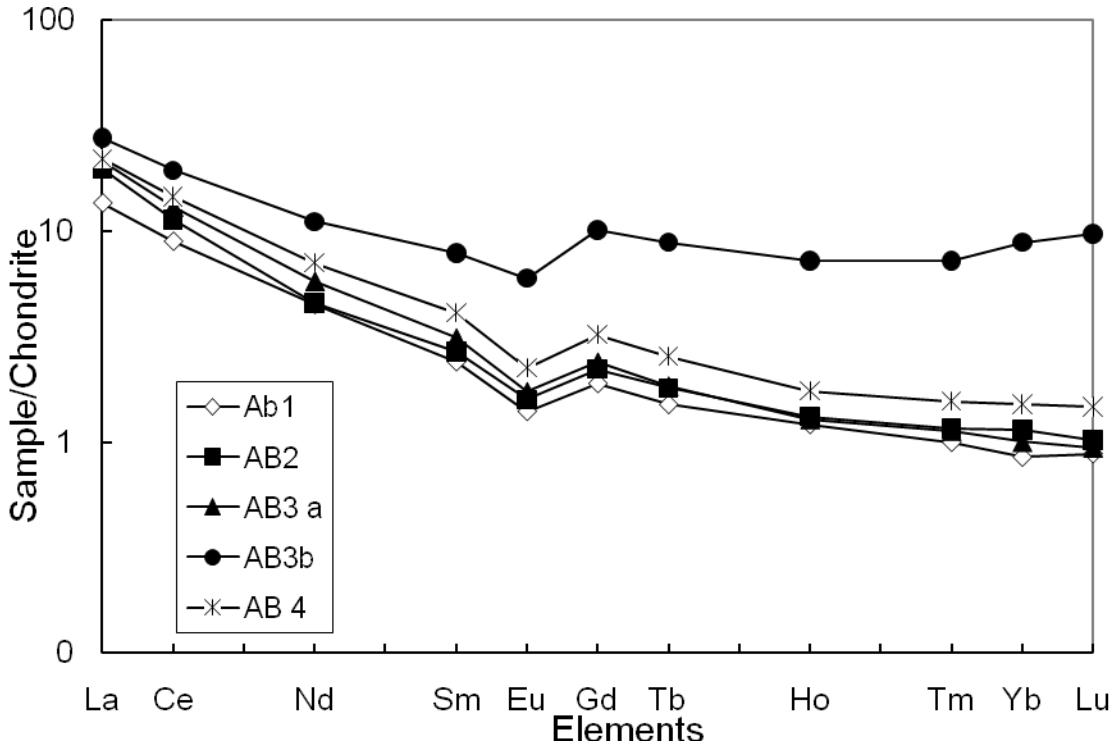


Figure 11. Chondrite-normalized REE diagram for samples from Absaloka mine as determined by INAA.

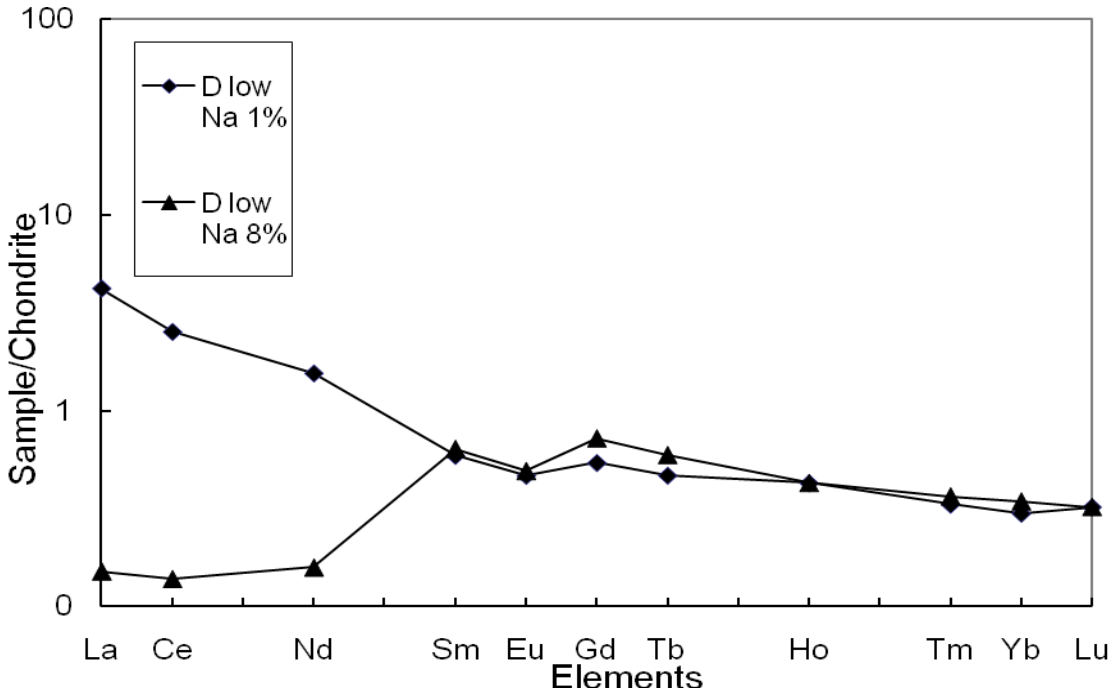


Figure 12. Chondrite-normalized REE diagram for samples from Decker mine as determined by INAA.

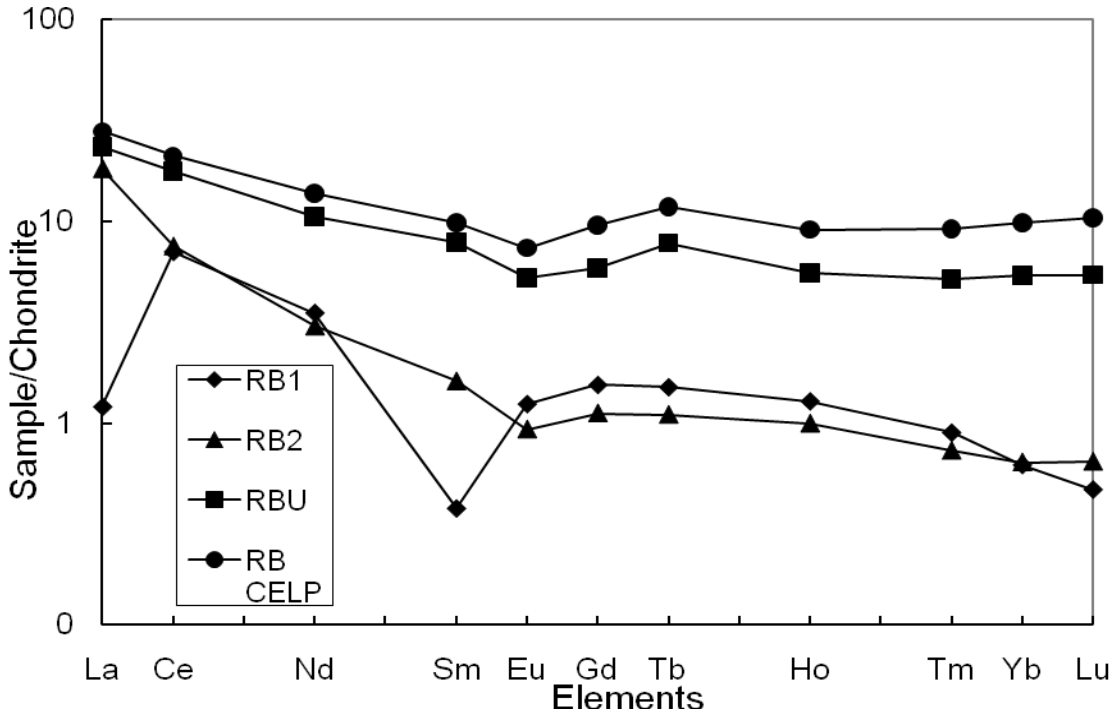


Figure 13. Chondrite-normalized REE diagram for samples from Rosebud mine as determined by INAA.

As, Be, Cd, Hg, Mn, Ni, Pb, Sb, Se, U, (Finkelman, 1994), and Th (Kizilshein and Kholodkov, 1999) have been identified as possible hazardous elements in coal. Of these elements of potential concern, As, Ni, Se, Sb, U, and Th were examined by INAA. A common theme for these is that the lowest concentration of each element is at one of the two Decker samples and highest is at RB CLEP or Ab 3b. The only apparent exception is for the lower end of the Ni range and that is accounted for by the fact that Ni is below detection range for both of the Decker samples. The abundances of these elements in this study are put into a local context in Table 3 comparing this study to Wyoming PRB coal and national average values.

Table 3. Relative Amounts of Potentially Hazardous Elements.

Element (US average)[1]	Range: This study, PRB, Mt Coals	Range: 4 sites, PRB, Wy Coals[2]
As (24[3])	0.02 at RB 1 to 5.81 at Ab 3b	1.0-2.6
Ni (14)	1.40 or 1.50 at RB 1 to 8.0 at RB CLEP	1.0 - 2.6
Se (2.8)	0.11 at D low Na 1% to 2.88 at Ab 3b	0.42 - 0.97
Sb (1.2)	0.03 at D low Na 8% to 4.84 at Ab 3b	0.088 -0.11
U (2.1)	0.10 at D low 8% to 5.38 at RB CLEP	0.27 - 0.58
Th (3.2)	0.10 at D low Na 8% to 6.99 at RB CLEP	0.69 - 1.4

[1]US average based on (Finkelman, 1993)
[2]Wy coals based on (Stricker et al 2007)
[3]Values in ppm

Arsenic and nickel both lie completely below the national average, selenium's upper range limit corresponds to the national average, and for all other elements the national average falls within the range. Overall PRB coal falls below the national average for these potentially hazardous elements. Standards of maximum permissible amounts of different elements in coal have not been established (Wang et al., 2010).

CHAPTER 4

X-RAY POWDER DIFFRACTION (XRD)

Instrumentation

X-ray powder diffraction (XRD) was used to determine mineral content of bulk coal samples (Van Alphen, 2007). XRD is particularly useful for identification of fine grained minerals including discrimination of clay species (Moore and Reynolds, 1997; Poppe et al., 2001). The main advantages of XRD are rapid identification of mineral phases based on their crystalline structures, the relatively mature crystal structure database that is used to compare X-ray diffraction spectra of unknown minerals (DDView, 2005) and relative ease of sample preparation. Detection limits are on the order of 1 wt% of a mineral in the sample matrix. However, XRD has many limitations: background noise from the amorphous materials (such as coal) can mask crystalline peaks (Van Alphen, 2007); and XRD cannot determine mineral sizes, mineral associations, or particle characteristics (Van Alphen, 2007; these properties have been examined using SEM/EDS methods, and will be discussed in the next chapter). A combination of XRD analysis to determine crystal structures, and SEM/EDS imaging and analysis to determine morphological and compositional information provides complementary data that have been used to identify minerals present in the PRB coal.

Sample Preparation

Powders of ash samples were isolated from each of the eleven samples. Residual organics were minimized by allowing each sample to react with hydrogen peroxide. The

dissolved ash was applied to a glass slide and allowed to dry. Random grain mounts were made by preparing a slurry in alcohol, dropping the slurry on a glass slide, and allowing it to air dry. (Moore and Reynolds, 1997)

Experimental Conditions

XRD analysis were preformed with an X1 Advanced Diffraction System by Scintag Inc. All experiments were run at 2 degrees per minute with a step size of 0.05 degrees in continuous scanning mode.

XRD spectra from the coal samples were compared to standardized mineral structure data of minerals expected to be present using the JCPDF data base and the search/match software function. The minerals that were chosen for the search/match routine are augite, blodite, calcite, diopside, dolomite, feldspars (microcline, orthoclase, sanidine, albite, oligoclase, andesine), gypsum, hornblende, illite, jarosite, kaolinite, marcasite, mirabilite, muscovite, nahcolite, natrojarosite, pyrite, quartz, and trona (specific JCPDF card file numbers are listed in Appendix B).

Analytical Results

Kaolinite is present in all samples, and in both of the Decker samples it is the only mineral identified. Variably present at Absaloka and/or Rosebud are other silicates (quartz, illite), carbonates (calcite and dolomite), a sulfate (gypsum) and a sulfide (pyrite). Illite and quartz are the two next most common minerals and they appear to be associated with each other at both Absaloka and Rosebud. The rest of the minerals (

gypsum at Absaloka and the carbonates at Rosebud) occur too rarely for postulating associations.

A display of all spectra from each mine plotted together for each mine is presented in Figures 14 - 16. The highest peak for each mineral is labeled; additional peaks are labeled as needed due to overlapping peaks complicating comparison.

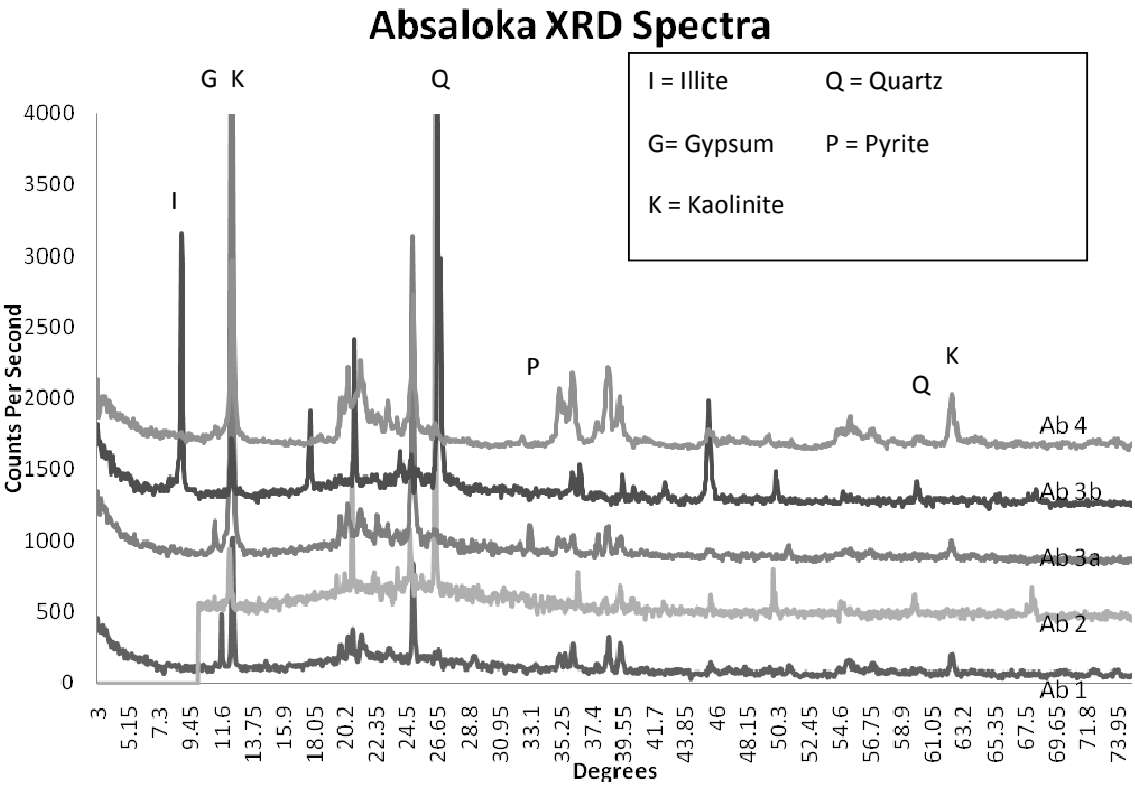


Figure 14. Absaloka coal XRD results.

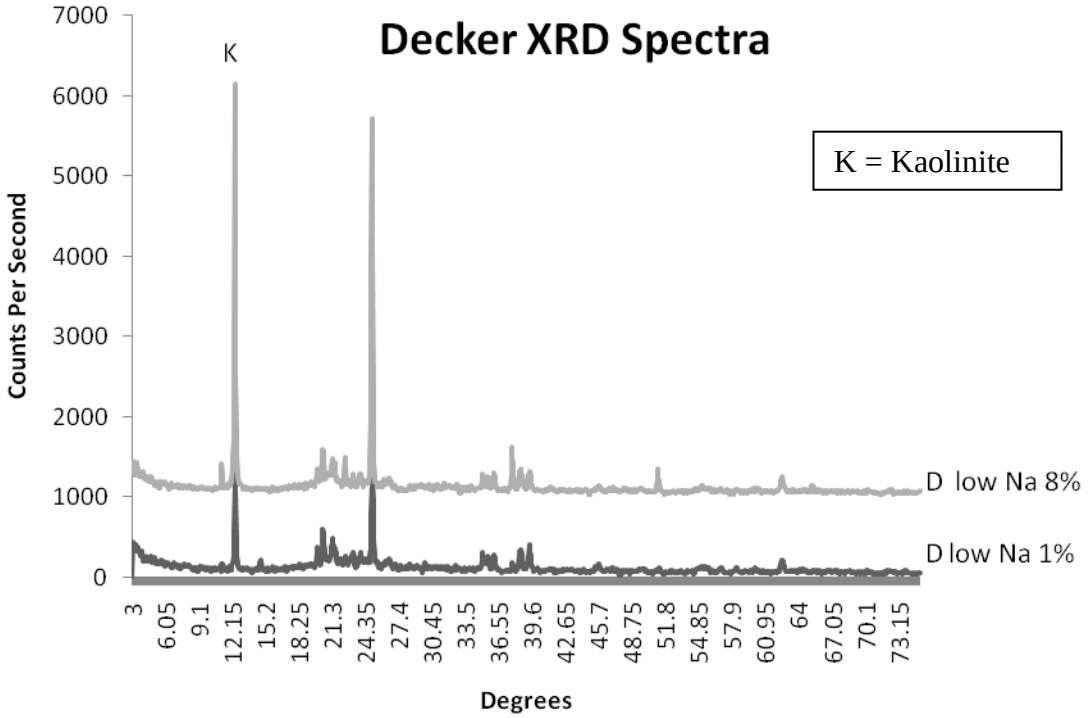


Figure 15. Decker coal XRD results.

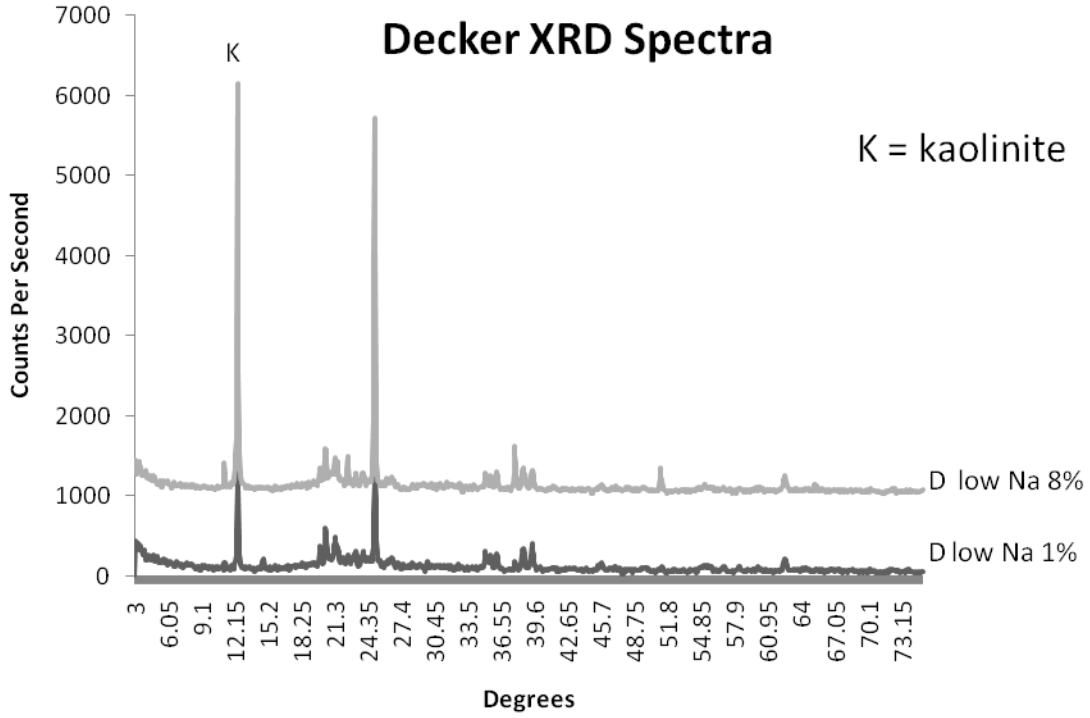


Figure 16. Rosebud coal XRD results.

Table 4. Summary of Minerals Identified in Three Montana Coal Mines (Ab, D, Rb) Using XRD.

	Ab 1	Ab 2	Ab 3a	Ab 3b	Ab 4	D 1 %	D 8%	RB 1	RB 2	RB CLEP	RB Upper
Calcite								x?[1]			
Dolomite								x?			x
Gypsum	x								x		
Kaolinite	x	x	x	x	x	x	x	x	x	x	x
Muscovite				x				x		x	x
Nahcolite									x?		
Pyrite			x							x?	
Quartz	x?	x		x				x			x

[1]Question marks indicate minerals of uncertain identification

Discussion

All the minerals identified in this study have been reported by others from XRD analysis of coals (e.g. Reyes et al., 2003; Matjie et al., 2005). Kaolinite is expected as a major or even exclusive mineral for ash layers in coal (Ward and Christie, 1994). Additionally, XRD results have been confirmed by SEM imaging and EDS elemental analysis (next section).

CHAPTER 5

SCANNING ELECTRON MICROSCOPY (SEM)

Instrumentation

A scanning electron microscopy was used to obtain high resolution images of coal samples. A JEOL-6100 SEM equipped with BSE detector and Noran and Rontec EDS detectors was used in this study. Two imaging modes were used: secondary electron images were obtained to characterize the size, morphology and distribution of mineral grains in the coal samples. Back-scattered electron (BSE) imaging was used to differentiate mineral phases based on differences in mean atomic number (Z) of the phases present (materials with high Z produce more back-scattered electrons, and thus, a brighter image). Energy dispersive X-ray spectrometry (EDS) was used to obtain qualitative elemental analyses of mineral phases. The combination of SEM/BSE imaging of phase morphology and EDS elemental analysis provides the basis for identification of minerals in the coal matrix EDS spectra provide surveys of elements present and their relative abundances; the detection limit is ~0.1% of a weight percent.

Sample Preparation

For each of the eleven samples a few representative coal fragments were selected for imaging and analysis with SEM and EDS. These include a representation of the whole coal typically in the form of cm-sized pieces or powders, and representations of heterogeneities, typically of visible ash and sulfide components. In the following sections the part representative of the whole coal is referred to as the bulk component.

Individual mineral grains (sulfides, silicates, carbonates and sulfates) that were disbursed in the bulk coal or concentrated in layers were selected for elemental analysis.

Pieces and powders were mounted with the use of double sided carbon tape. Additionally, graphite paint was applied to areas not of interest and the samples were coated in gold, both necessary to reduce charging. The samples were semi-flat, but not polished.

Experimental Procedures

SEM images were collected for each piece or powder analyzed to characterize the size and morphology of mineral grains in the coal. Additionally back scattered images (BSE) were collected in compositional mode for phase discrimination. Areas selected for EDS analysis were picked using these images to include all significant grain types in terms of shape and mean atomic number. Care was taken to locate the beam on areas free of visible contaminant particles, and to avoid grain boundaries and microcracks. Images were typically taken over a range of ~50X for overall reconnaissance of textures up to 1500x magnification to characterize ~micron sized textural features. Beam voltage used was between 15 and 20 KV depending on degree of charging, and to provide sufficient energy to produce characteristic x-rays for conducting elemental surveys of the entire periodic table using EDS. A sampling of representational images and spectra are provided in Appendices C and D, and the whole suite of 117 images (SEM and BSE) and 496 EDS spectra are available at ICAL.

Analytical Results

The mineralogy of coal deposits in the Powder River Basin, as determined from SEM imaging and EDS analysis, include: silicate, sulfide, sulfate, and carbonate minerals. It is important to note, however, that EDS spectra are semi-quantitative and identification of minerals is based on relative abundances of elements present and mineral morphology. The excitation volume from which the secondary X-rays emanate is on the order of 3 microns deep, so in many cases EDS spectra may derive from two or more overlapping grains, thus making a definite mineral identification difficult or impossible.

Pyrite is the dominant mineral in sulfide-rich samples. Pyrite occurs as pure pyrite, no arsenic or other replacement minerals are detected with the ~0.1% of a weight percent detection limits. However, other than calcite and ilmenite, all minerals occurring in the bulk and/or ash parts, are also present within the sulfide concentration (quartz, barite, an oxy-hydroxide, and possible illite, sulfur, jarosite, thenardite, and trona). Kaolinite is the dominant ash forming mineral in all the samples. Other minerals occurring in the ash are gypsum, calcite, and dolomite. The following two tables depict minerals present in each sample and whether they occur in the bulk, sulfide-rich layers, or ash-rich layers.

Table 5. Minerals in each Sample Based on SEM Imaging and EDS Elemental Analysis.

	Quartz SiO_2	Kaolinite $Al_2Si_2O_5(OH)_4$	Illite $(K,H_3O)(Al,Mg,Fe)_2(Si,Al)_4O_{10}[(OH)_2,(H_2O)]$	Iron Oxy-hydroxide	Sulfur S
Ab 1		x			
Ab2		x			
Ab3a		x			
Ab3b		x			
Ab4	x	x		x	
D low Na 1%	x	x			x?[1]
D low Na 8%		x			
RB 1		x			
RB 2	x	x			
RB Upper		x			
RB CLEP	x	x	x	x	

	Barite $BaSO_4$	Gypsum $CaSO_4$-2(H_2O)	Jarosite $KFe_3(SO_4)2(OH)_6$	Thenardite Na_2SO_4	Pyrite FeS_2
Ab 1					x
Ab2		x			x
Ab3a		x			x
Ab3b					x
Ab4					x
D low Na 1%	x	x	x?	x?	x
D low Na 8%		x			x
RB 1		x			x
RB 2		x			x
RB Upper		x	x?		x
RB CLEP		x			x

	Calcite $CaCO_3$	Dolomite $CaMg(CO_3)_2$	Trona $Na_3(HCO_3)(CO_3)$ - $2H_2O$	Ilmenite $FeTiO_3$
Ab 1				
Ab2				
Ab3a				
Ab3b	x	x		
Ab4	x			
D low Na 1%			x?	
D low Na 8%			x?	
RB 1	x			x
RB 2	x	x		
RB Upper		x		
RB CLEP				

[1]Question marks indicate minerals of uncertain identification

Table 6. Minerals in each Component Based on SEM/EDS Interpretations.

	Quartz SiO_2	Kaolinite $Al_2Si_2O_5(OH)_4$	Illite $(K,H_3O)(Al,Mg,Fe)_2(Si,Al)_4O_{10}[(OH)_2,(H_2O)]$	Iron Oxy-hydroxide	Sulfur S
Ab 1		x			
Ab2		x			
Ab3a		x			
Ab3b		x			
Ab4	x	x		x	
D low Na 1%	x	x			x?[1]
D low Na 8%		x			
RB 1		x			
RB 2	x	x			
RB Upper		x			
RB CLEP	x	x	x	x	

	Barite $BaSO_4$	Gypsum $CaSO_4$-2(H_2O)	Jarosite $KFe_3(SO_4)2(OH)_6$	Thenardite Na_2SO_4	Pyrite FeS_2
Ab 1					x
Ab2		x			x
Ab3a		x			x
Ab3b					x
Ab4					x
D low Na 1%	x	x	x?	x?	x
D low Na 8%		x			x
RB 1		x			x
RB 2		x			x
RB Upper		x	x?		x
RB CLEP		x			x

	Calcite $CaCO_3$	Dolomite $CaMg(CO_3)_2$	Trona $Na_3(HCO_3)(CO_3)$ - $2H_2O$	Ilmenite $FeTiO_3$
Ab 1				
Ab2				
Ab3a				
Ab3b	x	x		
Ab4	x			
D low Na 1%			x?	
D low Na 8%			x?	
RB 1	x			x
RB 2	x	x		
RB Upper		x		
RB CLEP				

[1]Question marks indicate minerals of uncertain identification

Discussion

SEM imaging and EDS elemental analysis largely served to confirm XRD determinations of the dominant mineralogy in the coal samples. However, SEM/EDS results also are used to identify minerals in trace abundances (<0.1 %) and to further determine the textural relations among the minerals present.

A selection of kaolinite and pyrite images from this study were compared with the literature to interpret significance. Previous work of Alonso- Azcárate et al. (2001) addresses the variation in morphology seen in pyrite of this study. Kaolinite in this study shows less variability of form or habit than pyrite. It is present in ash components at all sites with platy habit (Figure 17).

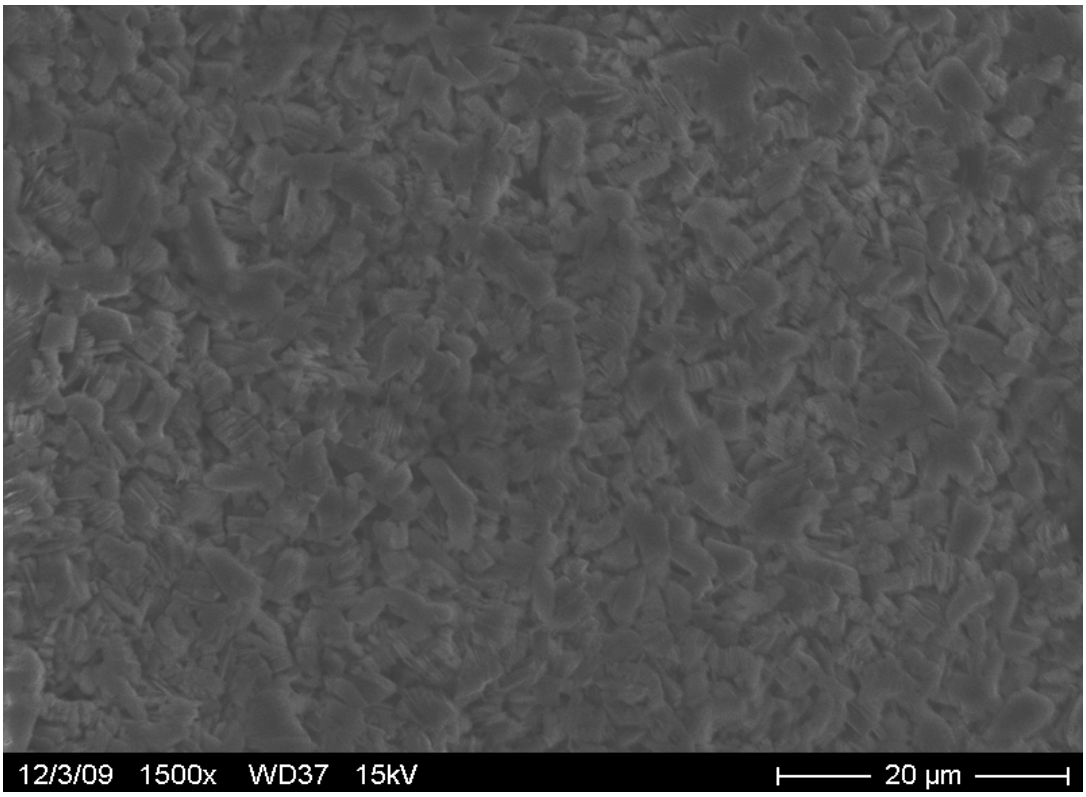


Figure 17. SEM image of kaolinite in an ash rich part of a sample from D low 1% Na.

An interpretation of pyrite images was given by Alonso- Azcárate et al. (2001) based on metasediments of Spain. The large array of pyrite habits were simplified into two groups based on a small number of forms (Alonso-Azcárate et al., 2001). Cubic, platy, or elongate crystals comprise Alonso-Azcárate group one and striated pyritohedron, irregular dodecahedron, striated cubo-pyritohedral, blocky crystals, and fine grained aggregates comprise group two (Alonso-Azcárate et al., 2001). Representative images of each of his groups are shown in his paper.

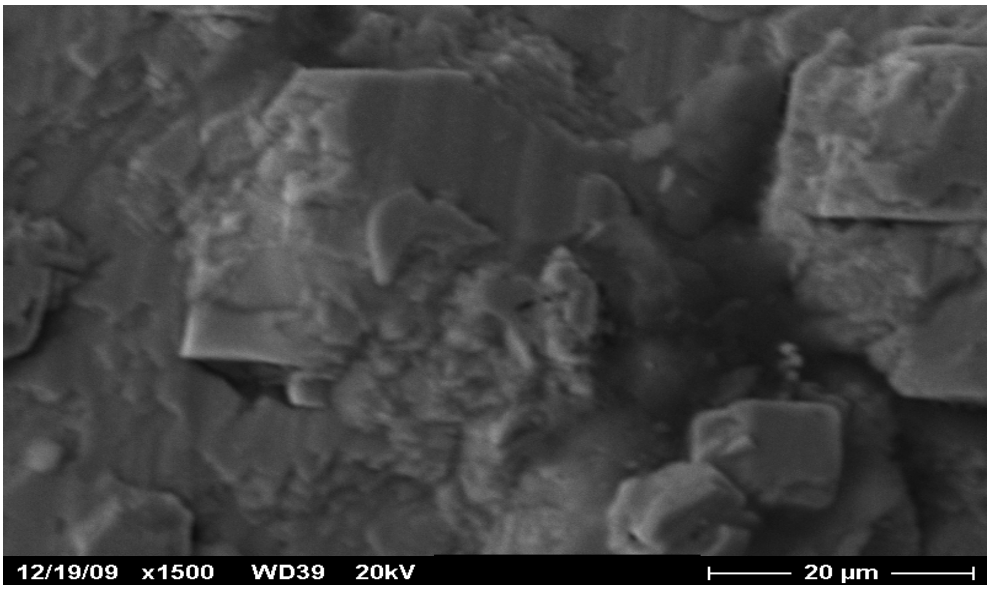
The differences in morphology are based on a continuum of processes that control crystal growth based on nucleation based, surface area rate controlled growth to continuous, diffusion rate controlled crystal formation (Alonso-Azcárate et al., 2001). This in turn is linked to pyrite saturation and/or temperature of formation (Alonso-Azcárate et al., 2001). Group one crystals form during initial nucleation controlled conditions, typically of relatively low temperatures and levels of pyrite saturation (Alonso-Azcárate et al., 2001). Group two includes the later, faster end member of nucleation formation through continuous growth, typically with higher temperatures and higher levels of pyrite saturation (Alonso-Azcárate et al., 2001). Blocky crystals are a specific case in which reactants concentration is distant from crystals favoring the development of outgrowths away from the central crystal resulting in a blocky form (Alonso-Azcárate et al., 2001). Experimentally grown pyrite during late, fast, pyrite saturated stages, also included dendritic pyrite due to conditions similar to those detailed for blocky crystal formation (Murowick and Barnes, 1987).

Samples analyzed from the PRB contain (Table 7) an even distribution from Alonso-Azcárate group 1 (cubic) through dendritic crystal forms. Only the fine grained

aggregate form is not present. Figure 18 shows two examples of pyrite crystal forms, one with cubo-pyritohedra form and one with dendritic habit.

Pyrite in this study displays formation from nucleation controlled through continuous growth (Alonso-Azcárate et al., 2001 and Murowick and Barnes, 1987). The presence of blocky and dendritic pyrite, paired with the absence of fine grained aggregates indicates that during the final stages of pyrite formation the reactants are concentrated a distance from the crystals (Alonso-Azcárate et al., 2001 and Murowick and Barnes, 1987).

In addition to increasing understanding of pyrite development, characterizing pyrite form is significant with respect to potential environmental hazards (Diehl et al., 2005). Pyrite in forms with greater surface area, such as blocky and dendritic forms found in this study, weather quicker and are of greater environmental concern (Diehl et al., 2005). This is especially true if hazardous elements are associated with the pyrite as will be discussed in upcoming sections with regards to this study.



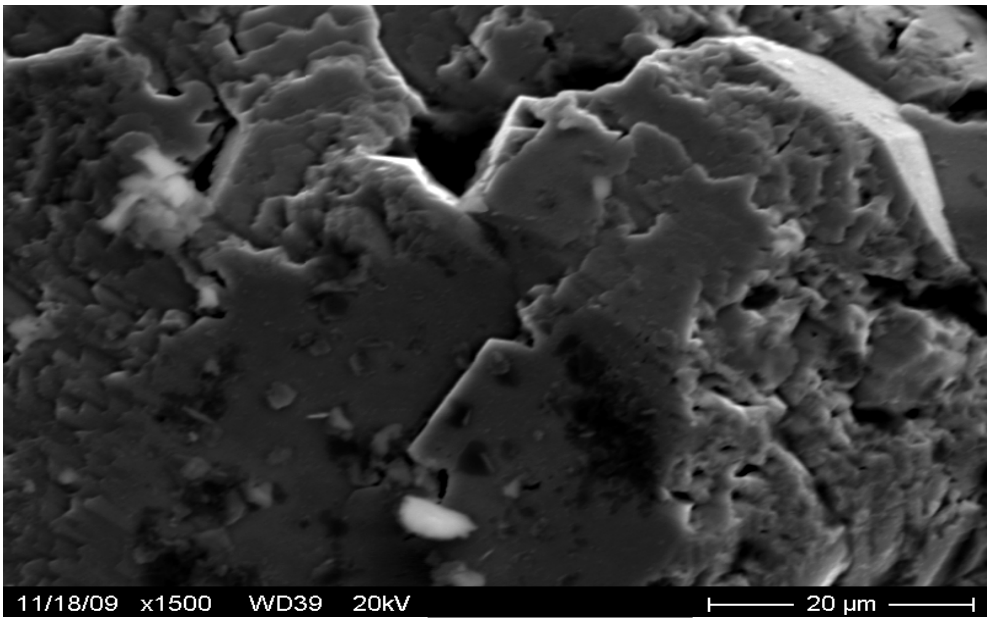


Figure 18. SEM images of cubo-pyritohedra pyrite from a sulfide rich piece from Ab 1 (top) and dendritic pyrite from a sulfide rich piece from Ab 2 (bottom)..

Table 7. Classification of Pyrite in this Study According to Alonso-Azcárate et al. (2001) and Murowick and Barnes (1987).

	Alonso-Azcárate Group 1	Pyritohedra and cubo-pyritohedra	Blocky	Dendritic	Fine grained aggregate
Ab 1		x			
Ab2				x	
Ab3a	x				
Ab3b		x			
Ab4			x		
D low Na 1%		x			
D low Na 8%				x	
RB 1	x				
RB 2	x				
RB Upper			x		
RB CLEP	x				

CHAPTER 6

X-RAY PHOTOELECTRON SPECTROSCOPY (XPS)

Instrumentation

X-ray photoelectron Spectroscopy (XPS) was used to a) produce a survey of elements present, and b) determine the chemical (valence) state of selected elements using a multiplex routine. The principles of XPS analysis have been reviewed by Hochella (1988). In brief, a) XPS is a surface-sensitive spectroscopy, with photoelectrons emitted from only the top few atomic layers (10's of Angstroms), b) elements of atomic number 3 or larger can be detected, thus allowing for a full survey of the Periodic Table, and c) small changes in the binding energy of electrons can be measured (better than ~0.l eV accuracy) and thus, the chemical state of elements can be determined. Each element has unique configuration of electrons and associated energies (Hochella, 1988). As a result, photoelectrons emitted after excitation by an X-ray beam will produce spectra detected by XPS indicative of what elements are present, with the exception of H and He (Hochella, 1988). Most elements have at most five intense lines in a spectrum, so line overlap is rarely a problem (Hochella, 1988). X-ray photoelectron spectroscopy additionally indicates the chemical state of elements (Fyfe et al., 1982). A multiplex routine is used to collect detailed XPS data for elements of interest; small shifts in binding energies reveal changes in the chemical state of these elements.

XPS analyses were preformed on a PHI 5600 model and data analysis was performed using the program Augerscan 2. The Handbook of X-ray Photoelectron Spectroscopy was used for elemental identification and interpretation of XPS data

(Moulder et al., 1992). The spectra were taken with the X-ray source operating at 400 W power, an electron take off angle of 45 degrees to the sample plane, a monochromatic Al K alpha X-ray (with a 2 mm X-ray source) perpendicular to the analyzer axis was used in all XPS data acquisitions. The analyzer aperture was set to analyze an area of ~800 micrometer on surface and with analysis maintained at constant energy resolution (~ 0.1 % of pass energy) (Moulder et al., 1992). The Al X-ray source spectra are likewise provided in the Handbook (Moulder et al., 1992).

Sample Preparation for Bulk Coal Surveys

Representative coal samples were prepared by a) removing visible areas of heterogeneity (e.g. ash layers) b) crushing multiple fragments of coal (~10 pieces) in a mortar and pestle, c) securing to a holder by double sided carbon tape and d) running duplicate samples to test for homogeneity. These samples are referred to as the bulk coal surveys. XPS analysis of uncrushed materials is only representational of the outer surface, but by crushing/pulverizing the material an XPS analysis can be representational of the whole bulk of the coal (Gong et al., 1999). According to Weitzsacker and Gardella (1996), it is an advantage of XPS that it can analyze powders since coal is often used in a powder form. Wojtowicz et al. (1995) demonstrated that when conducted under identical operating conditions XPS analysis of powders and fresh sample surfaces yield differences no greater than attributable to ‘experimental error’ (Wojtowicz et al 1995).

Samples were prepared in a manner to minimize contamination and yield good data. Washing of the crushing tools (mortar, pestle, and hammer) between each use, first with water and then with 70 percent ethanol minimizes cross-sample contamination.

Powders for XPS were pressed into indium foil, which is placed into the sample holders. The method found most acceptable for producing non-contaminated samples is making a stack consisting of a glass slide overlain by a tissue upon which the indium foil is placed and powder placed on it, overlain by tissue and then finally another glass slide. Firm pressure was used to secure the coal into the indium without breaking the glass slide. Gentle shaking of the foil ensures coal powder does not remain loose. Keeping the layer of powder thin minimizes charging issues, though charging still occurs and the neutralizer gun is required for most runs. Although thin, the powder forms a continuous layer so indium peaks from the substrate do not overwhelm results. Indium peaks were labeled on the surveys but not included in atomic concentrations. Duplicate runs from at least two distinct powder mounts were run to check for possible contamination and homogeneity of the samples.

Experimental Procedures for Bulk Coal Surveys

Surveys were taken of at least two independently made powders of the bulk coal from each sample. More surveys were taken if one or both of the original two seemed possibly contaminated as outlined above. Surveys were carried out with 0.4 eV per step, 10 sweeps, 46.95 pass energy, and 3.1 eV work function; an electron volt (eV) is the energy of an electron accelerated by one volt potential. Spectra were produced for an energy range of 0 to 1200 eV, to sample energies that represent most elements on the Periodic Table (Moulder et al., 1992). Carbon calibration was done for every survey to assure correct calibration of the peaks. The 1s peaks of carbon, oxygen, and nitrogen were used along with the 2p peaks of aluminum, calcium, sulfur, and silicon. A sampling

of representational spectra from bulk coal surveys are provided in Appendix E, and the whole collection of 50 XPS surveys and multiplex analysis of XPS spectra are available from ICAL.

Analysis Procedures for Bulk Coal Surveys

Peaks with a high signal to noise ratio were selected to identify the full complement of elements present in each coal sample. A computer program, Augerscan, generated lists of possible elements in given valence states corresponding to the peak position. Additional restrictions on possible elements represented are found by referencing the Handbook of X-ray Photoelectron Spectroscopy (Moulder et al., 1992) which shows all peaks that must be present for an element to be present. Therefore, although the lists generated by Augerscan are long, many possibilities were eliminated quickly because other peaks are not visible where needed in correspondence with other valence states of a given element. After labeling peaks, Augerscan computes relative atomic concentrations. The atomic concentration is based on peak area, which is considered more accurate than the alternative method based on peak height sensitivity (Moulder et al., 1992). The sensitivity is ~0.1% atomic concentration (Evens et al., 1999).

Analytical Results

At a broad scale, the coal is all very similar (Figure 19) in terms of the elements present and their relative abundances. The average carbon content is 75, 78, and 71wt% for the Absaloka, Decker, and Rosebud Mines respectively. Again looking at Absaloka,

Decker, and Rosebud respectively there is 20, 17, and 23 wt% oxygen. This leaves 5, 5, and 6 wt% for other components in the Absaloka, Decker, and Rosebud Mines, respectively.

Absaloka, Decker, and Rosebud Mines appear to be grossly similar in terms of the elements present, but differences emerge in their relative abundances. In addition, Absaloka and Rosebud are more similar to each other than either is to Decker, which based on relative distances between them would be expected.

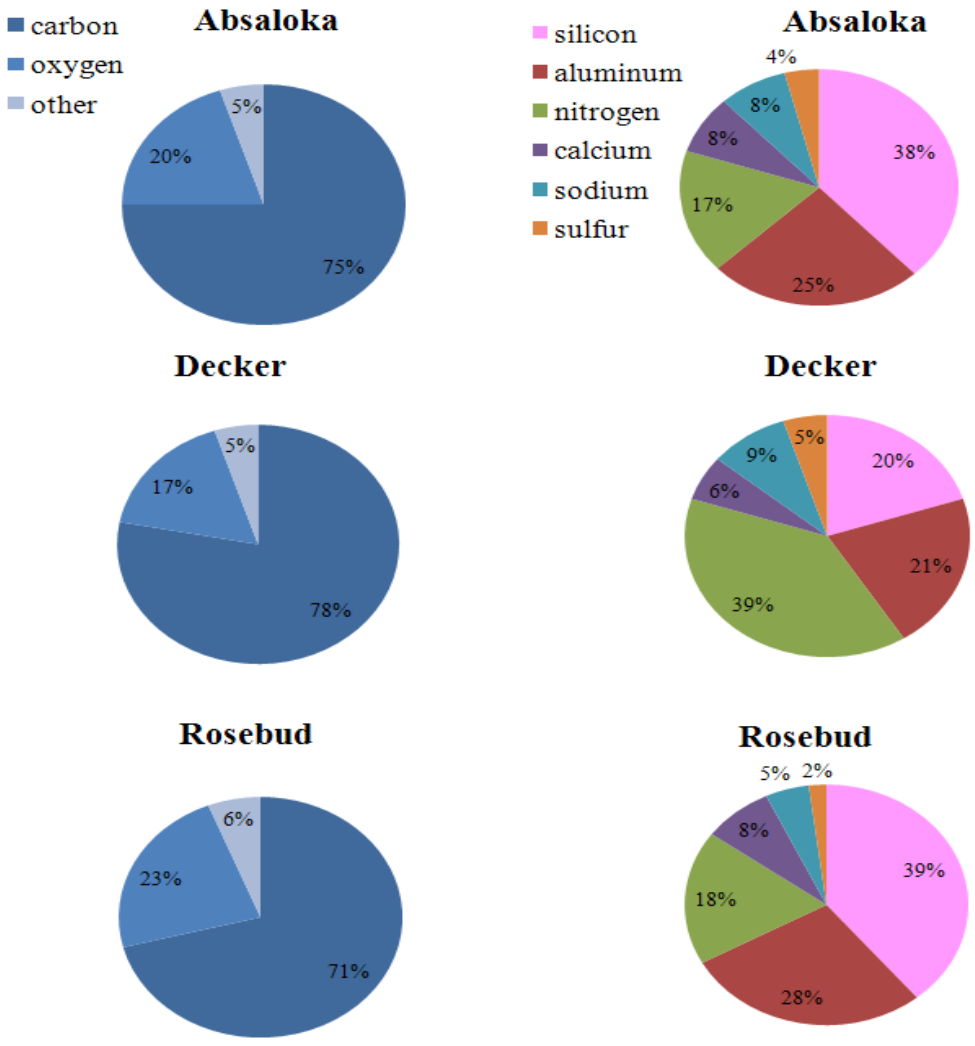


Figure 19. Pie charts illustrating atomic concentrations based on XPS in coal samples from three coal mines.

Figure 20 compares XPS elemental concentration averages as atomic concentrations for Absaloka, Decker, and Rosebud Mines to the coals of the APCSP (Weitzsacker and Gardella, 1992). XPS results were all plotted as relative atomic concentrations, normalized to 100% excluding carbon and oxygen. Table 8 gives the abbreviations for the APCSP coals along with their locality (state and coal seam) and rank.

Table 8. Complete Argonne Coals List with Locations and Ranks.

Abbreviation	Seam	State	Rank
UPFR	Upper Freeport	Pennsylvania	medium volatile, bituminous
WYAN	Wyodak-Anderson	Wyoming	subbituminous
ILLI	Illinois No. 6	Illinois	high volatile, bituminous
PITT	Pittsburgh (No. 8)	Pennsylvania	high volatile, bituminous
POCA	Pocahontas No. 3	Virginia	low volatile bituminous
BLCA	Blind Canyon	Utah	high volatile bituminous
LEST	Lewiston-Stockton	West Virginia	high volatile bituminous
BZAP	Beulah-Zap	North Dakota	lignite

Table modified from Vorres (1990) with abbreviations from (Weitzsacker and Gardella, 1992)

A graph (Figure 20) of atomic concentrations for Absaloka, Decker, Rosebud, and all the APCSP coals illustrates consistency in trends of atomic concentrations for all the coals. These plots are based on wt% normalized in the absence of carbon and oxygen. The APCSP consists of eight coals picked as representational of United States' coal (Vorres,1993); therefore, based on Figure 20, these coals appear typical of United States coal. No element stands out as significantly more or less abundant in coals from Absaloka, Rosebud, and Decker mines when compared with the representative data of the APCSP data; however, the Absaloka, Rosebud, and Decker mines in this study typically have less Al and Si (ash content) than the APCSP coals.

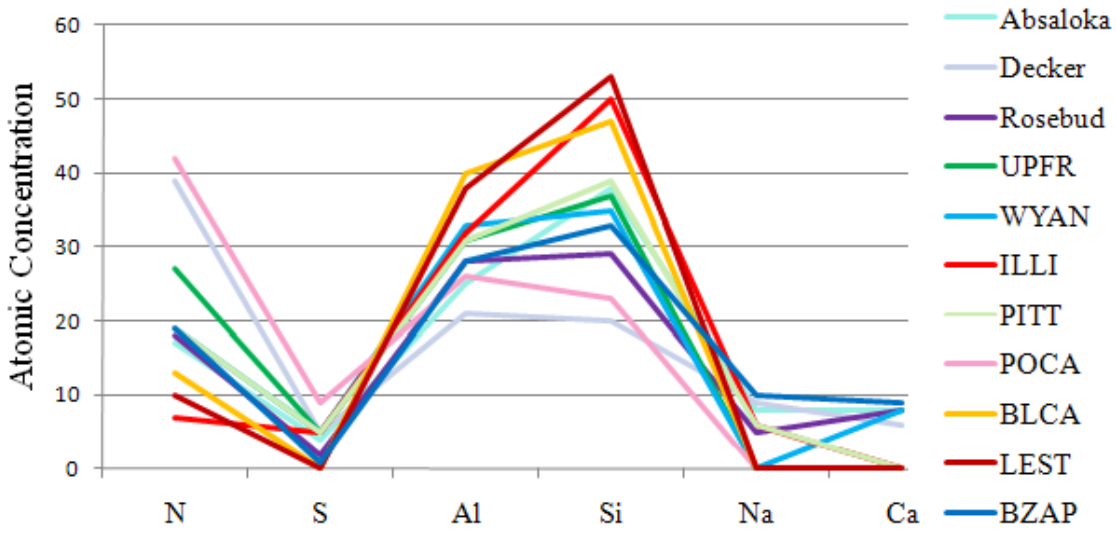


Figure 20. Relative atomic concentration according to XPS, excluding carbon and oxygen, for Absaloka, Decker, Rosebud, and each of the APCSP coals (Weitzsacker and Gardella, 1992).

Three identified elements, sulfur, sodium, and nitrogen are of particular interest as discussed in the introduction. As expected for PRB coal (Considine, 2009), sulfur is in low abundance. Sodium was only identified using XPS for samples at Ab 3b, Ab 4, D low Na 8%, and RB 1. However, one key point about this data is that it was based on the bulk homogenous part of the coal and therefore will underestimate total abundance of elements concentrated in heterogeneous parts such as sulfide and ash components. This explains why the Decker samples do not have 1% and 8% sodium, as indicated in their names. However, some degree of correlation is still found in that both for Decker and Rosebud, the samples labeled as having more sodium are found to have sodium and in the ones labeled as lower in sodium, sodium is not detected; Absaloka sample names give no indication of sodium content. Nitrogen occurs in all samples, and in general is greatest at Decker and least at Absaloka. The following graph gives the abundance of each of these

elements for each of the eleven samples. Note this is plotted as true abundance; carbon and oxygen are not excluded.

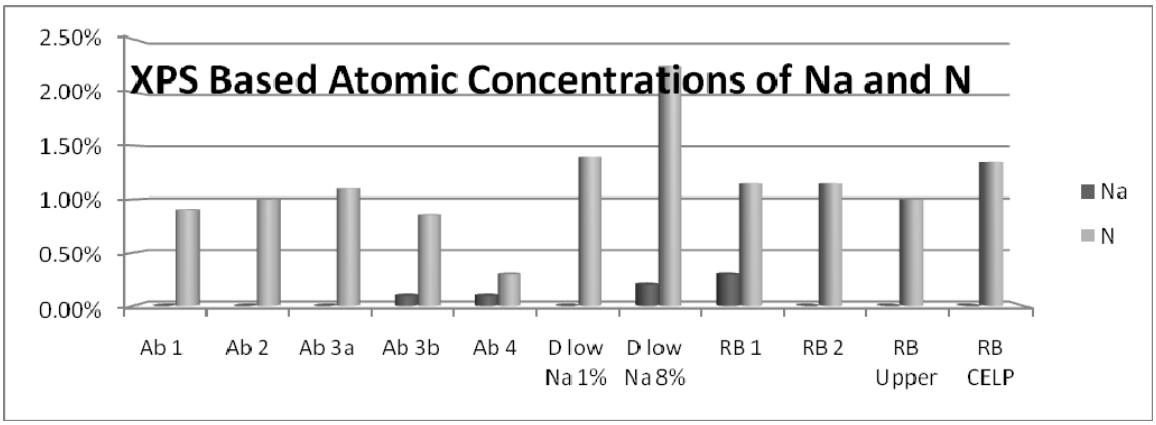


Figure 21. Absolute at.% of Na and N in various Montana coals determined by XPS.

Additional Surveys Beyond the Bulk Coal

Additional XPS surveys were done on areas of high sulfide (pyrite) components and an ash component. The pyrite from Ab 1 and an ash material from Ab 4 naturally formed thin flakes so they were pressed into indium foil without powdering. Standard procedure, including powdering, was preformed for the sulfide mineral from RB Upper.

An XPS survey of the ash indicates atomic concentration of 66.9% oxygen, 12.9% silicon, 10.5% aluminum, 9.2% carbon, 0.5 % sodium, and 0.1% calcium and is interpreted as being representative of a clay-rich substrate. A pyrite sample from Ab 1 yielded atomic concentration of 42.2% carbon, 42.2% oxygen, 8.6% sulfur, 3.1% iron, 1.8% nitrogen, 1.7% sodium, and 0.3% selenium. An XPS survey of the sulfide from RB Upper indicates atomic concentration of 33.1% carbon, 27.2% oxygen, 15.7% sulfur, 8.1% iron, 5.0% selenium, 5.3 % aluminum, 2.2% silicon, 2.1% nitrogen, 0.8% barium, 0.3% cobalt, and 0.1% calcium. A significant point to remember here is that Se and Co

were not detected in pyrite by EDS, with detection limits of 0.1 wt%; detection by XPS but not EDS indicates the Se and Co signal comes from the surfaces of pyrite. Therefore the Se and Co are probably sorbing onto a pyrite substrate rather than occurring as a solid solution in pyrite.

Multiplex Analysis of XPS Spectra

A multiplex routine was used to conduct detailed surveys of pre-selected energy windows to determine the chemical state of specific elements. Multiplexes were done for one sample from each of the mines, RB 1 from Rosebud mine, D low Na 8% from Decker mine and Ab 3a from Absaloka mine. Chemical states of nitrogen and sulfur (where present) have been analyzed in detail. Multiplex analysis of XPS spectra is done under the condition of a principal carbon peak at 285 eV. This calibration is necessary to correct for peak shifts that may be the result of sample charging (Wojtowicz et al 1995). The number of sweeps was determined based on a combination of peak size and significance, with particular focus put on nitrogen and sulfur due to their environmental significance. The elements aluminum, calcium, silicon, and sodium were not curve fitted because deconvolutable peaks of multiple valence states are not expected. Peak positions found were compared with values reported in the literature, summarized in Table 9, and no more than 0.1 eV was allowed for variation while labeling peaks.

Table 9. XPS Peak Positions from the Literature Exhibiting the Chemical Shifts Associated with Various Ionic States.

Element	Form	Energy (Ev)	Ref.
Nitrogen	pyridinic nitrogen	398.5 – 398.9	Buckley et al., 1995; Gong et al 1997; Gong et al., 1999; Grzybek et al., 2002; Kambara et al., 1995; Kelemen et al., 1994; Kozlowski, 2004; Wojtowicz et al., 1995
	nitrile	399.1	Gong et al., 1999
	amine	3991. – 399.3	Kelemen et al., 1994
	pyrrolic nitrogen	400.1 – 400.5	Buckley et al., 1995; Gong et al. 1997; Grzybek et al., 2002; Kambara et al., 1995; Kelemen et al., 1994; Kozlowski, 2004; Wojtowicz et al., 1995
	quaternary nitrogen	401.4 - 401.5	Kambara et al., 1995; Kozlowski, 2004; Schmiers et al., 1999; Wojtowicz et al., 1995
	electron deficient pyridine nitrogen	401.5	Buckley et al., 1995
	ammonium species	401.7 – 402.2	Gong et al., 1997
	graphene sheet	401.3	Gong et al., 1999
	N-oxide	402.9 - 403.0	Kelemen et al., 1994; Kozlowski, 2004
	nitro	405.3 – 405.9	Kelemen et al., 1994
Sulfur	thiols	162.0 – 163.3	Domazetis et al., 2006
	pyrite	162.5	Kelemen, 1990; Kozlowski, 2004
	sulphides	163.3	Domazetis et al., 2006; George et al., 1991; Kozlowski, 2004; Liu et al., 2007
	thiophenes	163.9 – 164.1	Domazetis et al., 2006; George et al., 1991; Grzybek and Kreiner, 1997 Kozlowski, 2004; Liu et al., 2007
	sulfoxides	165.2 - 167.9	Domazetis et al., 2006; Grzybek et al., 2002; Kozlowski, 2004; Liu et al., 2007
	sulfones	167.9 – 168.4	Domazetis et al., 2006; Grzybek et al., 2002; Kozlowski, 2004; Lui et al., 2007
	sulfonic	169.5 – 170.4	Domazetis et al., 2006
Oxygen	molecular	529.9 – 530.0	Domazetis et al., 2006
	carbonyl groups	531.3 – 531.4	Grzybek et al., 2002; Grzybek and Kreiner, 1997
	hydroxyl groups and ether linkages	532.8	Grzybek et al., 2002
	carboxyl groups	534.1 – 534.4	Grzybek et al., 2002; Grzybek and Kreiner, 1997

Results from Multiplex Analysis of XPS Spectra

A multiplex routine was used to acquire high resolution peak profiles of XPS spectra for elements of specific interest. The fine structure of XPS peaks can be resolved by deconvoluting the spectra with curve fitting routines to reveal shifts in binding energies that are related to the bound state or types of chemical bonds for the element of interest. This is done after carbon calibration to a primary carbon peak of 285 eV is

preformed. The relative height of these peaks can provide semi-quantitative determinations of the relative abundances of elements in difference valence states. In this study, the multiplex routine was used to analyze N, S, and O in detail. The relative abundance of different ionic states of nitrogen, sulfur, and oxygen from PRB coals analyzed in this study is summarized in Table 10. Key positions in Table 9 are used to identify the chemical forms used in Table 10. Representative multiplex analysis of XPS spectra are shown in Figures 22-26.

Table 10. Relative Concentrations of Various N, S, and O Components Determined by XPS Curve Fittings.

Sample	Element	Peak Position (eV)	Form	Atomic Concentration
Ab 3a	Nitrogen	398.50[1]	pyridinic	30.1
		400.18	pyrrolic	52.9
		401.41	quaternary	17.0
	Sulfur	164.18	thiophenes	100
	Oxygen	531.33	carbonyl groups	27.2
		532.8	hydroxyl groups and ether linkages	56.2
		534.06	carboxyl groups	16.6
D low Na 8%	Nitrogen	398.50	pyridinic	29.6
		400.18	pyrrolic	51.3
		401.4	quaternary	19.1
	Sulfur	164.10	thiophenes	78.7
		162.50	pyrite	21.3
	Oxygen	531.28	carbonyl groups	21.4
		532.80	hydroxyl groups and ether linkages	35.3
		534.10	carboxyl groups	43.3
RB 1	Nitrogen	393.87	pyridinic	26.7
		400.56	pyrrolic	66.7
		401.77	quaternary	6.7
	Sulfur	Not detected		
	Oxygen	531.32	C=O	17.3
		532.79	C-O	8.3
		534.1	COO-	42.2
		530.36	O^{2}-	32.3

[1]Peak positions reported after calibration with the carbon 285 eV peak

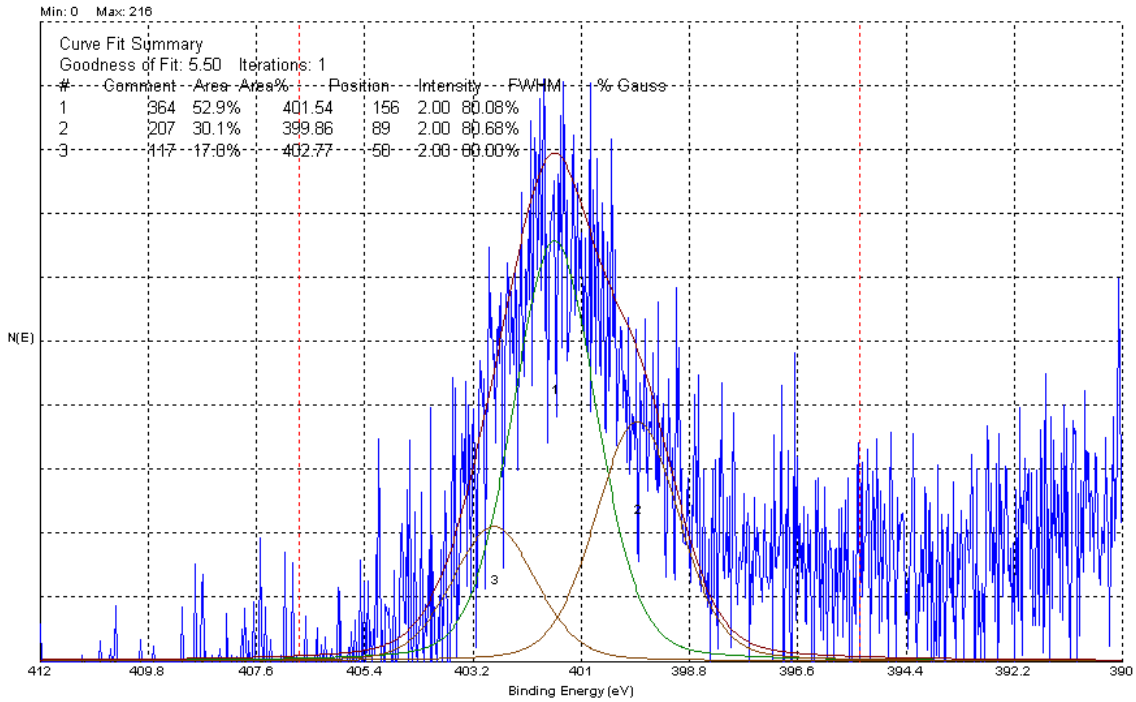


Figure 22. A representative N 1s XPS profile and the XPS curve fits for a Decker coal sample. Deconvoluted peaks correspond to 1) pyrrolic nitrogen, 2) pyridinic nitrogen, and 3) quaternary nitrogen.

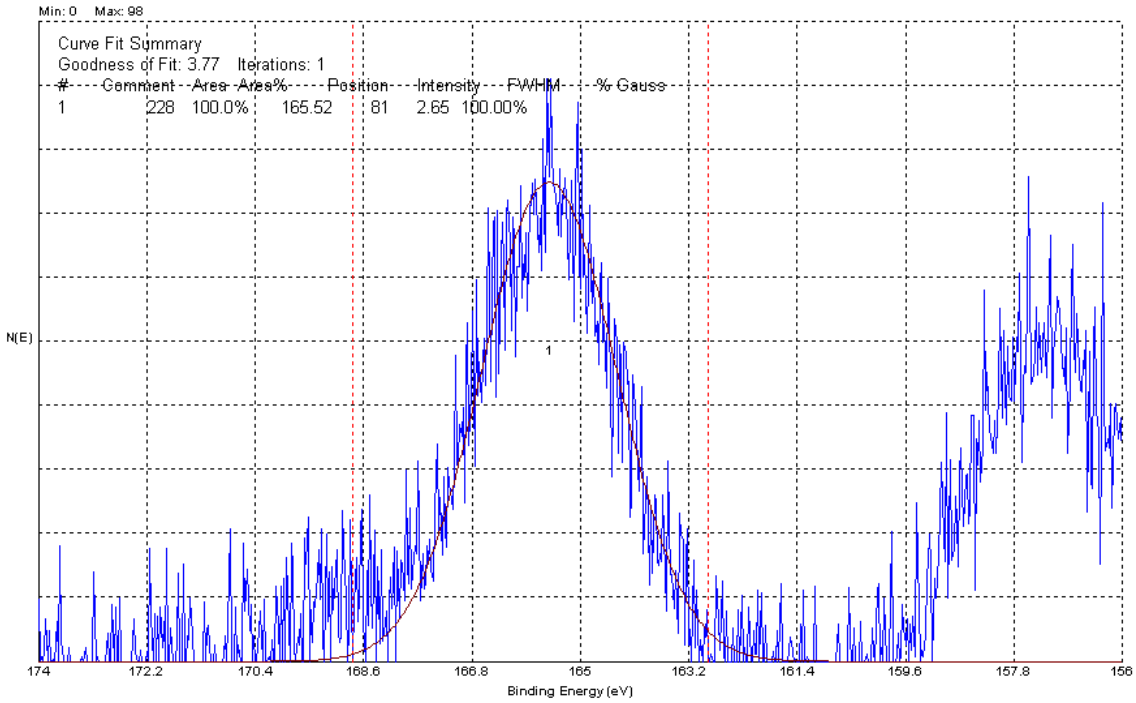


Figure 23. A representative S 2p XPS profile and the XPS curve fit for an Absaloka coal sample. Sulfur here is recognized only as thiophenes.

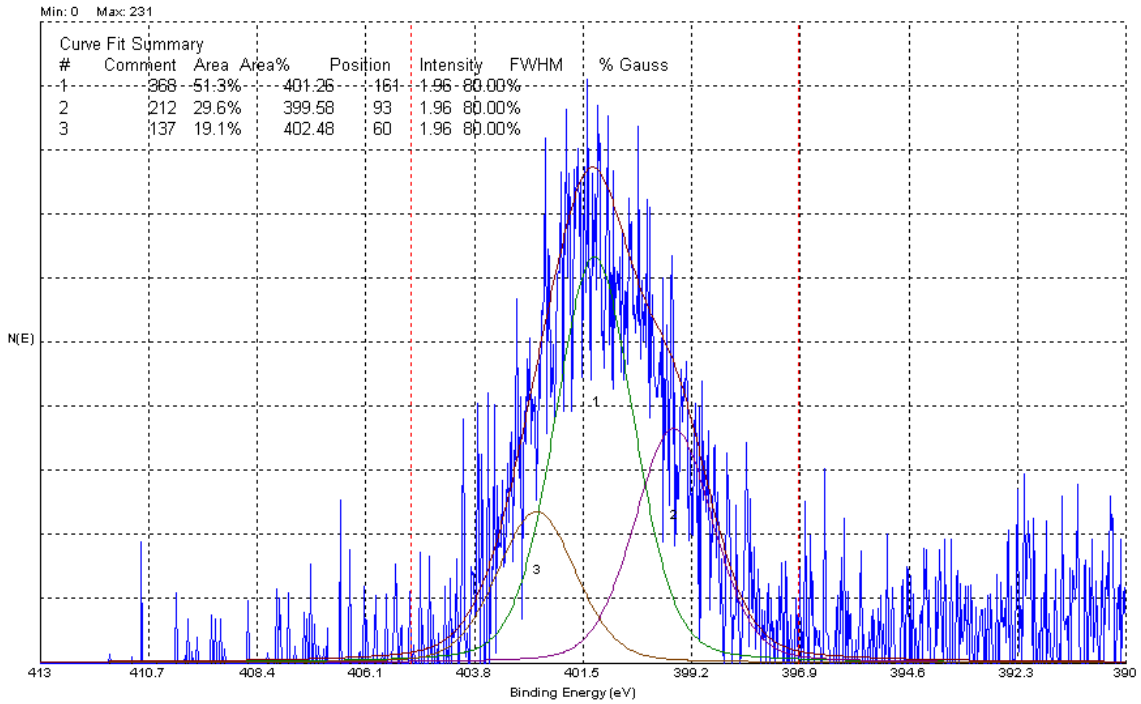


Figure 24. A representative N 1s XPS profile and the XPS curve fits for a Decker coal sample. Deconvoluted peaks correspond to 1) pyrrolic nitrogen, 2) pyridinic nitrogen, and 3) quaternary nitrogen.

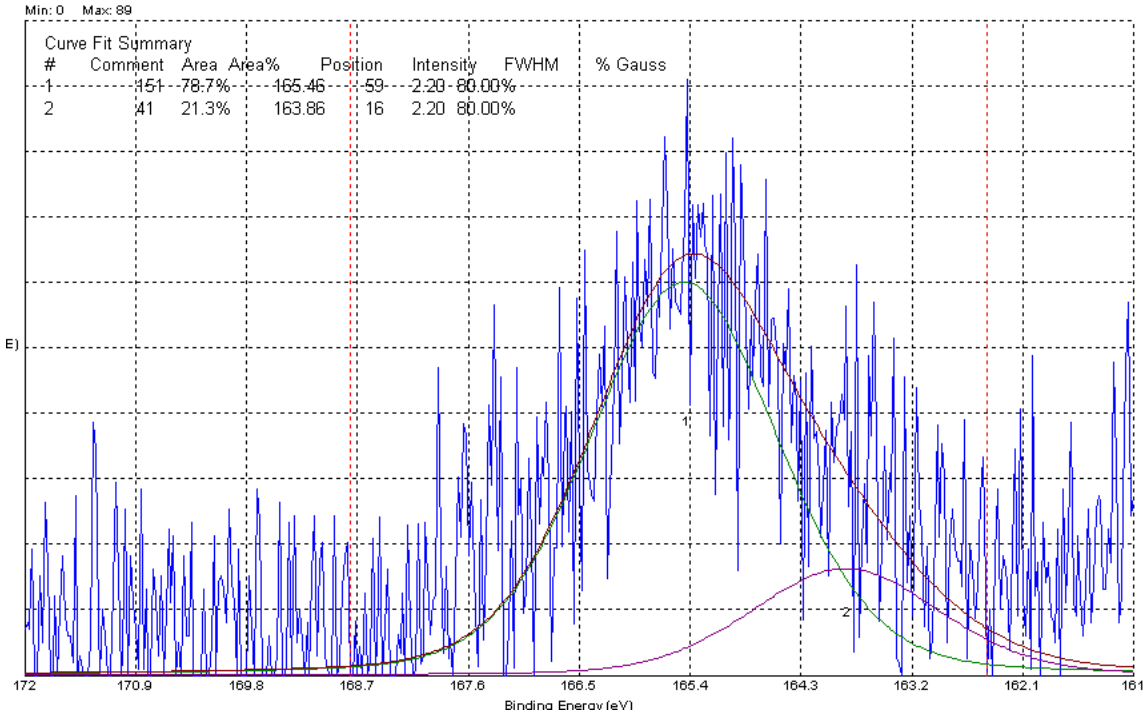


Figure 25. A representative S 2p XPS profile and the XPS curve fits for a Decker coal sample. Deconvoluted peaks correspond to 1) thiophenes and 2) pyrite.

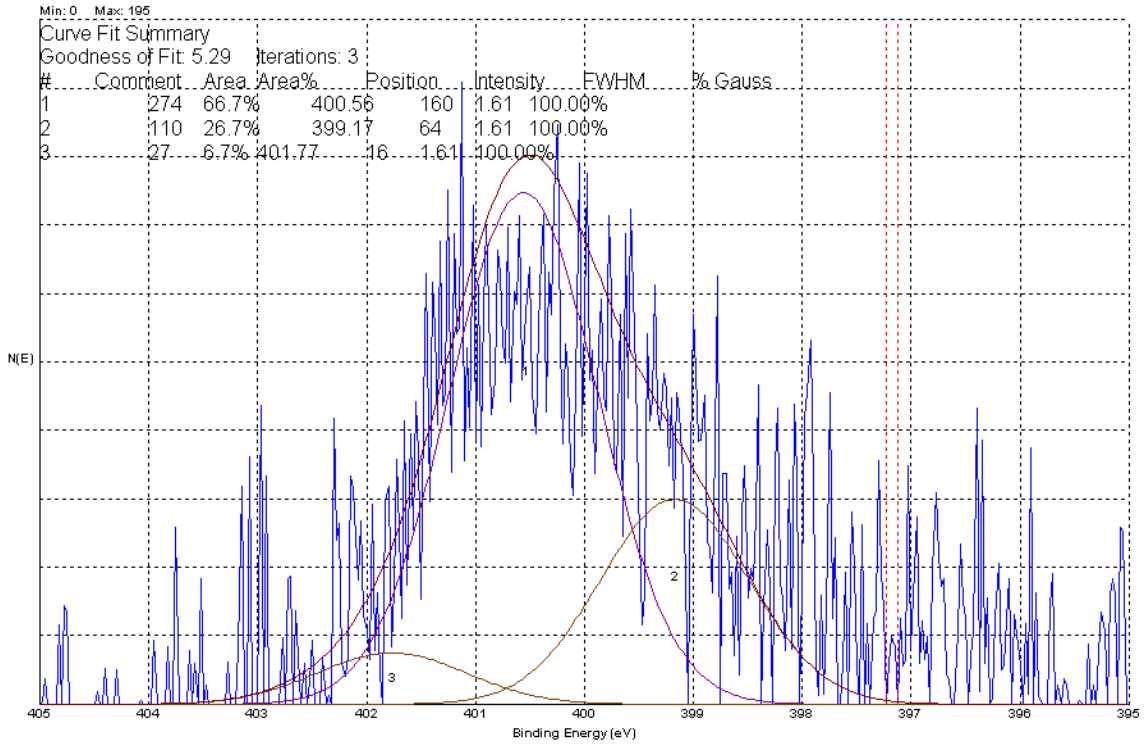


Figure 26. representative N 1s XPS profile and the XPS curve fits for a Rosebud coal sample. Deconvoluted peaks correspond to 1) pyrrolic nitrogen, 2) pyridinic nitrogen, and 3) quaternary nitrogen.

Discussion of Multiplex Analysis of XPS Spectra

The chemical state of nitrogen and nitrogen-bearing compounds is of particular interest to coal geochemistry, because of the potential of creating NO_x compounds during combustion. In this study, N was found to exist in three chemical states. Pyrrolic is the most common functional form of nitrogen, accounting for greater than fifty percent the total nitrogen in twenty coals of varying ranks studied by XPS by Kambara et al (1993); pyridinic is the next most common (Kelemen, 1994). In the twenty coals, nitrogen occurs as only pyrrolic, pyridinic, and quaternary forms (Kambara et al., 1993). In this study, PRB coals were found to contain these three components with pyrrolic accounting for the majority, and a greater contribution coming from pyridinic than quaternary forms.

Quaternary nitrogen may decrease in correlation to increasing rank (Kelemen et al., 1994). This has been studied using carbon concentration as an indicator of rank (e.g. Kelemen et al., 2006 and Wojtowicz et al., 1995). In this study, proportion of nitrogen in quaternary form versus carbon content (Figure 27) does not support such a trend. In the literature similar plots are presented as evidence for (Kelemen et al., 2006) and against (Wojtowicz et al., 1995) this conclusion.

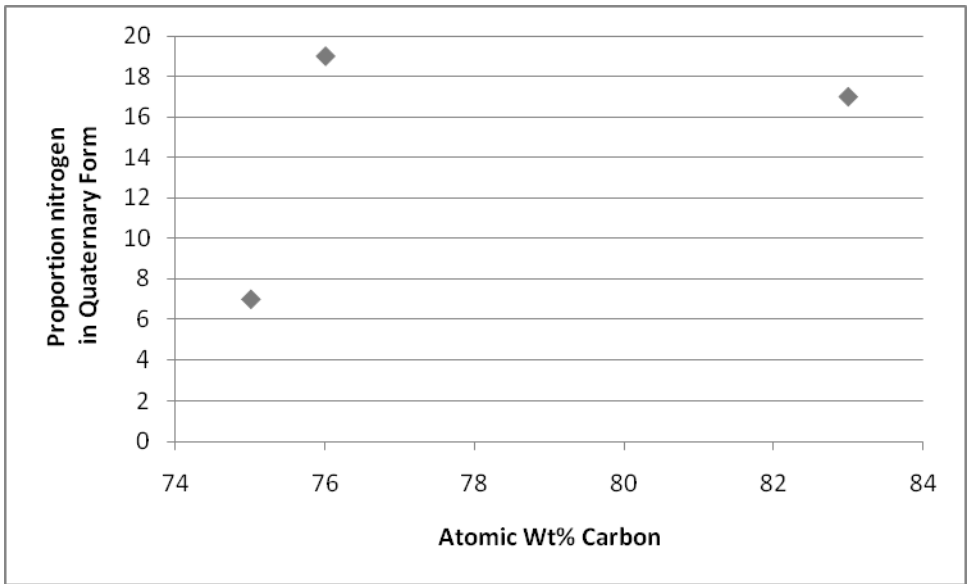


Figure 27. Proportion of nitrogen in quaternary form versus carbon content based on high resolution XPS surveys from the Absaloka, Decker and Rosebud coal mines.

Sulfur is only present as thiophenes at Ab 3a. At D low Na 8%, sulfur is 78.7% thiophenes and 21.3% pyrite. Sulfur is not identified at RB 1. The occurrence of sulfur in thiophenic form is expected, and the lack of both sulfides and sulfate likely only reflects the selection of "bulk" coal for these studies to the exclusion of samples with visible pyrite. For comparison, the sulfur of subbituminous coal from the Powder River basin in Wyoming contains 93% organic sulfur and 7% sulfate as determined by XPS; Pyrite was looked for but not found (Kelemen and Freud, 1990). Bulk analysis of the

coal determines it contains just less than 1% pyritic sulfur, about 6% sulfate sulfur and 93% organic sulfur (Kelemen and Freud, 1990). XPS of a variety of coals from the APCSP found sulfur mostly in sulfide and thiophenic forms (George, 1991); Additionally, pyrite is reported for one sample (George, 1991).

In summary of the literature of XPS analysis of coal, Gong et al. (1998) conclude oxygen occurs mainly in three functional forms, hydroxyl groups and ether linkages C-O, carbonyl groups C=O, and carboxyl groups O=C-OH; the carboxyl groups can also be denoted as, COO^- (e.g. Grzybek et al., 2004). In this study of PRB coal, these functional groups completely described the oxygen, except for at RB 1, where an additional peak corresponding to O^{-2} is present. Surfaces of demineralized lignites through bituminous coals are characterized mostly by C-O, with some C=O, and occasional COO- (Grzybek et al., 2004). Grzybek et al. (2004) suggest during oxidation, oxygen functionalities in coal might follow an oxidation path of C-O to C=O to COO- and then to CO_2. The higher proportions of C=O and COO- found in the PRB coals, with samples exposed to atmospheric conditions, is in accordance with this proposition. The occurrence of an O^{-2} at RB 1 is significant; a similar peak was identified by Domazetis et al. (2006) and was correlated to the presence of iron oxides.

CHAPTER 7

TIME-OF-FLIGHT SECONDARY ION MASS SPECTROMETRY (ToF-SIMS)

Instrumentation

ToF-SIMS is a surface-sensitive analytical method that uses a pulsed particle beam (Ga^+ ions) to ablate atoms and molecular complexes (neutrals, positive and negative ions) from the outermost atomic layers of a material (1-2 atomic layers, <1 nm). Ablated material is accelerated into a mass spectrometer; and the time-of-flight of the particles is proportional to the square root of their mass, thus producing a mass spectrum. The analytical capabilities of ToF-SIMS include mass resolution of 10^{-3} atomic mass units (amu), a mass range of $1\text{-}10^4$ amu, trace element detection typically on the order of parts per million, micron resolution imaging of any mass of interest, and depth profiling using the calibrated Ga^+ ion gun to analyze successively deeper layers in a material. Relative abundances of surface components can be obtained using ToF-SIMS, but these analytical results are semi-quantitative due to uncertainties of matrix effects, ablation rates of different ions or complexes, and lack of well-characterized standards. However, ToF-SIMS is particularly useful in identifying molecular compounds, including molecular fragments that derive from other macromolecules (typically complex organic compounds) (Benninghoven, 1994; Van Vaeck et al., 1999). In this study, ToF-SIMS was used to obtain surveys of elements and compounds present including detection of trace elements, elemental mapping of coal surfaces, and depth profiles across the surfaces

of coal particles. The instrument used in this project is a Charles Evans TRIFT ToF-SIMS.

ToF-SIMS has previously been used in the characterization of coal from a number of locations. Gong et al. (1997) used ToF-SIMS to confirm the presence of ammonium ions and ammonium-containing fragment ions in a bituminous coal. Additionally, imaging capabilities have been used to demonstrate the spatial association of ammonium with clay minerals (Gong et al., 1997). ToF-SIMS surveys have been used to demonstrate the relative abundance of elements present in coals before and after cleansing treatments such as acid washing (Domazetis et al., 2006). Cluster analysis of ToF-SIMS data has been used to discriminate different coals according to their elemental abundances (Pei et al.,2008) forming groups which correlate well with combustion properties.

Sample Preparation

Representative samples chosen for ToF-SIMS analysis are Ab 2, D low Na 8%, and RB Upper based on XPS bulk surveys. Duplicate samples of powders prepared for XPS analysis were used for the ToF-SIMS studies. Powders were pressed into indium foil as described for XPS sample preparation. The main difference is that the powder was applied much more sparingly, as a complete covering causes charging issues.

Experimental Procedures for Positive Spectrum

Three positive ToF-SIM spectra were obtained for each sample. These three spectra were taken at the same spot, one without sputtering, one after two minutes of

sputtering with a raster size of 200 microns, and a final one after another two minutes of sputtering with raster size again at 200 microns. Sputtering rate was calibrated using an atomic force microscope and is determined to be ~.014 micron per minute at ~ 1 nA ion current at 13 KeV energy at the target point. The analyzed area was 140 x 140 microns. At RB Upper, however, only two spectra were recorded, one before sputtering and one after the full four minutes with a raster size of 200 microns. Data analysis using the WinCadence® software includes a peak-matching function to identify possible elements, isotopes, or molecular compounds for a given mass. Representative ToF-SIMS spectra are provided in Appendix F, and all three spectra are available at ICAL.

ToF-SIMS- Analysis of Positive ToF-SIMS Spectra with 4 Minutes Sputtering

ToF-SIMS data can be overwhelming (Pei et al., 2008) so analysis of the mass spectra was focused on 219 elements and compounds reported for coal from the literature (Agroskin 1966; Buckley and Lamb, 1996; Domazetis 2006; Gong et al., 1997; Thomas 2002). Each ToF-SIMS mass spectrum was analyzed after four minutes of sputtering in the range of 0- 100 amu since masses >100 amu are rare in coal (Pei et al 2008). From 100 to 3000 amu only a broad survey of prominent masses was completed and these were mostly found to be complex organic molecular compounds. The focus of the present study is on inorganic elements or compounds. For this reason the analysis was focused on spectra gathered in positive ToF-SIMS mode; in positive mode inorganic peaks dominant and in negative mode organic peaks dominant (Pei et al., 2008). The four minute total sputter time, corresponding to ~55 – 60 nm depth, was sufficient to cleanse

material surfaces of most organic compounds and adventitious compounds sorbed from the atmosphere as environmental contaminants.

ToF-SIMS- Data for Positive
ToF-SIMS Spectra with 4 Minutes Sputtering

ToF-SIMS analysis is inherently semi-quantitative due to uncertainties in matrix effects and lack of standards appropriate for quantifying components on material surfaces (Benninghoven, 1994). However, the relative magnitude of mass peaks is still informative, and is presented in Table 11. In general, the major lithophile elements (Si, Al, Na, K, Ca, Fe, Mg) are accounted for along with their hydride or oxide forms. Nitrogen compounds (H3N and H4N) are also present, but are not major components in any of the samples.

Although minor abundance isotopes for each element are not directly included in the results, a search was conducted for all minor abundance isotopes which should occur in at least one sample with a peak of ten or greater counts. These are ^{6}Li, ^{25}Mg, ^{26}Mg, ^{29}Si, ^{30}Si, ^{41}K, ^{42}Ca, ^{43}Ca, ^{44}Ca, ^{48}Ca, ^{46}Ti, ^{47}Ti, ^{49}Ti, ^{50}Ti, ^{54}Fe, ^{86}Sr, and ^{87}Sr. This serves as confirmation of the identified elements. In some cases, a minor abundance isotope peak is expected in an area previously designated to another element. These cases are HSi and ^{29}Si, HCa and ^{41}K, and Ti and ^{48}Ca. In all of these cases, the centroid for the whole peak falls within .01 amu of both components. Therefore rather than try to directly deconvolute the peak, the integral for the whole peak was taken and the expected contribution from the minor abundance isotope, as calculated from the major abundance version of the element, was subtracted to figure out the peak count of the element of interest.

Table 11. Components Listed by Decreasing Abundance Based on Positive ToF-SIMS after Four Minutes Sputtering.

	Absaloka	Decker	Rosebud
1	Al	Na	Al
2	Ca	Ca	Si
3	Si	Al	Ca
4	Na	K	K
5	Si_2H	Si	HSi
6	H	H	Mg
7	Mg	Si_2H	SiOH
8	K	Mg	H
9	HSi	HCa	Na
10	SiOH	HSi	Si_2H
11	HCa	SiOH	HCa
12	Li	Fe	Li
13	Ti	CaO	Ti
14	Sr	Sr	Fe
15	CaO	Li	CaO
16	S_2	Si O_2 H	Sr
17	Fe	H_4N	S_2
18	SiO_2H	SiO_2H_3	SiO_2H
19	H_4N	Ti	H_4N
20	Zn	S_2	N
21	SiO_2	B	Zn
22	H_3N	N	H_3N
23	Na_2O	S	Mn
24	B	Cr	SiO_2
25	Mn	Zn	Na_2O
26	SiO_2H_3	SiO_2	SiO_2H_3
27	FeO_2H	FeO_2H	B
28	N	H_3N	H_3O
29	Cr	H_3O	Cr
30	H_2	Na_2O	H_2
31	Cu	H_2	TiO_2
32	TiO_2	TiO_2	FeO_2H
33	H_3O	Cu	S
34	Cu	S	Cu

Analysis of ToF-SIMS Images

Images were taken of many elements and compounds to document the occurrence and distribution of these elements in the PRB coals (e.g. disseminated throughout the matrix, concentrated in or on mineral substrates, or concentrated in fractures or pore space). None of the abundant elements concentrate mainly on fracture or in mineral poor areas. Of the abundant elements hydrogen is the most dispersed. In order to assess the association of elements with mineral substrates, maps were obtained for elements that occur in minerals known to occur in the PRB coals (i.e. those identified by XRD and SEM/EDS) and then compared with the distribution of other elements or compounds that were detected in the initial ToF-SIMS surveys. In reviewing these elemental maps only spatial proximity and correlation can be demonstrated, chemical association is an interpretation.

The strongest pairing is Al and Si (Figure 28), which is interpreted as clay minerals (in agreement with XRD and SEM/EDS analysis), and it was observed in all three samples. The distribution of Li, H_4N, and Ca correlates with Al and Si (clays). K and clays appear overall correlated though unique concentration areas for both stand out at Ab 2 and D low Na 8%. Mg correlates to clays at D low Na 8%, but correlations are weak or absent at Ab 2 and RB Upper. Na is not correlated with clays at Ab 2, includes a good matching with clays and additional areas of strong concentration that are not concentrated in clays at D low Na 8%, and is correlated with clays at RB Upper. Sr appears correlated with clays at D low Na 8%; however, it is not correlated to clays at either Ab 2 nor RB Upper. H_3N, N, SiO_2H_3, S_2, Si_2H, and Cu lack substantial indication of clay correlations. The distribution of H is very diffuse; however, it does include areas

of clay concentration and shows some tendency for greater concentrations in these areas. Furthermore, H can come from the organic remnants on the surface even after sputtering.

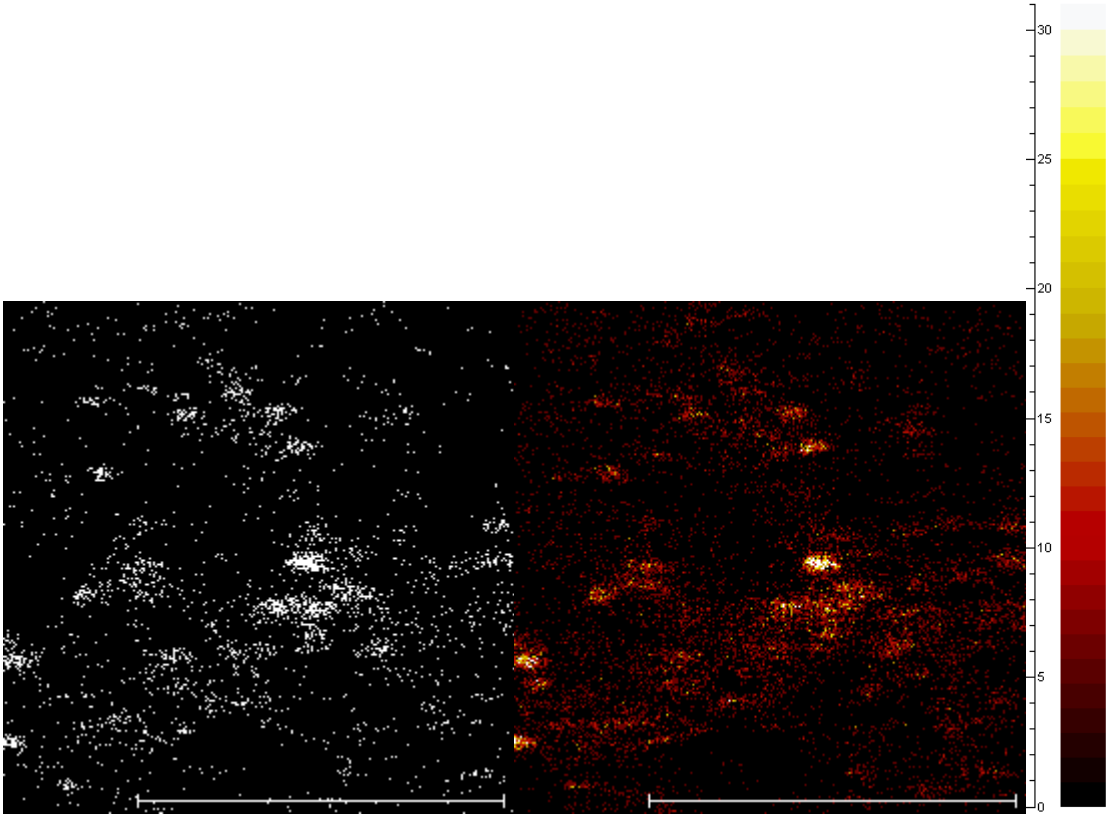


Figure 28. ToF-SIMS elemental maps for D low Na 8% of aluminum (left) and silicon (right). Scale bars are 100 micron each. Intensity scale, far right, shows the number of ions coming into the detector per a given unit of time with lighter colors indicating more ions.

Additional Search for Trace Elements Using ToF-SIMS

ToF-SIMS surveys were searched specifically to identify the presence or absence of potentially hazardous elements previously reported in coal (Kizilshtein and Kholodkov, 1999 and Finkelman, 1994). The use of ToF-SIMS to determine the absence or possible presence of hazardous elements is justified because ToF-SIMS is a very sensitive method for identification that is appropriate for use on heterogeneous material

including coal (Domazetis et al., 2006). The elements searched for were As, Be, Cd, Hg, Mn, Ni, Pb, Sb, Se, U, (Finkelman, 1994), and Th (Kizilshtein and Kholodkov, 1999). In all cases, these elements were either not detected or were detected just above background levels in the ToF-SIMS spectra (Table 12).

Table 12. Maximum Peak Counts for Select Elements Based on Positive ToF-SIMS after Four Minutes Sputtering.

Element	Absaloka	Decker	Rosebud
U	x	x	1
As	4	8	4
Ni	X	2	2
Sb	3	2	5
Se	6	4	5
Mn	14	7	31

Additional images were taken of these potentially hazardous elements to examine distribution and association patterns. The low count rate for all of these elements indicates that they are disseminated in the coal matrix in very low concentrations (< ~10 ppm); no concentrating agent or mechanism could be identified in these coal samples. Figures 29 – 32 show representative elemental maps for Cr, Mn and Zn compared with the total ion map for RB Upper.

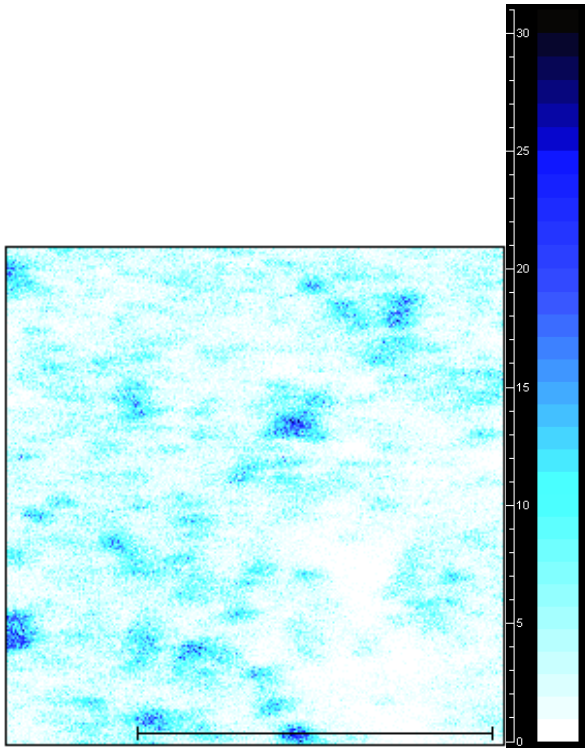


Figure 29. ToF-SIMS total ion image from RB Upper. Scale bar is 100 micron. Intensity scale, far right, shows the number of ions coming into the detector per a given unit of time with darker colors indicating more ions. This scale also applies to the next three images.

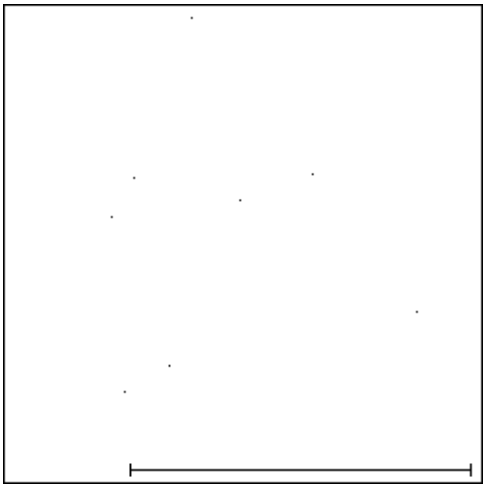


Figure 30. ToF-SIMS Cr+ ion image from RB Upper. Scale bar is 100 micron.

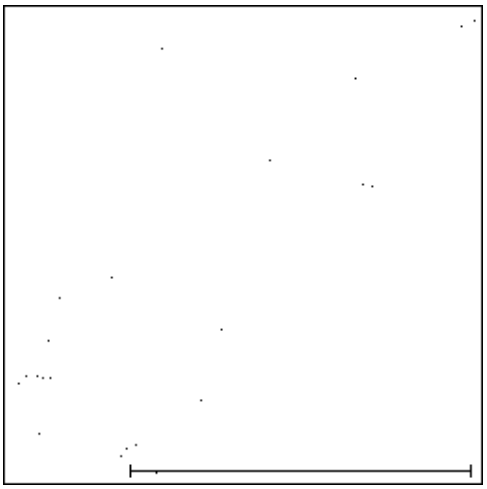


Figure 31. ToF-SIMS Mn+ ion image from RB Upper. Scale bar equals 100 micron.

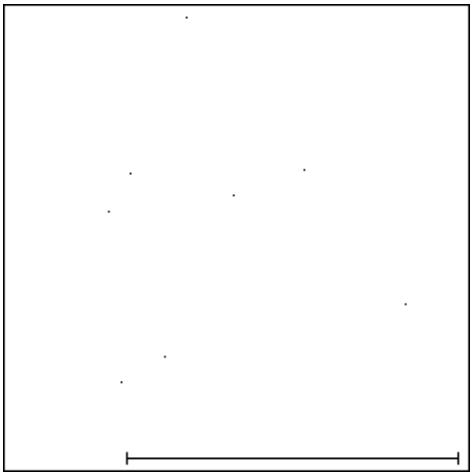


Figure 32. ToF-SIMS Zn+ ion image from RB Upper. Scale bar equals 100 micron.

Analysis of Negative ToF-SIMS Spectra with 4 Minutes Sputtering

Negative spectra were also gathered for representative samples from each mine. A list of likely components identified from the literature (e.g. Buckley and Lamb, 1996; Domazetis et al., 2006;) were searched for and ranked in order of abundance (Table 13). The dominant anions and anionic complexes are: O, C_2, H, OH, F, S, Cl, and simple

alkane compounds. Although identified in the literature, SO_3, SO_4, and HSO_4 are not listed because they were not confidently identified at any of the PRB mines.

Table 13. Top Ten Components, Found by Negative ToF-SIMS after 4 Minutes Sputtering, Listed in Order of Decreasing Abundance.

	Absaloka	Decker	Rosebud
1	O	O	O
2	C_2	C_2	C_2
3	H	F	CN/C_2H_2
4	OH	CN/C_2H_2	C_2H
5	CH	C_2H	OH
6	C_2H	OH	H
7	CN/C_2H_2	H	F
8	C	C	C
9	F	CH	CH
10	S	Cl	Cl

CHAPTER 8

DISCUSSION

Coal is an abundant and relied-on energy source; however, much focused attention resolves around coal being a source of greenhouse gas emissions, fly ash, and potentially hazardous elements. This has lead to an increase in research and development of clean coal technologies, this research indicates that in order to decide the best method for clean coal combustion one must understand the geochemistry and mineralogy of coal. Furthermore, this information must be assessed at a local level because critical differences can exist on fine scales within a deposit, and between different deposits. Therefore, this study has documented the chemistry and mineralogy of eleven samples from three mines from the Montana portion of the Powder River Basin- Decker, Rosebud, and Absaloka. These samples were provided by the mines, from active production units, as representative of their coal. A variety of independent analytical methods are used to geochemically and mineralogical characterize this coal.

The main contributions of this work are 1) an inventory of the elements present in bulk samples, and the distribution of these elements in coal, 2) an inventory of the minerals present (including their occurrence and distribution), 3) an additional focus on major elements of concern N, Na, and S (and particularly the chemical state of N and S), and 4) analysis of potentially hazardous trace elements

Composition

This study has created an inventory of elements present; the two techniques used in this study to yield quantifiable elemental information are XPS and INAA. XPS recognizes carbon and oxygen as accounting for 94 - 95 % of the atomic concentration at all three mines. The remaining inorganic part is composed of silicon, aluminum, nitrogen, calcium, sodium, and sulfur. As represented by XPS of the coals analyzed here in comparison to the coals from the APCSP (Weitzsacker and Gardella, 1992), Montana coal of the PRB has elemental abundances that fall at or below the national average of a variety of different United States coal. Sulfur content is low, as expected for Powder River basin coal. Neither sodium nor nitrogen content are particularly high, however these elements still demand attention, since they are major elements with negative effects during coal combustion. REEs measured by INAA revealed granitic source area patterns, but with lower than expected total values for granitic rocks (Cullers and Graf, 1984). At Decker and Rosebud mines there is significant depletion of LREEs which may indicate mixing with another source material, possibly a more mafic crustal component.

Particular focus has been paid to potentially hazardous elements. An understanding of potential hazards of elements is beneficial in terms both of understanding dangers and appreciating coals which are low in such elements. Potentially hazardous elements include those elements listed as hazardous air pollutants according to the Clean Air Act which are also known to occur in coal, and Th (Kizilshtein and Kholodkov, 1999). According to INAA, arsenic and nickel are both less abundant than the national average in all eleven samples. However, concentrations of some specific trace elements that are equal to or greater than national average

concentrations are found in RB Upper (Th), RB CLEP (Sb, U, and Th), and Ab 3b (Se, Sb, U, and Th). Further testing with ToF-SIMs reveals Be, Cd, Hg, Pb, and Th are absent or below detection limits. U is not detected at Ab 2 or at D low Na 8%. Mn is present at Absaloka and Rosebud, but unlikely at Decker.

Se is also detected by XPS in a sulfide (pyrite) sample. However EDS elemental analysis shows pyrite to be pure iron sulfide with no other substituting component (detection limits of 0.1 wt% and depth of analysis of ~3 microns under the electron beam). Therefore, Se is concentrated with, but does not substitute into, pyrite; most likely it is sorbed onto pyrite surfaces rather then entering the pyrite structure in compositional solid solution. Cobalt is also identified as an element that may be concentrated on sulfide surfaces. Although cobalt is not an element originally identified as potentially hazardous in this study, the hazard potential for cobalt, along with all searched for potentially hazardous elements identified in these samples by at least one technique is addressed in the hazard potential section.

For further comparisons, including elements of United States coal according to rank and elements averaged for coal worldwide are provided in Appendix G from The National Research Council (1980).

Mineralogy

The mineralogy of the PRB coals, including occurrence, distribution and composition, has been characterized through interpretation of SEM images and EDS analytical data, and prominent minerals within ash layers have been confirmed using XRD. Minerals identified by XRD are kaolinite, quartz, illite, dolomite, gypsum, pyrite,

and calcite. Kaolinite dominates in all of them, with quartz and illite being next most common, and gypsum, calcite, and dolomite locally occurring. XRD results are consistent with the observed mineralogy identified for coals worldwide (Sakurovs, 2007). SEM imaging and EDS elemental analysis serve as a confirmation of XRD results. The minerals identified by SEM include all the minerals identified by XRD. Also, kaolinite is identified as the dominant ash forming mineral, in agreement with XRD. However, SEM and EDS were also done on bulk coal samples and sulfide rich areas in addition to the coal seams. Pyrite is recognized as the most abundant sulfide mineral. Additional minerals identified include: barite, ilmenite and possible illite, sulfur, jarosite, thenardite, and trona.

Blocky and dendritic pyrite in some samples indicate reactants originate over a large distance from the site of crystal growth (Alonso-Azcárate et al., 2001 and Murowick and Barnes, 1987). Furthermore, the increased surface areas present greater opportunity for weathering, releasing oxidation producing iron-oxyhdroxides and acid discharge into the environment (Diehl et al., 2005 and Waanders et al., 2003). Since, as mentioned with reference to Se previously, with the SEM detection level of <0.1 wt %, no hazardous elements are detected in the pyrite, the potential problem of release of hazardous trace elements substituted into the pyrite being released is not an issue.

Clays may be undesirable due to swelling ability (Thomas, 2002). However, kaolinite is not a swelling clay, and therefore the dominance of kaolinite rather than other clays is desirable. Also clays reflect environment of deposition; here kaolinite as the dominant clay mineral is logical since that is indicative of a non-marine environment of deposition (Thomas, 2002).

Focus on Nitrogen and Sodium

Nitrogen was studied in detail using XPS because slight shifts in the binding energy can be used to interpret the chemical state of nitrogen in the natural coal samples. The negative environmental impacts of nitrogen are not well predictable but may be related to chemical state. XPS on nitrogen looked at the chemical states present. In order of decreasing abundance the detected forms are pyrrolic, pyridinic, and quaternary nitrogen; this matches with literature expectations (e.g. Kambara et al., 1995 and Kelemen et al., 1994). However the proportion of quaternary nitrogen for the samples from Absaloka and Decker is higher than expected. Although not well established, the elevated abundance of quaternary nitrogen may mean more NO_x forms during combustion (Kambara et al, 1993).

Although not hazardous, sodium is significant because of fouling, corrosive material build up, on broiler surfaces formed by sodium during coal combustion (Chadwick and Domazetis, 1995). Sodium is identified by the bulk coal surveys taken with XPS and INAA. As shown below (Figures 33 and 34), these results do not correlate exactly. However, both methods show sodium is only present in very small amounts, and the magnitudes reported are similar. With INAA there is a range of values from 1 to 3,195 ppm and with XPS it ranges from 0 to .30% atomic concentration. The low values likely reflect both techniques being done on bulk coal samples that are relatively ash free; this can explain for example the lack of even close to an 8% sodium reading for the coal from Decker labeled as having 8% sodium. As for the apparent lack of correlation between INAA and XPS, since all the values are so low, it may be explainable in terms of natural variation. Alternatively it may represent the differences in the instruments. XPS

is a surface analysis technique, and so even though the coal was powdered allowing the whole coal to be analyzed, at the level of an individual grain of powder, XPS still only analyzed the surface of it. INAA analyzes the whole coal. If the difference is real and related to surface versus whole coal examination, it may relate back to the notion that sodium concentration is largely a function of post deposition interactions with groundwater (Hildebrand, 1986). Either way this calls for more studies, either to figure out the range of natural variation or to realize the difference due to technique.

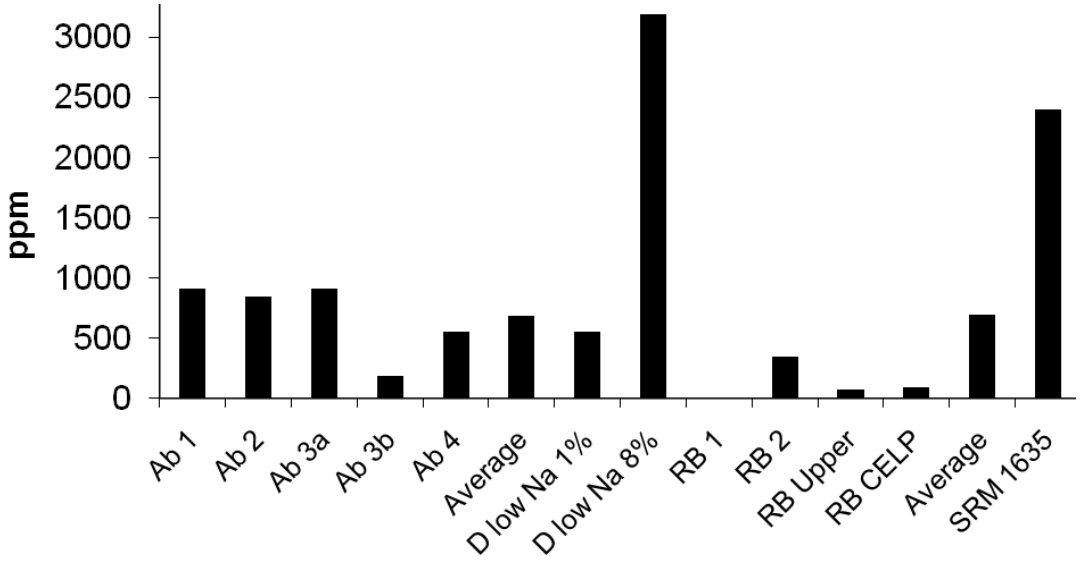


Figure 33. Na in ppm as determined by INAA in various coal mines.

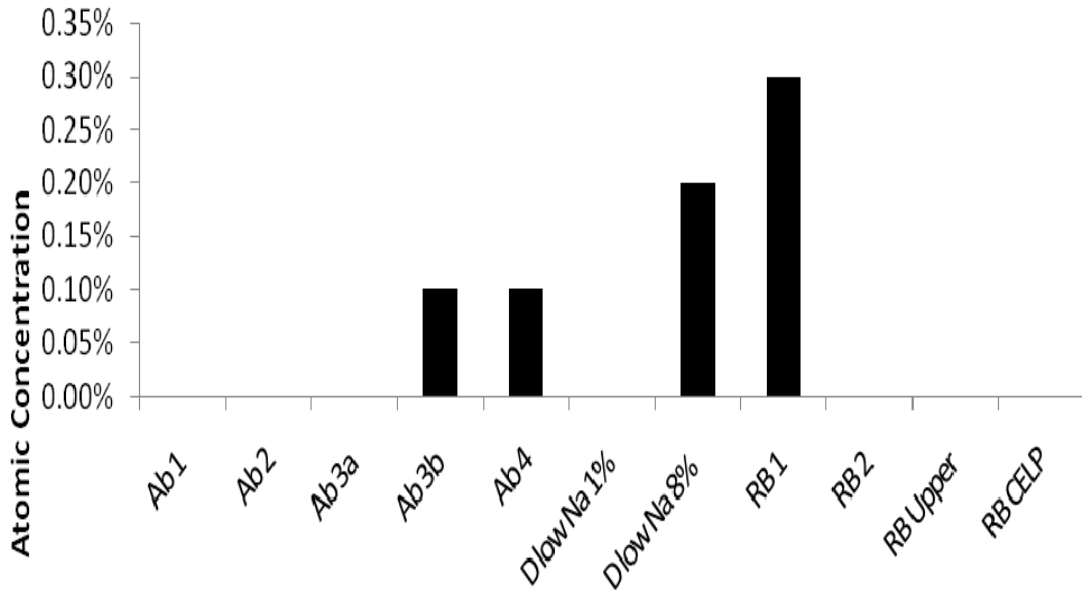


Figure 34. Na atomic concentration as determined by XPS in various coal mines.

Hazards Potential

Currently guidelines of recommended or maximum permissible levels for these elements are lacking. A preliminary set of environmental acceptable concentrations (EAC) and highest permissible concentration limits (HPCL) has been proposed by Wang et al. (2010) (Table 14) for some elements. As, Cr, and Ni are present at all localities in environmental acceptable concentrations (based on Wang et al., 2010). Se is present at one site at a level above environmentally acceptable but still way beneath the highest possible concentration limit; in all other samples Se is present in an environmental acceptable concentration. For PRB coals analyzed by Stricker et al., (2007) no element occurs at or above proposed EACs (Wang et al, 2010).

Table 14. Na atomic concentration as determined by XPS in various coal mines.

Element	EAC	HPCL
S	0.5%	1.5%
As	6.5	20
Be	1	3
Cd	0.8	2.5
Cl	400	1200
Cr	15	45
F	120	200
Hg	0.15	0.50
Mn	80	240
Ni	30	90
Pb	15	45
Se	2.5	8

Table from Wang (et al., 2010)

Human Health Implications for Trace Elements in Coal

Selenium metal has low toxicity; however, SeO_2, which results from coal combustion, will react in water to form selenite, a highly toxic selenium compound (Guijian et al., 2007). Selenium contaminated water from coal combustion is known to inversely affect not only fish communities but the whole wetland ecosystem. Furthermore, the effects are long lived. In the case of Belews Lake, North Carolina, effects of selenium input from a coal-fired facility remained for more than ten years after selenium input had ceased (Lemly, 1996). From 1961 to 1964 a selenium poisoning endemic caused nearly 50% morbidity rates in Enshi Country, Hubei Province of China; the selenium poisoning resulted from high selenium stony coal weathering and the selenium being taken up by crops (Yang et al., 1983).

Mn, although a possibly dangerous element, is not likely to be a concern with regards to coal combustion. A study on trace element partitioning based on combustion in a pulverized coal boiler classifies Mn as hardly volatile (Huang et al., 2004). In

another study on trace element partitioning, based on a stroker fire combustion unit, Mn is mostly incorporated into glassy and refractory bottom ash phases (Li et al., 2005); Occurrence as glassy and refractory phases means low mobility (Li et al., 2005). When a bituminous coal, Illinois #6 of the Argonne premium coal sample program, is gasified in a integrated gasification combined-cycle (IGCC) unit, Mn is again classified as relatively non-mobile (Helble et al., 1996).

Arsenic harms the cardiovascular system, gastrointestinal tract, kidney, nervous system, skin, blood and liver (Gupta, 1999). It is also a possible carcinogen (Gupta, 1999). However, health problems related to arsenic are rare in the United States; health problems relating to arsenic are mostly limited to developing nations in which coal is used domestically (USGS, 2006), such as the southwest Guizhou Province in China where domestic use of high arsenic coals resulted in over 3000 cases of fatal arsenic poisoning (Ding et al., 2001).

Nickel from power plants typically remains air borne for days, after which it mostly ends up in soils (ATSDR, 2005). If subjected to acidic conditions some of the nickel can be taken up by groundwater and some plants will accumulate nickel (ATSDR, 2005). However, most nickel remains strongly bonded to soils and therefore does not concentrate in waters or plants, so it does not present a health hazard (ATSDR, 2005). In Pench Valley (central India) coal, nickel concentrations range from 59 to 78 ppm (Gupta, 1999). Analytical results for natural waters show that nickel is below detection limit in all the water samples of the area (Gupta, 1999). The presence of humic substances in aquatic water suggests that nickel tends to concentrate under reducing conditions (Gupta, 1999). The aforementioned study demonstrates how nickel concentrations of natural

water are dependent on the availability and non-availability of organic substances under reducing conditions (Gupta, 1999). Nickel content, below detection limit in natural waters of the area, most probably attributed to the high oxidation state, not allowing setting up of reducing condition to enrich nickel in available humic substances (Gupta, 1999).

Antimony is most hazardous when exposed to in low quantities for an extended period of time. Antimony is released into the air by coal plants and stays suspended for days. Long term effects of breathing in antimony include irritation of the eyes, skin, and lungs or at higher concentrations lung, heart, and stomach problems.

Uranium is raised as a possible element of concern since it is radioactive; however, even assuming a tenfold increase in concentration from raw coal to coal ash, the concentrations of uranium are within the ranges found in many common soils and rocks (Figure 35) (USGS, 1997). The same holds true for other radioactive elements in coal, radium, radon, and thorium (USGS, 1997)

Although cobalt can cause respiratory problems and skin irritations (HSE, 1998), little is written about cobalt in coal. This makes sense since according to Gibbs et al. (2008) it is highly immobile in all conditions in all coals. However in a couple instances water sources enriched in cobalt have been related to coal (e.g. Hatcher et al., 1992 and Duong et al., 1995).

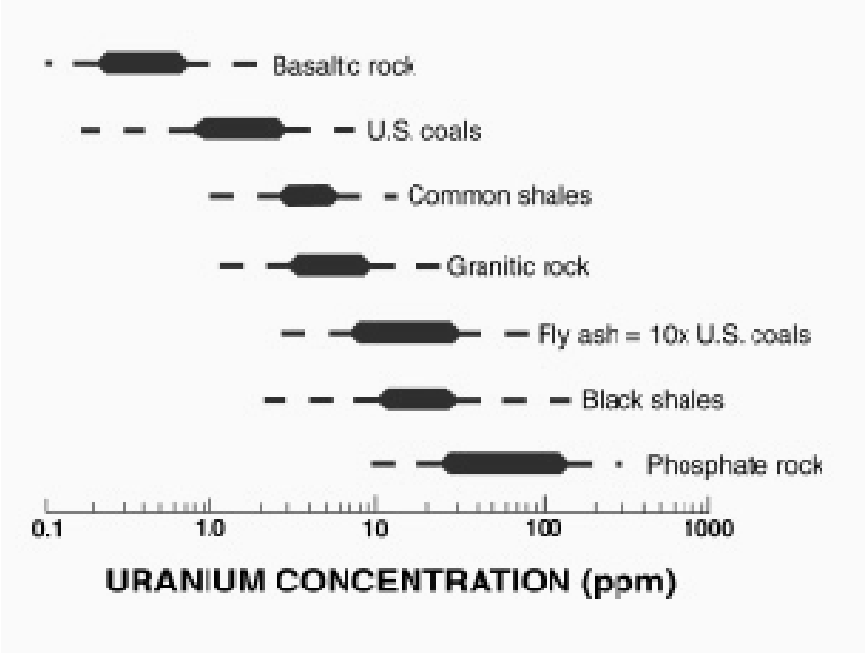


Figure 35. Comparison of uranium levels in coal in comparison to other natural sources (from USGS, 1997).

Suggestions for Future Work

As mentioned above, one key component still missing is quantification of the minerals present. Also, it would be interesting to look into the mechanisms responsible for concentrating elements in the coals (depositional, diagenetic, groundwater). This might include doing a detailed stratigraphic study of the coal to look for elemental variation on a small scale. Future work should also be done to better understand how coal mineralogy and geochemistry effects coal combustion and associated environmental and health implications.

REFERENCES CITED

Agroskin, A.A., 1966, Chemistry and Technology of Coal: English translation from Russian, Israel Program for Scientific Translations, Jerusalem, 240 p.

Alonso-Azcárate, J., Rodas M., Fernández-Díaz, L., Bottrell, S.H., Mas, J.R., and López-Andrés, S., 2001, Causes of variation in crystal morphology in metamorphogenic pyrite deposits of the Cameros Basin (N Spain): Geological Journal, v. 36, i. 2, p. 159–170.

Beer, J.M., 2000, Combustion technology developments in power generation in response to environmental challenges: Progress in Energy and Combustion Science, v. 26, no. 4–6, p. 301–327.

Benninghoven, A., 1994, Chemical-analysis of inorganic and organic-surfaces and thin-films by static time-of-flight secondary-ion mass-spectrometry (ToF-SIMS): Angewandte Chemie-International Edition in English, v. 33, no. 10, p. 1023–1043.

Brown, J., Kronberg, B., and Fyfe, W., 1981, Semi-quantitative ESCA examination of coal and coal ash surfaces: Fuel, v. 60, i. 5, p. 439–446.

Buckley, A.N., and Lamb, R.N., 1996, Surface chemical analysis in coal preparation research. Complementary information from XPS and ToF-SIMS: International Journal of Coal Geology, v. 32, no. 1–4, p. 87–106.

Cameron, C.C., Esterle, J.S., and Palmer, C.A., 1989, The geology, botany and chemistry of selected peat-forming environments from temperate and tropical latitudes: International Journal of Coal Geology, v. 12, no. 1–4, p. 105–156.

Chadwick, B.L., Domazetis, G., and Morrison, R.J.S., 1995, Multiwavelength monitoring of photofragment fluorescence after 193-nm photolysis of NaCl and NaOH - application to measuring the sodium species released from coal at high-temperatures: Analytical Chemistry, v. 67, no. 4, p. 710–716.

Considine, T.J., 2009, Powder River basin coal: powering America, Final report to the Wyoming Mining Association.

Cullers, R.L., and Graf, J.L., 1984, Rare earth elements in igneous rocks of the continental crust: intermediate and silicic rocks – ore petrogenesis *in* Henderson, P. ed., Rare earth element geochemistry: Elsevier, p. 275–316.

Devic, G., and Pfendt, P., 2007, Diagenetic relationships between sulphur species and formation of pyrite in coals and sediments: Energy Sources Part a-Recovery Utilization and Environmental Effects, v. 29, i. 16, p. 1487–1498.

Diehl, S.F., Goldhaber, M.B., Koenig, A.E., Tuttle, M.L.W., and Ruppert, L.F., 2005, Concentration of arsenic, selenium, and other trace elements in pyrite in

Appalachian coals of Alabama and Kentucky *in* Barnhisel, R.I., ed., Raising Reclamation to New Heights: Proceedings of the 22nd Annual Meeting of the American Society of Mining and Reclamation, June 19–23, Breckenridge, Colorado, p. 283–301.

Domazetis, G., Raoarun, M., James, B.D., Liesegang, J., Pigram, P. J., Brack, N., and Glaisher, R., 2006, Analytical and characterization studies of organic and inorganic species in brown coal: Energy & Fuels, v. 20, no. 4, p. 1556–1564.

Eby, N., 2007, Geochemical Instrumentation and Analysis: Science Education Resource Center at Carleton College: http://serc.carleton.edu/research_education/geochemsheets/techniques/INAA.html (March, 2010).

Ellis, M.S., Gunther, G.L., Flores, R.M., Ochs, A.M., Stricker, G.D., Roberts, S.B., Taber, T.T., Bader, L.R., and Schuenemeyer, J.H., 1999, Preliminary Report on Coal Resources of the Wyodak-Anderson Coal Zone, Powder River Basin, Wyoming and Montana: U.S. Geological Survey Open-File Report 98-0789-A, 32 pp.

Evans, C. and associates, 1999, Analytical resolution versus sensitivity diagram.

Finkelman, R. B., 1993, Trace and Minor Elements in Coal *in* Engel, M.H., and Macko, S.A., eds., Organic Geochemistry: New York, Plenum Press p. 593–607.

Finkelman, R.B., 1994, Trace elements in coal: A USGS perspective of the Clean Air Act: American Chemical Society, Division of Fuel Chemistry Preprints, v. 39, p. 519–523.

Flores, R. M., 2004, Coalbed methane in the Powder River Basin, Wyoming and Montana: An assessment of the Tertiary-Upper Cretaceous coalbed methane total petroleum system: U.S. Geological Survey Digital Data Series DDS-69-C, chapter 2, 56 p.

Flores, R.M., and Bader,L.R., 1999, Fort Union Coal in the Powder River Basin, Wyoming and Montana: a synthesis: the 1999 resource assessment of selected Tertiary coal beds and zones in the Northern Rocky Mountains and Great Plains region, U.S. Geological Survey Professional Paper 1625-A.

Franco, A., and Diaz, A.R., 2009, The future challenges for "clean coal technologies": joining efficiency increase and pollutant emission control: Energy, v. 34, no. 3, p. 348–354.

Fyfe, W. S., Kronberg, B. I., and Brown, J.R., 1982, Variations in the inorganic-chemistry of coal: American Chemical Society, Division Fuel Chemistry preprint, v. 27, no.1, p. 116–123.

George, G.N., Gorbaty, M.L., Kelemen, S.R., and Sansone, M., 1991, Direct determination and quantification of sulfur forms in coals from the Argonne premium sample program: Energy & Fuels, v. 5, no. 1, p. 93–97.

Gong, B., Buckley, A.N., Lamb, R.N., and Nelson, P.F., 1999, XPS determination of the forms of nitrogen in coal pyrolysis chars: Surface and Interface Analysis, v. 28, no. 1, p. 126–130.

Gong, B., Pigram, P.J., and Lamb, R.N., 1997, Identification of inorganic nitrogen in an Australian bituminous coal using X-ray photoelectron spectroscopy (XPS) and time-of-flight secondary ion mass spectrometry (TOFSIMS): International Journal of Coal Geology, v. 34, no. 1–2, p. 53–68.

_____, 1998, Surface studies of low-temperature oxidation of bituminous coal vitrain bands using XPS and SIMS: Fuel, v. 77, no. 9-10, p. 1081–1087.

Goodarzi, F., 2006, Characteristics and composition of fly ash from Canadian coal-fired power plants: Fuel, v. 85, no. 10–11, p. 1418–1427.

Grzybek, T., Pietrzak, R., and Wachowska, H., 2002, X-ray photoelectron spectroscopy study of oxidized coals with different sulphur content: Fuel Processing Technology, v. 77, p. 1–7.

Hildebrand, R.T., 1986, Influence of groundwater composition on sodium content of coal in Powder River Basin, Southeastern Montana and Northeastern Wyoming: Aapg Bulletin-American Association of Petroleum Geologists, v. 70, no. 8, p. 1043–1043.

Hochella, M.F., 1988, Auger-electron and x-ray photoelectron spectroscopies: Reviews in Mineralogy, v. 18, p. 573–637.

ICDD DDView version 3.1 using PDF 2, 2005.

Kambara, S., Takarada, T., Yamamoto, Y., and Kato, K., 1993, Relation between functional forms of coal nitrogen and formation of NO(x) precursors during rapid pyrolysis: Energy & Fuels, v. 7, no. 6, p. 1013–1020.

Kambara, S., Takarada, T., Toyoshima, M., and Kato, K., 1995, Relation between functional forms of coal nitrogen and NOx emissions from pulverized coal combustion: Fuel, v. 74, no. 9, p. 1247–1253.

Kelemen, S.R., and Freund, H., 1990, Oxidation-kinetics of Wyoming Powder River Basin Coal in O_2 between 295 K and 398 K: Energy & Fuels, v. 4, no. 2, p. 165–171.

Kelemen, S.R., Gorbaty, M.L., and Kwiatek, P.J., 1994, Quantification of nitrogen forms in Argonne premium coals: Energy & Fuels, v. 8, no. 4, p. 896–906.

Kelemen, S.R., Gorbaty, M.L., Kwiatek, P.J., Fletcher, T.H., Watt, M., Solum, M.S., and Pugmire, R.J., 1998, Nitrogen transformations in coal during pyrolysis: Energy & Fuels, v. 12, no. 1, p. 159–173.

Kelemen, S.R., Afeworki, M., Gorbaty, M.L., Kwiatek, P.J., Sansone, M., Walters, C.C., and Cohen, A.D., 2006, Thermal transformations of nitrogen and sulfur forms in peat related to coalification: Energy & Fuels, v. 20, no. 2, p. 635–652.

Kizilshtein, L.Y., and Kholodkov, Y.I., 1999, Ecologically hazardous elements in coals of the Donets Basin: International Journal of Coal Geology, v. 40, no. 2–3, p. 189–197.

Kolker, A., and Finkelman, R.B., 1998, Potentially hazardous elements in coal: Modes of occurrence and summary of concentration data for coal components: International Journal of Coal Preparation and Utilization, v. 19, no. 3, p. 133–157.

Kong, L.B., Karner, F.R., Benson, S.A., and Steadman, E.N., 1993, Petrographic analysis of the Rosebud seam at the Absaloka, Big sky, and Rosebud mines, Powder River Basin, Montana: Organic Geochemistry, v. 20, no. 6, p. 811–822.

Kotz, J.C., Treichel, P., and Weaver G.C., 2006, Chemistry and chemical reactivity sixth edition: Brook/Cole, p. 1680.

Kronberg, B.I., Brown, J.R., Fyfe, W.S., Peirce, M., and Winder, C.G., 1981, Distributions of trace-elements in Western Canadian coal ashes: Fuel, v. 60, no. 1, p. 59–63.

Kunce, M., Hamilton, S., and Gerking S., 2004, Marketable permits, low-sulfur coal, and the behavior of railroads: http://www.bus.ucf.edu/wp/Working%20Papers/2004/04-20Gerking.pdf

Matjie, R.H., Van Alphen, C., and Pistorius, P.C., 2006, Mineralogical characterization of Secunda gasifier feedstock and coarse ash: Minerals Engineering, v. 19, no. 3, p. 256–261.

Moore, D.M. and Reynolds, R.C. Jr., 1997, X-Ray diffraction and the identification and analysis of clay minerals. 2nd Ed: Oxford University Press, New York, p. 332.

Moulder, J.F., Stickle, W.F., Sobol, P.E., and Bomben, K.D., 1992, *in* Chastain, J., Ed., Handbook of X-Ray Photoelectron Spectra—A Reference Book of Standard Spectra for Identification and Interpretation of XPS Data, Perkin-Elmer, Eden Prairie, Minnesota, p. 217.

Murowchick, J.B. and Barnes, H.L., 1987, Effects of temperature and degree of supersaturation on pyrite morphology: American Mineralogist, v. 72 p. 1241–1250.

Nabeel, A., Khan, M.A., Husain, S., Krishnamacharyulu, B., Rao, R.N., and Sharma, D.K., 2000, Basic studies of coal to enhance its development as a clean fuel: Energy Sources, v. 22, no. 1, p. 57–65.

Nakamura, Y., 1974, Oxidation behavior of an iron-chromium alloy containing yttrium or rare-earth elements between 900 degrees and 1200 degrees C: Metallurgical transactions, v. 5, no. 4, p. 909–913.

Pei, L., Jiang, G., Tyler, B.J., Baxter, L.L., and Linford, M.R., 2008, Time-of-flight secondary ion mass spectrometry of a range of coal samples: A chemometrics (PCA, cluster, and PLS) analysis: Energy & Fuels, v. 22, no. 2, p. 1059–1072.

Pourkashanian, W.A., Jones, J.M., and Skorvpska, N., 2000, Combustion and gasification of coal: part of applied energy technology series Taylor & Francis, New York 263 p.

Reyes, F., Pérez Alcázar, G.A., Barraza, J.M., Bohórquez, A., Tabares, J.A., and Speziali, N.L., 2003, Mossbauer and XRD characterization of the mineral matter of coal from the Guachinte mine in Colombia: Hyperfine Interactions, v. 148, no. 1–4, p. 39–46.

Richards, M., 2008, City of Colstrip Comprehensive growth policy: http://www.cityofcolstrip.com/documents/Growth%20Plan/Colstrip%20Comprehensive%20Growth%20Plan%2008%20for%20website.pdf (August, 2009).

Roberts, S.B., Wilde, E.M., Rossi, G.S., Blake, D., Bader, L.R., Ellis, M.S., Stricker, G.L., Ochs, A.M., Kinney, S.A., Schuenemeyer, J.H., and Power, H.C., 1999, Colstrip Coalfield, Powder River Basin, Montana: Geology, coal quality, and coal resources: USGS Geological Survey Professional Paper 1625.

Smith, K.K., 2005, Powering Our Future: An Energy Sourcebook for Sustainable Living: Lincoln, Nebraska, Alternative Energy Institute, 378 p.

Speight, J.G., 2005, Handbook of Coal Analysis: New Jersey, John Wiley & Sons, 239 p.

Stanczyk, K., 2004, Temperature-time sieve - A case of nitrogen in coal: Energy & Fuels, v. 18, no. 2, p. 405–409.

Sticker and G.D. and Ellis and M.S., 1999, Coal Quality and Geochemistry, Powder River Basin, Wyoming and Montana: U.S. Geological Survey Professional Paper 1625-A.

Struck, D.G., Western Interstate Commission for Higher Education. Resources Development Internship Program; Montana. Dept. of Natural Resources and Conservation, 1975, Conflictive land use: coal strip mining and agriculture: Boulder, Colo.: Western Interstate Commission for Higher Education, 22 p.

Suzuki, S. and Hirai S., 1992, Multielement analysis of environmental reference materials by instrumental neutron activation analysis: Analytical sciences, v.8, p. 437–441.

Thomas, L., 2002, Coal Geology: Chichester, John Wiley and Sons Ltd, 384 p.

US Energy Information Administration, 2008, Annual coal report. DOE/EIA 0584: http://www.eia.doe.gov/cneaf/coal/page/acr/acr_sum.html#fes1 (May, 2010)

US National Committee for geochemistry Assembly of Mathematical and physical sciences, National Research Council, 1980, Trace-Element Geochemistry of Coal Resource Development Related to Environmental Quality and Health by the panel on the trace element geochemistry of coal resource development related to health subcommittee on the geochemical environment in relation to health and disease: National academy press, Washington DC, 153 p.

USGS, 1997, Radioactive Elements in Coal and Fly ash: abundance, forms and Environmental Significance: U.S. Geological Survey Fact Sheet FS-163-97: http://pubs.usgs.gov/fs/1997/fs163-97/FS-163-97.pdf (March, 2010).

van Alphen, C., 2007, Automated mineralogical analysis of coal and ash products - Challenges and requirements: Minerals Engineering, v. 20, i. 5, p. 496–505.

Van Vaeck, L., Adriaens, A., and Gijbels, R., 1999, Static secondary ion mass spectrometry: (S-SIMS) Part 1. Methodology and structural interpretation: Mass Spectrometry Reviews, v. 18, no. 1, p. 1–47.

Vorres, K.S., 1993, Users Handbook for The Argonne Premium Coal Sample Program

Wang, W.F., Qin, Y., Wang, J.Y., Li, J., and Weiss, D. J., 2010, A preliminary method for determining acceptable trace element levels in coal: Energy, v. 35, no. 1, p. 70–76.

Ward, C.R., and Christie, P.J., 1994, Clays and other minerals in coal seams of the Moura-Baralaba area, Bowen Basin, Australia: International Journal of Coal Geology, v. 25, no. 3–4, p. 287–309.

Weitzsacker, C.L., and Gardella, J.A., 1992, Quantitative electron spectroscopic analysis of Argonne premium coals: Analytical Chemistry, v. 64, no. 9, p. 1068–1075.

Westmoreland, -(a), Westmoreland mining: http://www.westmoreland.com/coal.asp?topic=westmoreland_mining#rosebud

(March, 2009). –(b), Westmoreland resources: http://www.westmoreland.com/coal.asp?topic=westmoreland_resources (March, 2009).

Wojtowicz, M.A., Pels, J.R., and Moulijn, J.A., 1995, The fate of nitrogen functionalities in coal during pyrolysis and combustion: Fuel, v. 74, no. 4, p. 507–516.

APPENDICES

APPENDIX A

NOTE FROM NELSON EBY

Attached are the results for your coal samples. I also did a NIST standard and several replicate analyses so you can get an idea of the precision and accuracy of the method.

The samples were irradiated for 3 hours at 1 MW. They were counted for 10,000 seconds 5 to 7 days after irradiation and for 40,000 seconds 4 to 5 weeks after irradiation. The counting system consists of a high resolution Broad Energy Germanium Detector with quick response time electronics. The system is automated and we can, and do, change samples remotely using the internet. The spectra are analyzed using Canberra Genie software. Final data reduction is done using my own computer codes. Flux variations are determined by attaching an iron wire to each sample vial. I also correct for geometry and interferences. We have developed a set of absolute standard calibrations for the system which are tied to individual analyses using the flux and geometry corrections. ICP-MS and AA individual element liquid standards were used for the calibration. International rock standards
were used to check the element calibrations.

Hope you find the numbers useful.

All the best,
Nelson

APPENDIX B

SPECIFIC JCPDF CARD FILE NUMBERS

card # :	name :	formul-
33-1161	SILICON OXIDE / QUARTZ, SYN	SI O2
10-0357	POT SOD ALUMINUM SILICATE / SANIDINE, POTASSIAN, DISORDERED, SYN	(NA K) (SI3 AL) O8
11-0647	SODIUM SULFATE HYDRATE / MIRABILITE	NA2 S O4 . 10 H2 O
43-0685	POTASSIUM ALUMINUM SILICATE HYDROXIDE / MUSCOVITE-2M2	K AL2 (SI3 AL) O10 (O H)2
42-1340	IRON SULFIDE / PYRITE	FE S2
09-0465	SODIUM CALCIUM ALUMINUM SILICATE / ANORTHITE, SODIAN, ORDERED	(CA NA) (AL SI)2 SI2 O8
09-0466	SODIUM ALUMINUM SILICATE / ALBITE, ORDERED	NA AL SI3 O8
36-0425	SODIUM IRON SULFATE HYDROXIDE / NATROJAROSITE, SYN	NA FE3 (S O4)2 (O H)6
15-0700	SODIUM HYDROGEN CARBONATE / NAHCOLITE, SYN	NA H C O3
22-0827	POTASSIUM IRON SULFATE HYDROXIDE / JAROSITE, SYN	K FE3 (S O4)2 (O H)6
36-0426	CALCIUM MAGNESIUM CARBONATE / DOLOMITE	CA MG (C O3)2
41-1486	CALCIUM ALUMINUM SILICATE / ANORTHITE, ORDERED	CA AL2 SI2 O8
41-1370	CALCIUM MAGNESIUM ALUMINUM SILICATE / DIOPSIDE	CA (MG AL) (SI AL)2 O6
21-0149	CAL MAG IRON ALUM SILIC HYDROXIDE / MAGNESIOHORNBLENDE, FERROAN	CA2 (MG FE)5 (SI AL)8 O22 (O H)2
34-0175	POTASSIUM SODIUM ALUMINUM SILICATE HYDROXIDE / MUSCOVITE-2M2	(K NA) AL2 (SI AL)4 O10 (O H)2
41-1480	SODIUM CALCIUM ALUMINUM SILICATE / ALBITE, CALCIAN, ORDERED	(NA CA) AL (SI AL)3 O8
06-0263	POTASSIUM ALUMINUM SILICATE HYDROXIDE / MUSCOVITE-2M1	K AL2 (SI3 AL) O10 (O H F)2
19-0926	POTASSIUM ALUMINUM SILICATE / MICROCLINE, ORDERED	K AL SI3 O8
29-1496	POTASSIUM ALUMINUM SILICATE HYDROXIDE / ILLITE-1M	K .7 AL2 (SI AL)4 O10 (O H)2
20-0528	SODIUM CALCIUM ALUMINUM SILICATE / ANORTHITE, SODIAN, ORDERED	(CA NA) (AL SI)2 SI2 O8
19-1227	POTASSIUM SODIUM ALUMINUM SILICATE / SANIDINE	(K NA) (SI3 AL) O8
29-1447	SODIUM HYDROGEN CARBONATE HYDRATE / TRONA	NA3 H (C O3)2 . 2 H2 O
24-0201	CALCIUM IRON MAGNESIUM SILICATE / AUGITE	CA (FE MG) SI2 O6
31-0966	POTASSIUM ALUMINUM SILICATE / ORTHOCLASE	K AL SI3 O8
19-1184	SODIUM ALUMINUM SILICATE / ALBITE, ORDERED	NA AL SI3 O8
14-0164	ALUMINUM SILICATE HYDROXIDE / KAOLINITE-1A	AL2 SI2 O5 (O H)4
37-0475	IRON SULFIDE / MARCASITE	FE S2
33-0311	CALCIUM SULFATE HYDRATE / GYPSUM, SYN	CA S O4 . 2 H2 O
05-0586	CALCIUM CARBONATE / CALCITE, SYN	CA C O3

APPENDIX C

SAMPLING OF SEM IMAGES

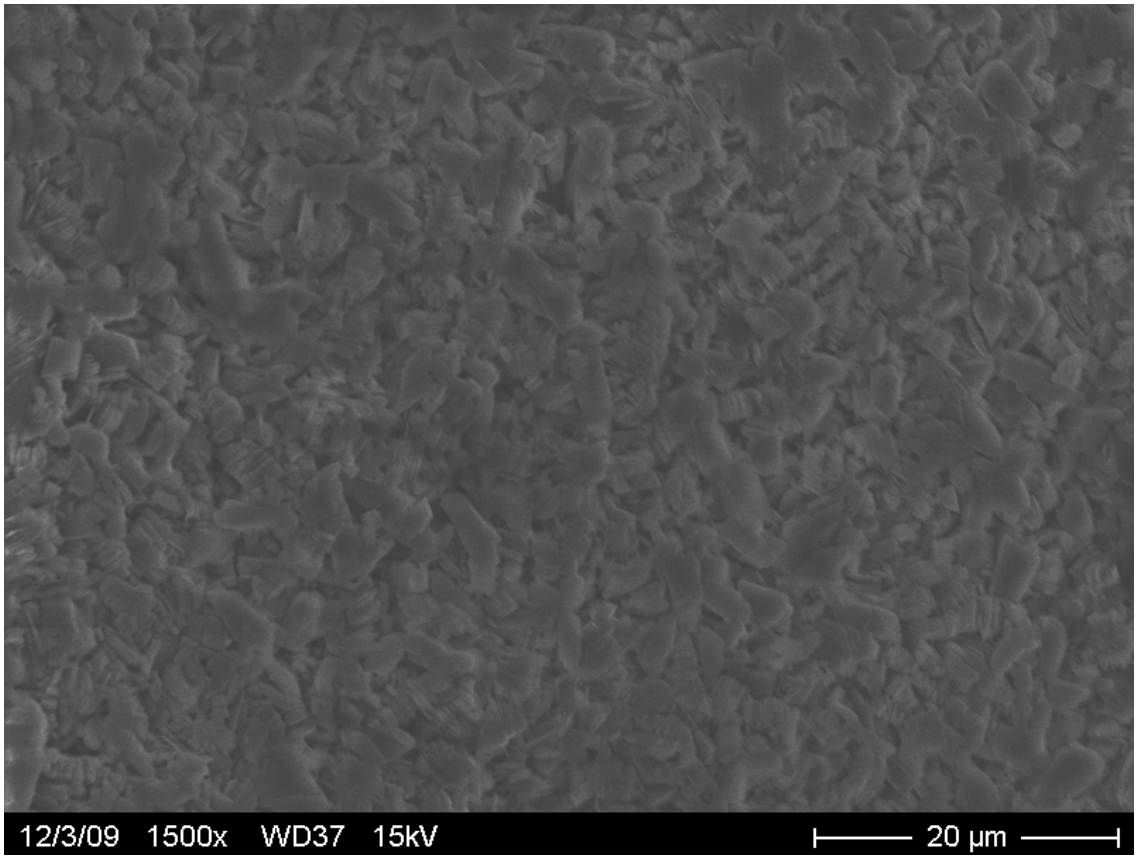


Figure 36. D low 1% Na ash rich. Kaolinite with platy habit.

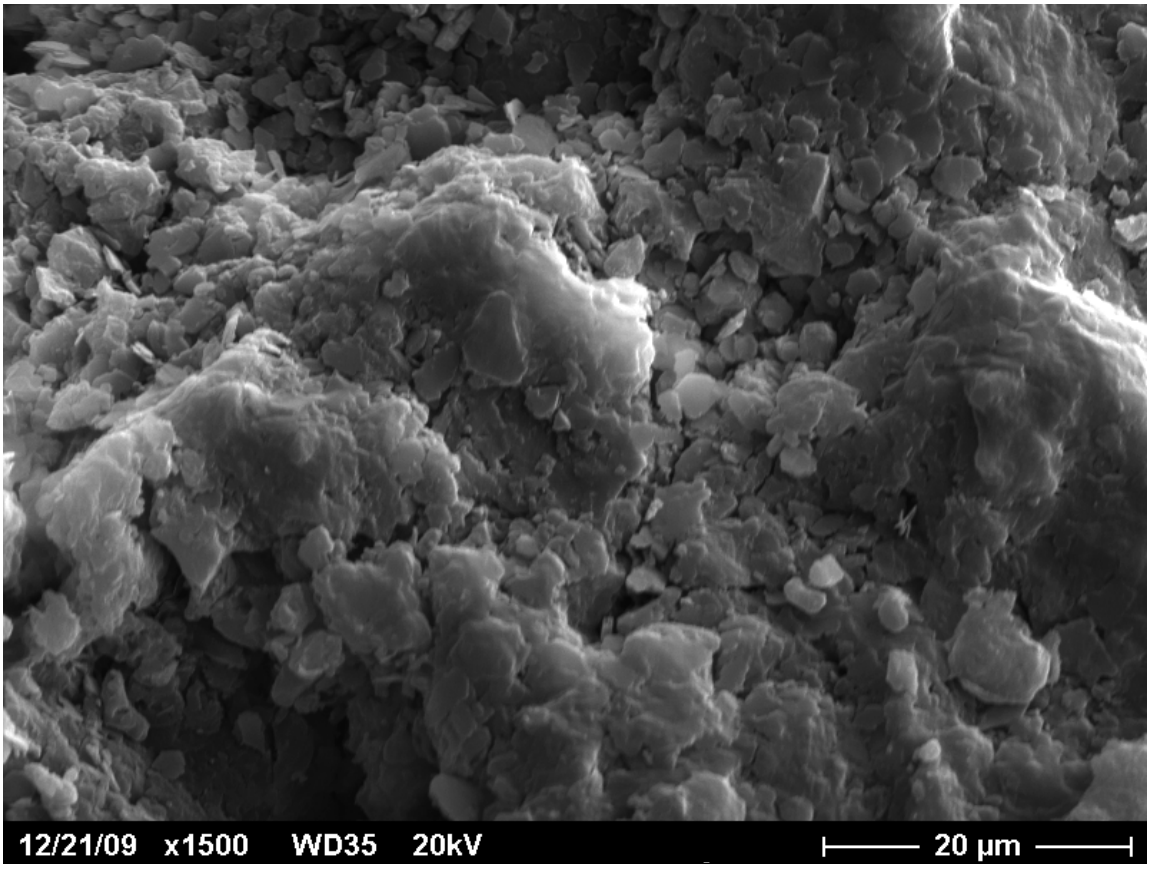


Figure 37. D low 8% Ash rich. Dominantly kaolinite, pyrite is also detected in low abundance throughout.

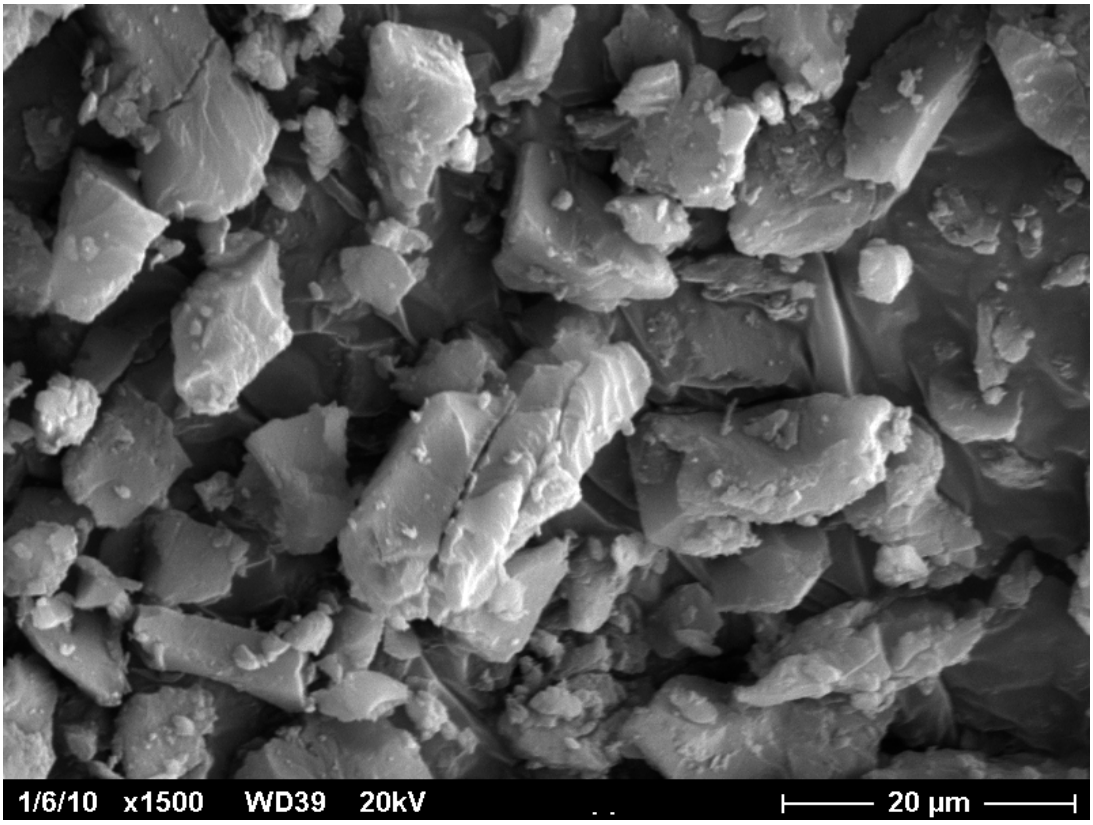


Figure 38. RB Upper Powder. Kaolinite and dolomite are the dominant minerals in this powder made in absence of visible ash and sulfide heterogeneities.

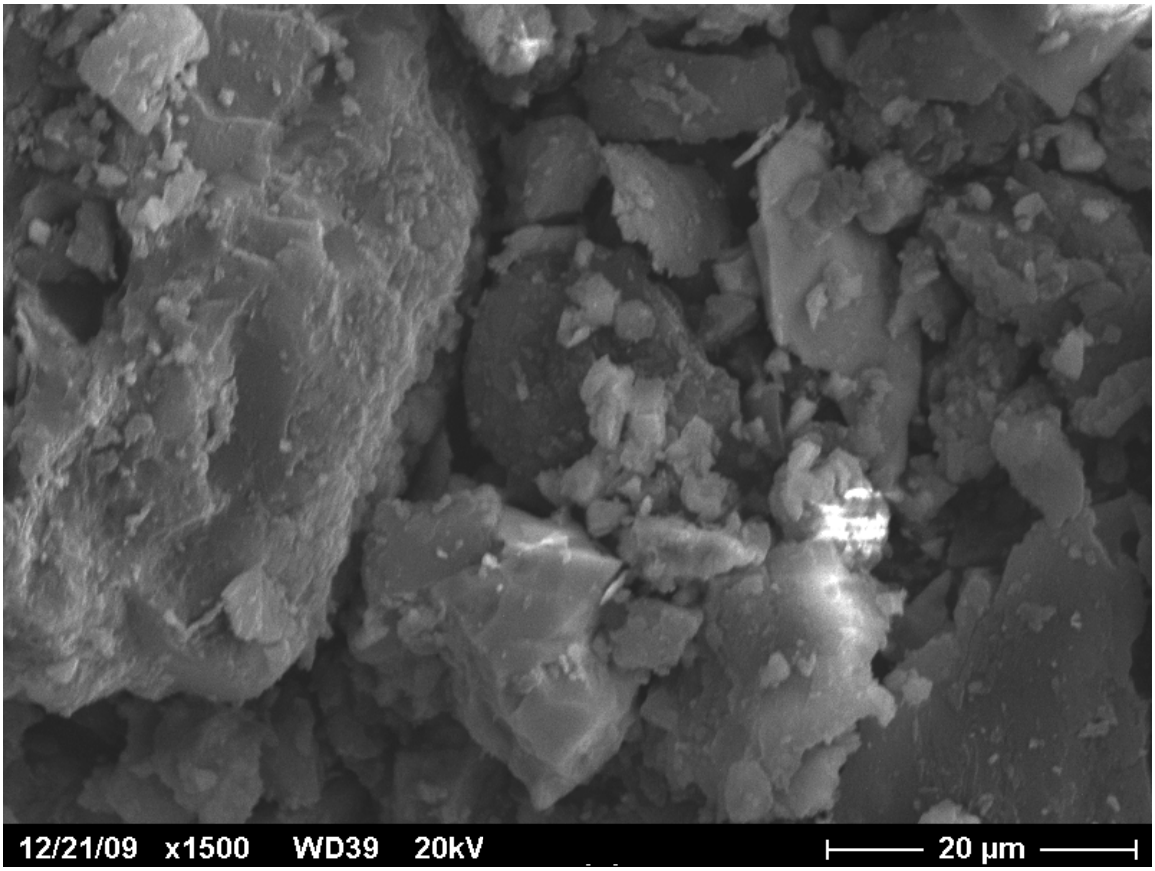


Figure 39. RB CLEP Powder. Pyrite is the dominant mineral in this powder made in absence of visible ash and sulfide heterogeneities.

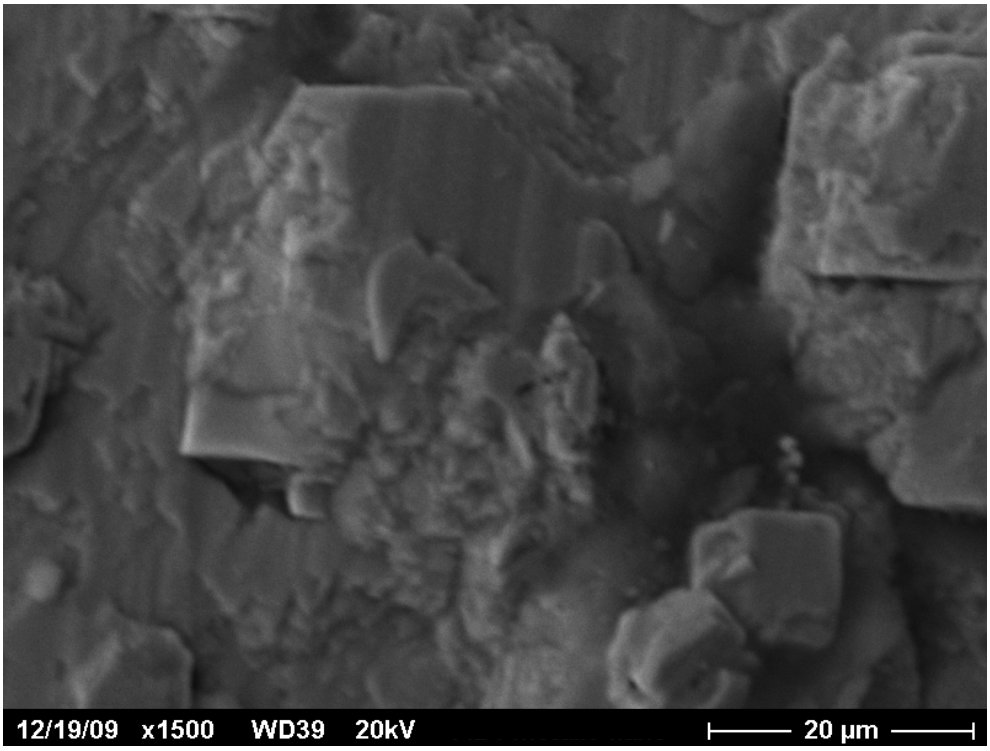


Figure 40. Ab 1 Sulfide rich. Cubo-pyritohedra pyrite dominants this sulfide component.

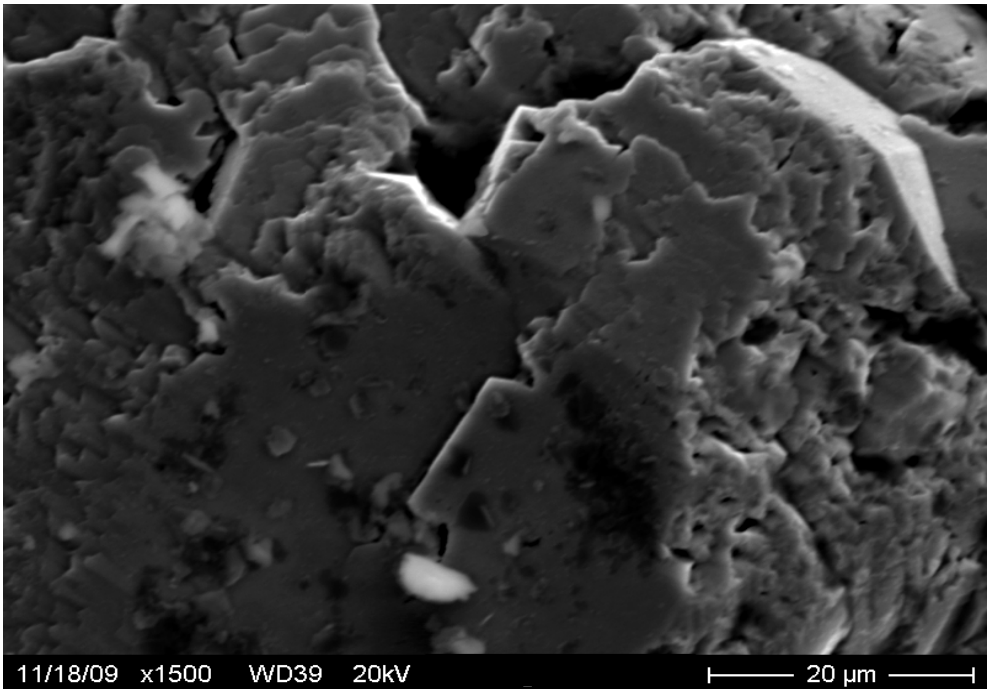


Figure 41. Ab 2 Sulfide rich. Dendritic pyrite dominants this sulfide component.

APPENDIX D

SAMPLING OF EDS SPECTRA

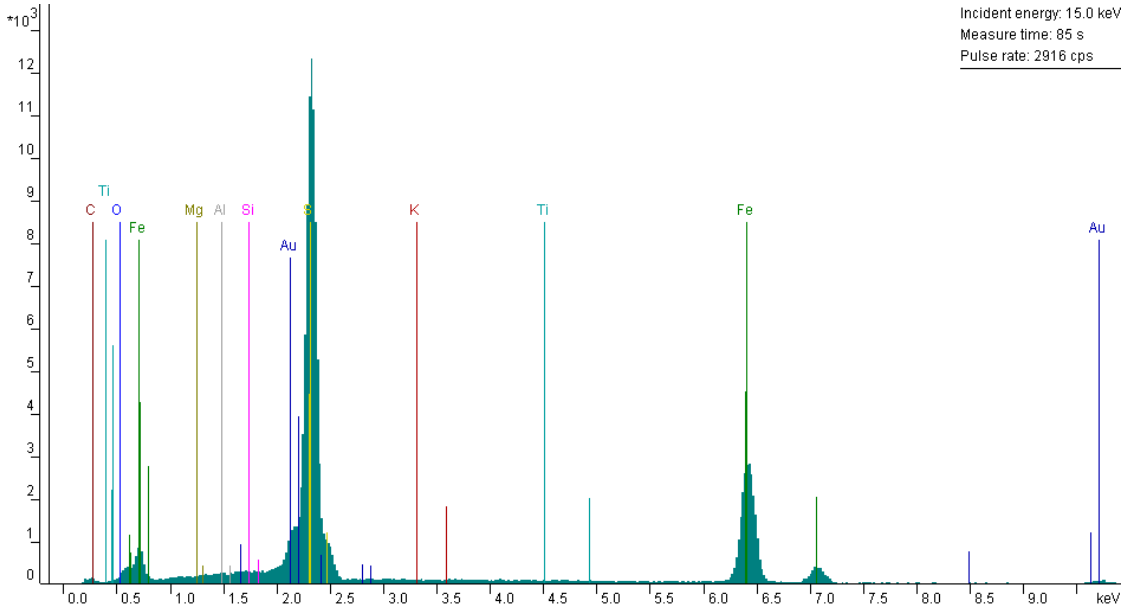


Figure 42. EDS spectra of pyrite in a powder from RB CLEP; note pyrite is pure.

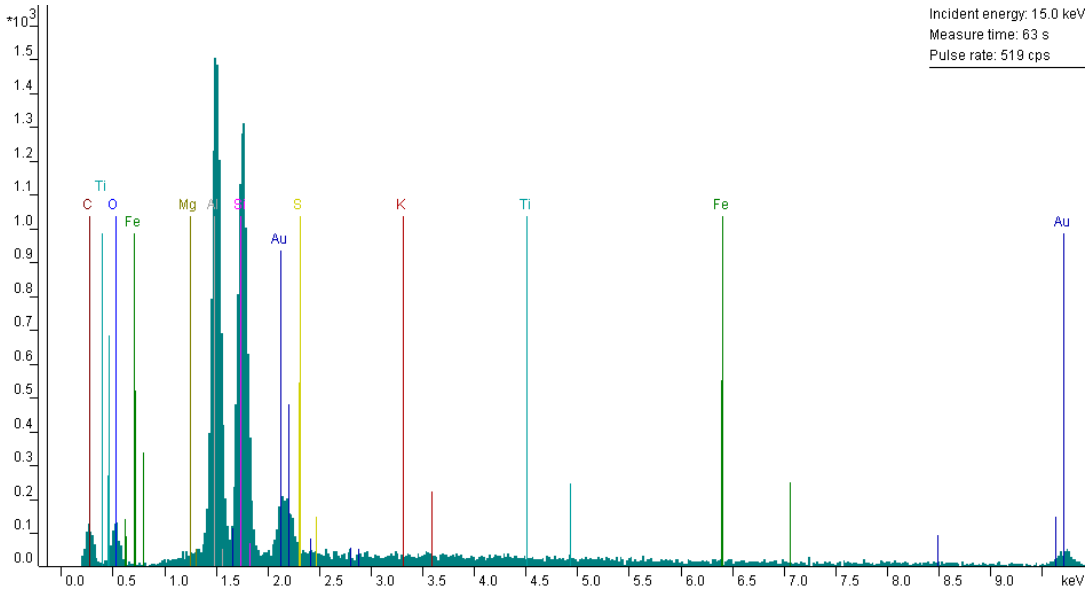


Figure 43. EDS spectra of kaolinite in a powder from Ab 4.

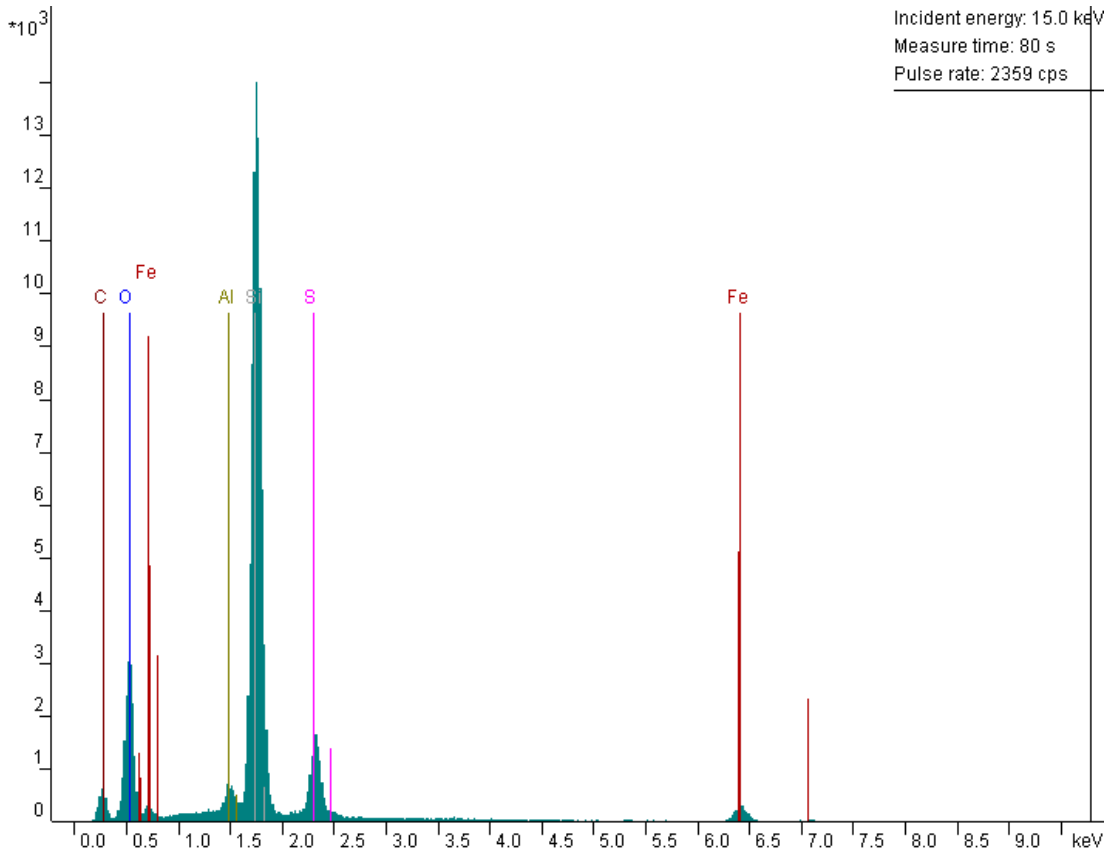
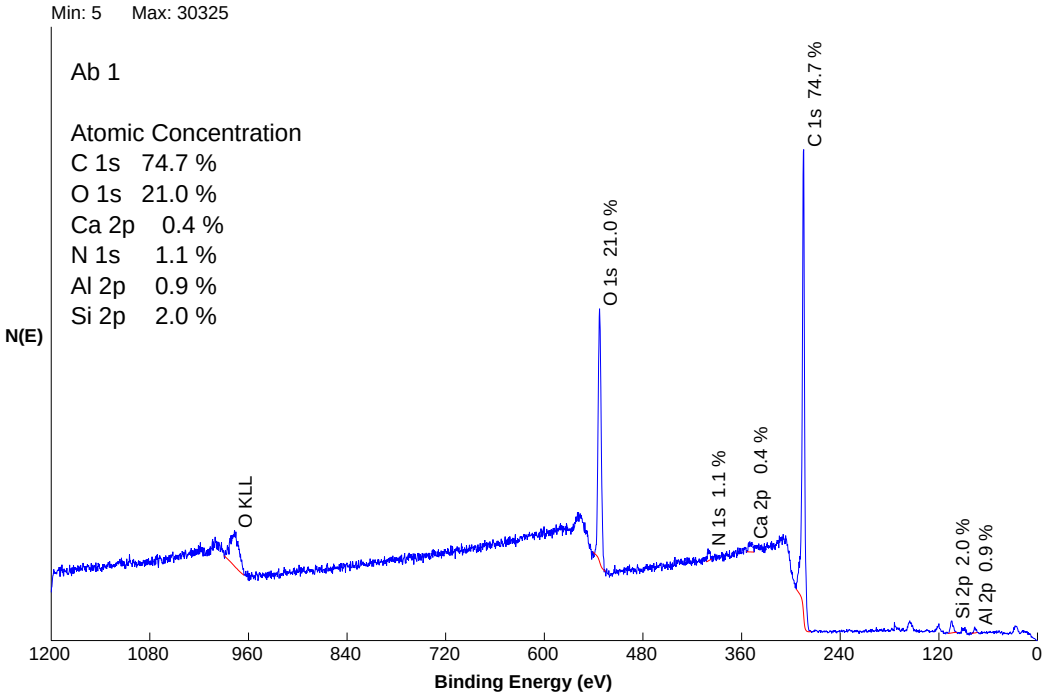
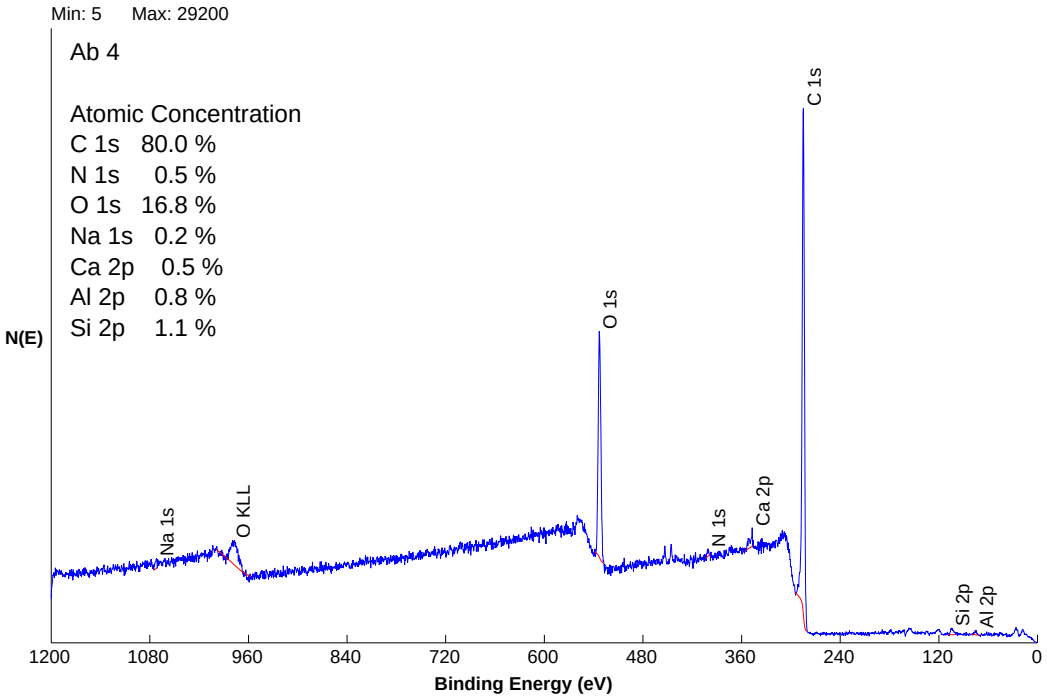


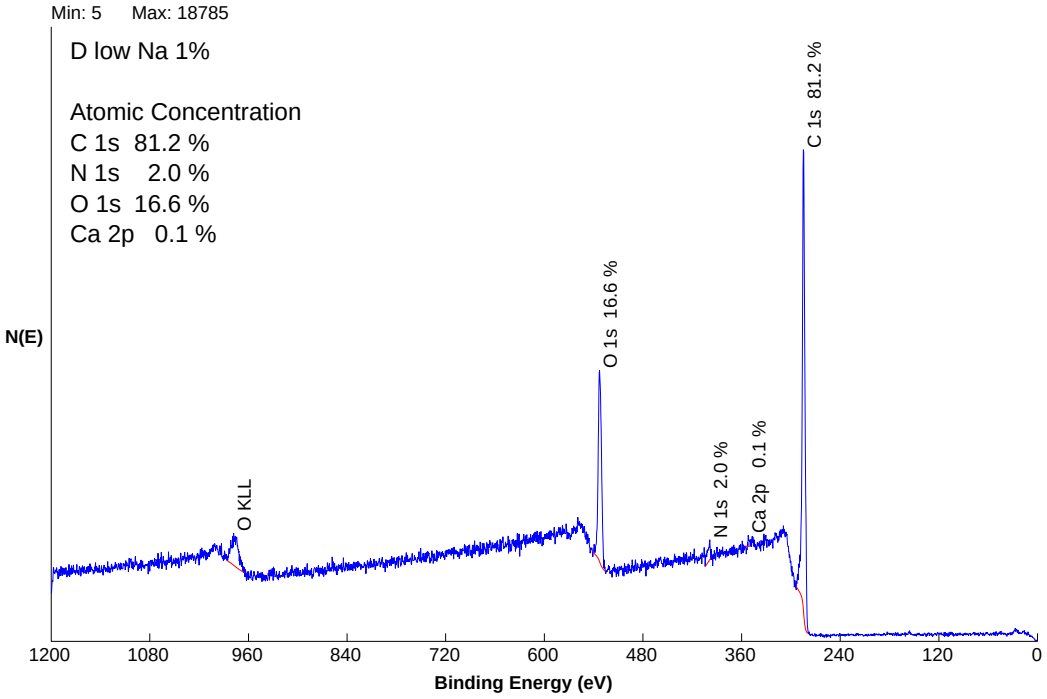
Figure 44. EDS spectra of mostly quartz and some pyrite in a sulfide rich piece from RB 1.

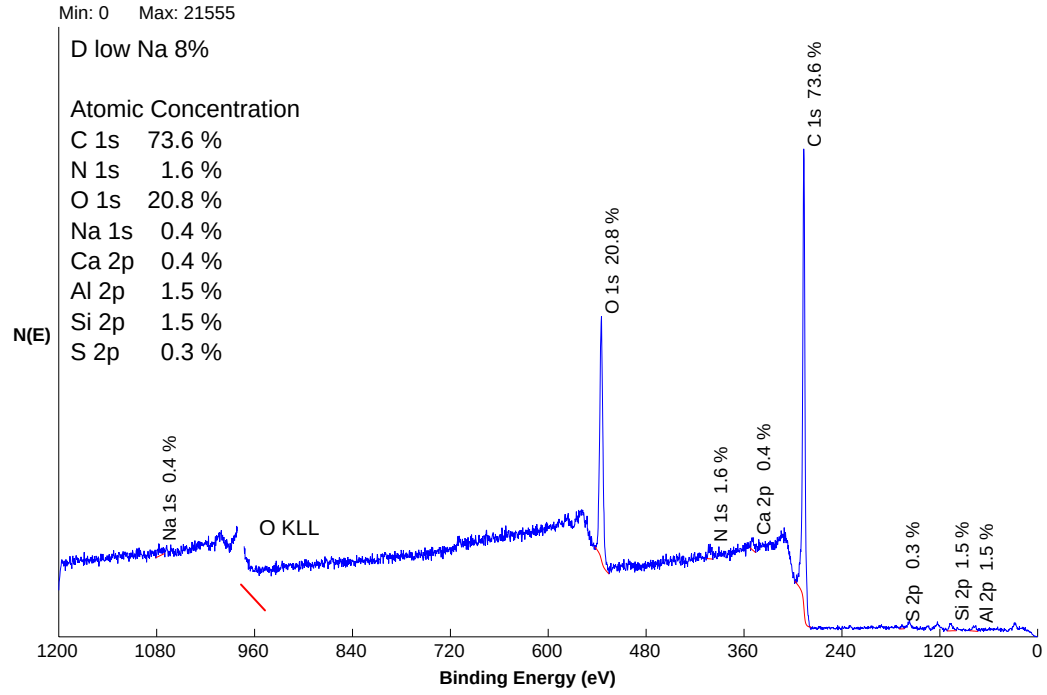
APPENDIX E

SAMPLING OF XPS SURVEYS


Min: 5 Max: 30325
Ab 1
Atomic Concentration
C 1s 74.7 %
O 1s 21.0 %
Ca 2p 0.4 %
N 1s 1.1 %
Al 2p 0.9 %
Si 2p 2.0 %
N(E)
C 1s 74.7 %
O 1s 21.0 %
N 1s 1.1 %
Ca 2p 0.4 %
Si 2p 2.0 %
Al 2p 0.9 %
O KLL
1200 1080 960 840 720 600 480 360 240 120 0
Binding Energy (eV)


Min: 5 Max: 29200
Ab 4
Atomic Concentration
C 1s 80.0 %
N 1s 0.5 %
O 1s 16.8 %
Na 1s 0.2 %
Ca 2p 0.5 %
Al 2p 0.8 %
Si 2p 1.1 %
N(E)
C 1s
O 1s
Na 1s
O KLL
N 1s
Ca 2p
Si 2p
Al 2p
1200 1080 960 840 720 600 480 360 240 120 0
Binding Energy (eV)


Min: 5 Max: 18785
D low Na 1%
Atomic Concentration
C 1s 81.2 %
N 1s 2.0 %
O 1s 16.6 %
Ca 2p 0.1 %
N(E)
C 1s 81.2 %
O 1s 16.6 %
N 1s 2.0 %
Ca 2p 0.1 %
O KLL
1200 1080 960 840 720 600 480 360 240 120 0
Binding Energy (eV)


Min: 0 Max: 21555
D low Na 8%
Atomic Concentration
C 1s 73.6 %
N 1s 1.6 %
O 1s 20.8 %
Na 1s 0.4 %
Ca 2p 0.4 %
Al 2p 1.5 %
Si 2p 1.5 %
S 2p 0.3 %
N(E)
C 1s 73.6 %
O 1s 20.8 %
N 1s 1.6 %
Ca 2p 0.4 %
Na 1s 0.4 %
S 2p 0.3 %
Si 2p 1.5 %
Al 2p 1.5 %
O KLL
1200 1080 960 840 720 600 480 360 240 120 0
Binding Energy (eV)

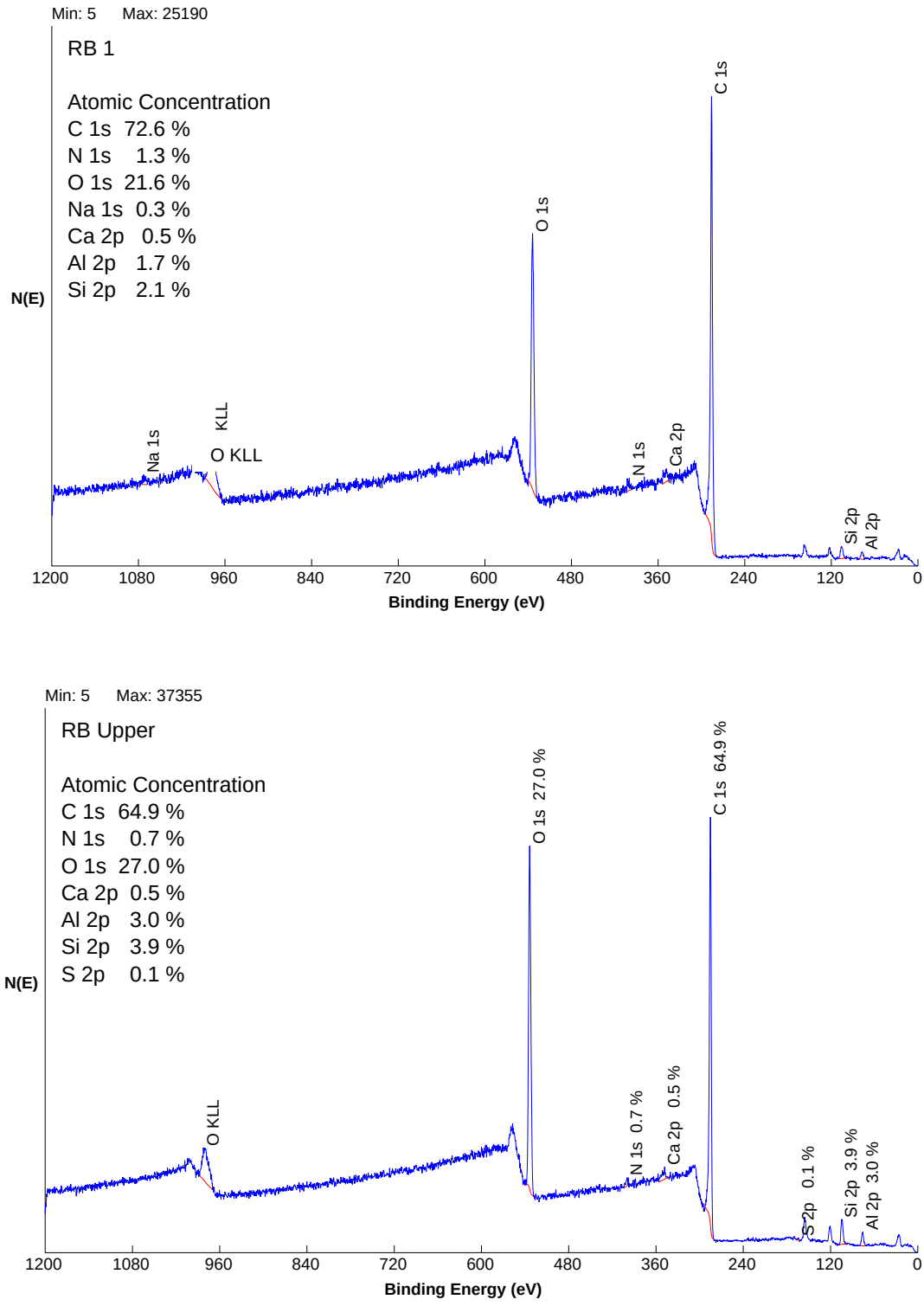


Figure 45. Spectra of XPS peaks. Auger peaks are also present; these are commonly wider such as displayed by the labeled O KLL peaks.

APPENDIX F

EXAMPLE ToFSIMs SPECTRA

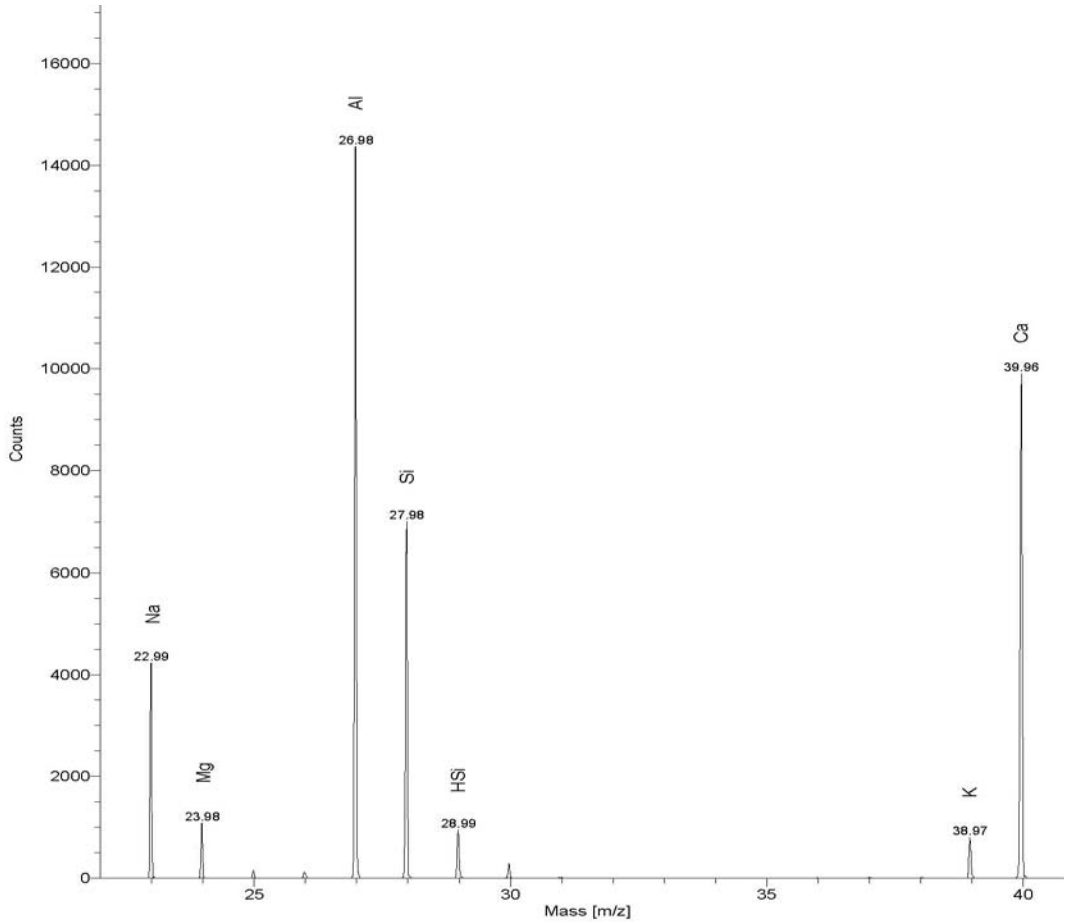


Figure 46. ToFSIMs spectra gathered in positive mode after four minutes sputtering of Ab 2.

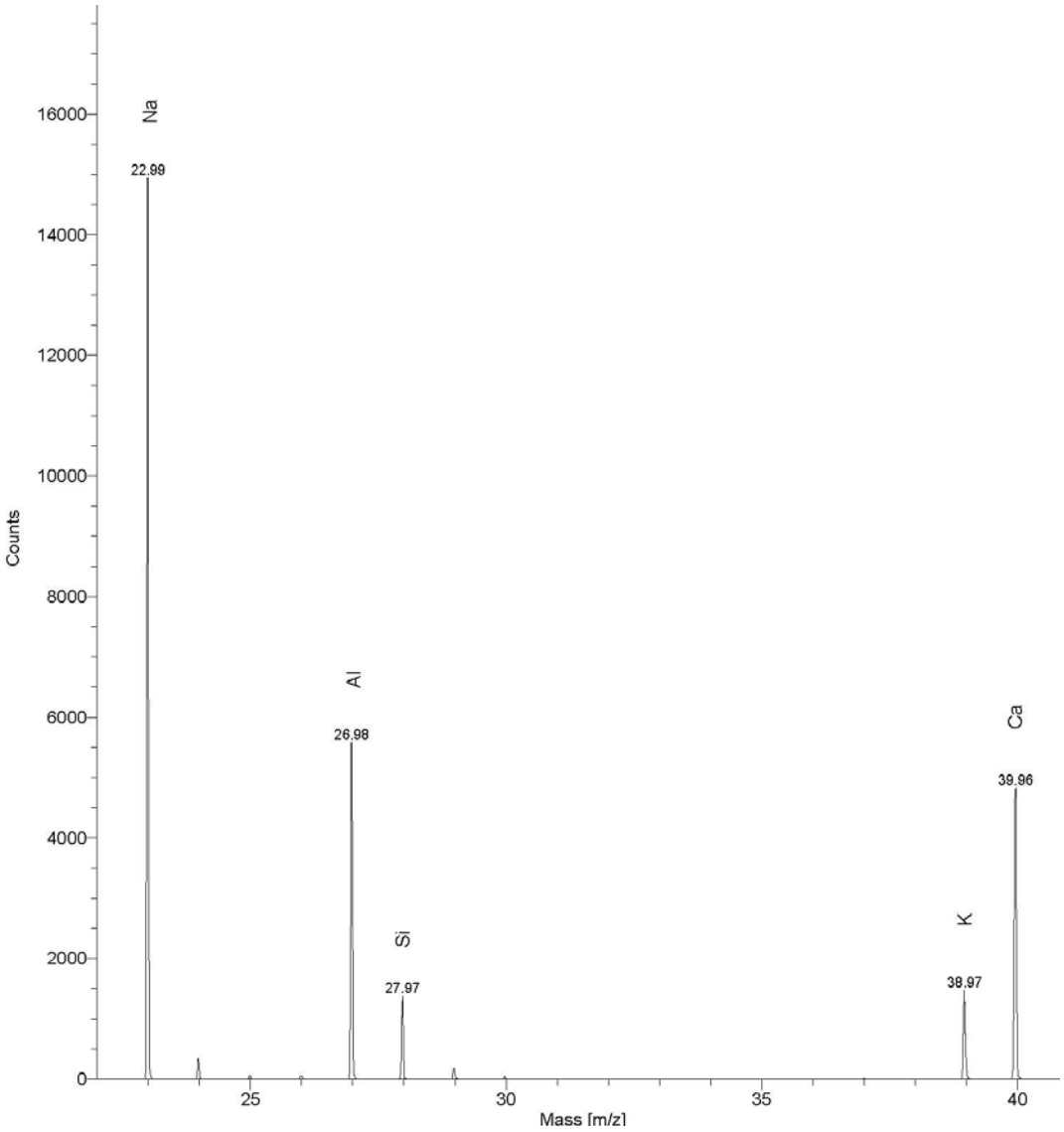


Figure 47. ToFSIMs spectra gathered in positive mode after four minutes sputtering of D low Na 8%.

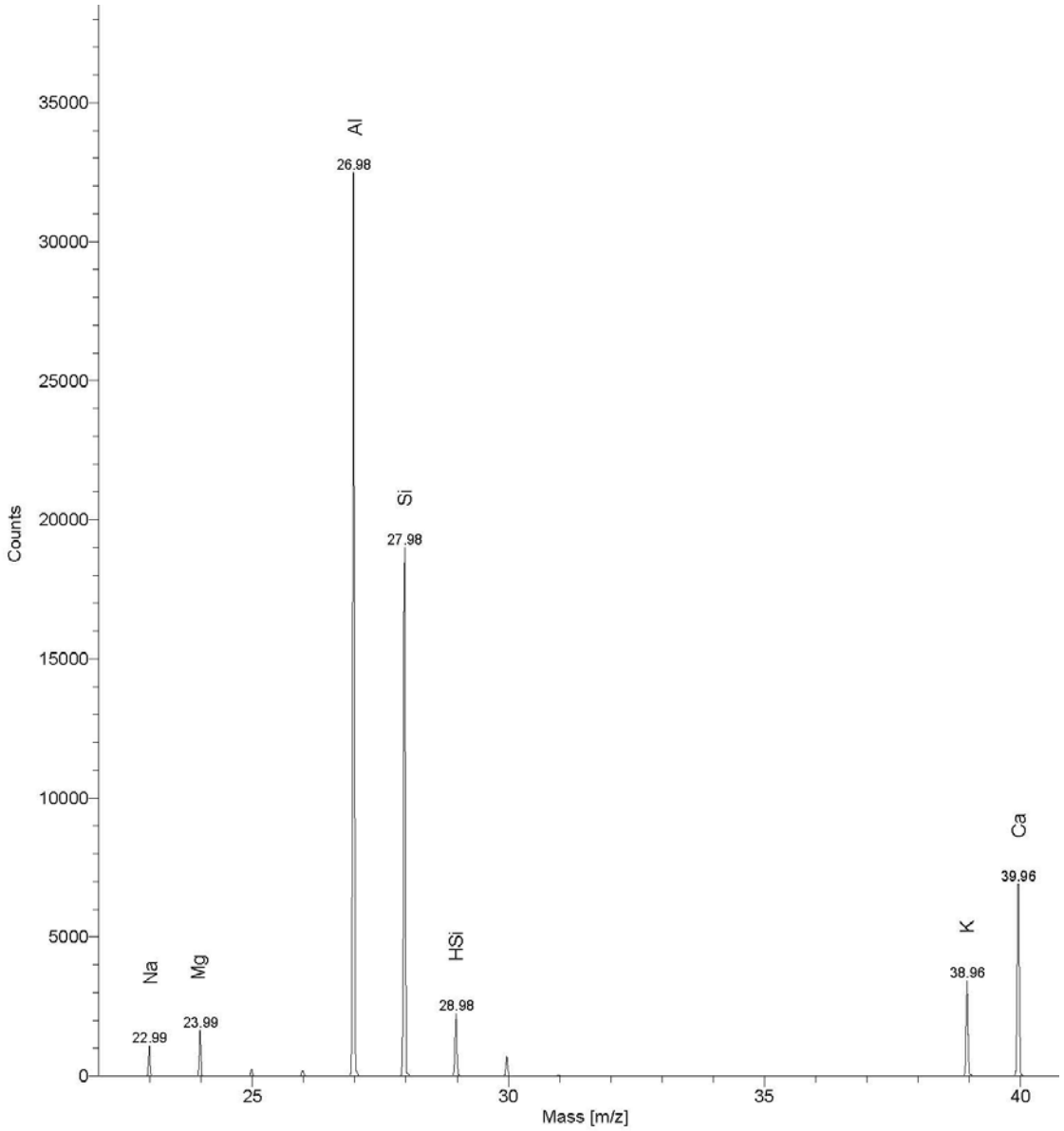


Figure 48. ToFSIMs spectra gathered in positive mode after four minutes sputtering of RB Upper.

APPENDIX G

ELEMENTS IN U.S. COALS BY RANK, AND U.S. AND WORLDWIDE AVERAGES, COMPILED BY THE NATIONAL RESEARCH COUNCIL (1980)

Table 15. Elements in U.S. Coals by Rank, and U.S. and Worldwide Averages.

Element	Anthracite	Bituminous	Sub-bituminous	Lignite	Average	Estimated Worldwide Average[c]
Major elements (percent)						
Sulfur (S)						
Phosphorus (P)	–	–	0.10	0.007	–	0.05
Silicon (Si)	2.7	2.6	2.0	4.9	2.6	2.8
Aluminum (Al)	2.0	1.4	1.0	1.6	1.4	1.0
Calcium (Ca)	0.07	0.33	0.78	1.2	0.54	1.0
Magnesium (Mg)	0.00	0.08	0.18	0.31	0.12	0.02
Sodium (Na)	0.05	0.04	0.10	0.21	0.06	0.02
Potassium (K)	0.24	0.21	0.06	0.20	0.18	0.01
Iron (Fe)	0.44	2.2	0.52	2.0	1.6	1.0
Manganese (Mn)	0.002	0.01	0.006	0.015	0.01	0.005
Titanium (Ti)	0.15	0.08	0.05	0.12	0.08	0.05
Minor and trace elements (ppm)						
Antimony (Sb)	0.9	1.4	0.7	0.7	1.1	3.0
Arsenic (As)	6	25	3	6	15	5.0
Barium (Ba)	100	100	300	300	150	500
Beryllium (Be)	1.5	2.0	0.7	2.0	2.0	3
Bismuth (Bi)	–	–	<0.6	<0.8	<0.7	5.5
Boron (B)	10	50	70	100	50	75
Bromine (Br)	–	–	2.3	3.2	2.6	–
Cadmium (Cd)	0.3	1.6	0.2	1.0	1.3	–
Cerium (Ce)	–	–	5.5	12.3	7.7	11.5
Cesium (Cs)	–	–	0.40	0.25	0.4	–
Chlorine (Cl)	–	–	255	110	207	1000
Chromium (Cr)	20	15	7	20	15	10
Cobalt (Co)	7	7	2	5	7	5
Copper (Cu)	27	22	10	20	19	15
Dysprosium (Dy)	–	–	2.7	1.4	2.2	–
Erbium (Er)	–	–	0.46	0.16	0.34	0.6
Europium (Eu)	–	–	0.61	0.13	0.45	0.7
Fluorine (F)	61	77	63	94	74	–
Gadolinium (Gd)	–	–	0.13	0.21	0.17	1.6
Gallium (Ga)	7	7	3	7	7	7
Germanium (Ge)	–	–	0.47	1.20	0.71	5
Hafnium (Hf)	–	–	0.75	0.30	0.60	-
Holmium (Ho)	–	–	0.13	0.06	0.11	0.3
Iodine (I)	–	–	1.0	1.3	1.10	–
Lanthanum (La)	–	–	7.5	3.2	6.1	10
Lead (Pb)	10	22	5	14	16	25
Lithium (Li)	33	23	7	19	20	65
Lutetium (Lu)	–	–	0.09	0.05	0.08	0.07
Mercury (Hg)	0.15	0.20	0.12	0.16	0.18	0.012
Molybdenum (Mo)	2	3	1.5	2	3	5
Neodymium (Nd)	–	–	50	11	37	4.7
Nickel (Ni)	20	20	5	15	15	15
Niobium (Nb)	–	–	5.4	2.7	4.5	–
Praseodymium (Pr)	–	–	6.1	2.7	2.7	2.2
Rubidium (Rb)	–	–	5.3	0.98	2.90	100
Samarium (Sm)	–	–	0.50	0.27	0.42	1.6
Scandium (Sc)	5	3	2	5	3	5
Selenium (Se)	3.5	4.6	1.3	5.3	4.1	3
Silver (Ag)	–	–	0.17	0.26	0.20	0.50
Strontium (Sr)	100	100	100	300	100	500
Tellurium (Te)	–	–	0.1	0.1	0.1	–
Terbium (Tb)	–	–	0.1	0.1	0.1	0.3
Thallium (Tl)	–	–	0.1	0.12	0.1	–
Thorium (Th)	–	–	2.3	1.2	1.9	–
Thulium (Tm)	–	–	0.07	0.07	0.07	–
Tin (Sn)	–	–	1.7	1.3	1.6	–
Tungsten (W)	–	–	2.2	3.3	2.5	–
Uranium (U)	1.5	1.9	1.3	2.5	1.6	1.0
Vanadium (V)	20	20	15	30	20	25
Ytterbium (Yb)	1	1	0.5	1.5	1	0.5
Yttrium (Y)	10	10	5	15	10	10
Zinc (Zn)	16	53	19	30	39	50
Zirconium (Zr)	50	30	20	50	30	–